



Validation and Verification of Torsional Dynamic Behavior of Test Bench
Through Multibody Simulations

Master Thesis

Design and Development for Mechanical and Automotive Engineering
(M.Eng)

Submitted by: Amit PANDIT

Matriculation Number: 762243

First Examiner: Prof. Dr.-Ing. Joachim BERKEMER

Second Examiner: Dr.-Ing. Tobias MEYER

Winter semester 2021

February 15, 2022

STATEMENT OF AUTHENTICITY

I hereby declare that I have written the attached work alone and without any other reference work than those mentioned. All thoughts or quotations taken directly or indirectly from other sources have been noted as such. Furthermore, I have not used the work, parts of this work or basic ideas from this work to achieve credits in any academic course at any time.



Esslingen, February 15, 2022

Amit PANDIT

ABSTRACT

The need for multibody model representing the torsional dynamics of the test bench is noticed for various purposes like understanding system dynamics with different generators, tuning of control system, component optimization, etc. Therefore, multibody models of three different test bench setups are created in MSC Adams and the torsional dynamics are validated against empirical results. A suitable approach has been used to estimate system damping and its implementation in multibody model. Consistent and lumped inertia models of the system are also created and appropriate method is employed for multibody optimization. Linearization process of the multibody model is also done and optimized parameters are verified with the existing metal properties.

Adams and ANSYS are used for creating flexible parts and the reasons for differences in the results are also explained. Control system is applied to multibody system in operational model and torsional dynamics are compared against experiment results. A case study is also done to find the probable cause of shift in torsional eigenfrequencies.

Contents

ABSTRACT	ii
LIST OF FIGURES	vi
LIST OF TABLES	ix
1 INTRODUCTION	1
1.1 Aim and objectives	3
1.2 Methodology	3
1.3 Outline of the thesis	4
2 STATE OF THE ART	4
2.1 Digital signal processing	5
2.1.1 Sampling process in time domain	5
2.1.2 Aliasing	6
2.1.3 Leakage and windowing	7
2.1.4 Fast Fourier Transform	9
2.1.5 Spectrogram	9
2.2 Finite element method (FEM)	10
2.2.1 Consistent inertia model	10
2.2.2 Lumped inertia model	12
2.3 Vibration system modeling and analysis methods	13
2.3.1 Modal analysis	15
2.4 Multibody modeling	16
2.4.1 Linearization	17
2.4.2 Flexible multibody system	19
2.5 Material properties	20
2.6 MATLAB optimization tool	22
2.7 Test bench overview	23
2.7.1 Customer 1	24
2.7.2 Without DUT	25

2.7.3 Customer 2	26
3 EXPERIMENTS	27
3.1 Experiment and results	28
3.1.1 Customer 1	28
3.1.2 Without DUT	31
3.1.3 Customer 2	34
3.2 Damping ratio calculation	36
3.2.1 Damping from experiment data	36
3.2.2 Modal space transformation	38
4 MULTIBODY MODELING	40
4.1 Model building Procedures	40
4.2 Realizing experimental damping ratio in multibody model	42
4.3 Known parameters	42
4.4 Calculation of stiffness and inertia from multibody model	43
4.5 Results from normal modes analysis	45
5 MATHEMATICAL MODELING	47
5.1 Customer 1	47
5.2 Without DUT	49
5.3 Customer 2	50
6 OPERATIONAL MODEL	50
6.1 Customer 1	52
6.2 Without DUT	54
6.3 Customer 2	57
7 LINEARIZATION OF MULTIBODY MODEL	60
8 COMPARISION OF RESULTS	61
9 MODEL OPTIMIZATION	64
9.1 Optimization of mathematical model	64

9.2 Optimization of Adams models	68
10 CASE STUDY OF LOW EIGENFREQUENCIES	72
11 CONCLUSIONS AND FUTURE PROSPECTS	75
REFERENCES	78
APPENDICES	81
A Flexible parts and units	81
B Stiffness calculation from multibody model	81
C Simulink model for optimization	82
D Simulink model to check sensitive parameters	83

List of Figures

1	Test bench setup at HiL-Grid-CoP	2
2	HiL control architecture	3
3	Digital Signal Processing (DSP)	5
4	Aliasing during sampling	6
5	Anti-aliasing filter	7
6	Ideal (left) and real (right) LPF	7
7	Leakage and truncation of data	8
8	Windowing	8
9	Uniformly distributed cylindrical mass	11
10	Two mass torsional system	14
11	Rayleigh Damping	21
12	3dB or Half Power Method	22
13	Asynchronous motor diagram	23
14	Power Transmission Shaft System (PTSS)	24
15	Testing hall overview of Customer 1	25
16	Components of interest of Customer 1	25
17	Testing hall overview of Without DUT	26
18	Components of interest of Without DUT	26
19	Testing hall overview of Customer 2	27
20	Components of interest of Customer 2	27
21	System torque and speed during Ramp (left) and Coast stop (right)	29
22	FFT during system ramp up and down	29
23	FFT during 'coast off'	30
24	Spectrogram plot during 'Ramp up and down' (left) and 'Coast Stop' (right)	30
25	Order during 'Ramp up and down' (left) and 'Coast Stop' (right) system	31
26	Flange torque and speed during 'Ramp up and down'	31
27	Flange torque and speed during 'Coast Stop'	32

28	FFT plot of system during 'Ramp up and down'	33
29	FFT plot of system during 'Coast Stop'	33
31	Order during 'Ramp up and down' (left) and 'Coast Stop' (right) system	33
30	Spectrogram plot of 'Ramp up and down' (left) and 'Coast Stop' (right) system	34
32	System torque and speed during Ramp (left) and Coast stop (right)	35
33	FFT plot of system during ramp-up and down	35
34	FFT plot of system during coast stop	36
35	Spectrogram plot of ramping (left) and coast stop (right) system	36
36	Oder during ramp (left) and coast stop (right) system	37
37	Torque and speed to different test	37
38	FFT plot using average and maximum data points	38
39	Constraints in multibody model	41
40	Angular twist vs axial length	43
41	Torsional stiffness vs time	44
42	Simple representation of 'Customer 1' setup	48
43	Simple representation of 'Without DUT' setup	50
44	Operational model	51
45	Air-gap torque and speed during system 'Ramp up'	52
46	Flange torque and speed during step air-gap torque	53
47	FFT during 'Ramp up'	53
48	FFT during step air-gap torque	54
49	Spectrogram plot during 'ramp up'	55
50	Air-gap torque and speed during system 'Ramp up'	55
51	Flange torque and speed during step air-gap torque	56
52	FFT during 'Ramp up'	56
53	FFT during step air-gap torque	56
54	Spectrogram plot during 'ramp up'	57
55	Air-gap torque and speed during system 'Ramp up'	58

56	Flange torque and speed during step air-gap torque	58
57	FFT during 'Ramp up'	58
58	FFT during step air-gap torque	59
59	Spectrogram plot during 'ramp up'	59
60	Frequency response of linearized model of 'Customer 1'	60
61	Frequency response of linearized model of 'Without DUT'	61
62	Frequency response of linearized model of 'Customer 2'	61
63	Common part of 'Customer 1' and 'Customer 2' model	65
64	Change in frequency against inertia, stiffness and damping of 'Without DUT'	66
65	Change in frequency against inertia, stiffness and damping of 'Customer 1'	67
66	Change in frequency against inertia, stiffness and damping of 'Customer 2'	68
67	Torsional Stiffness of part 1 vs. Young's modulus	70
68	Torsional Stiffness of part 2 vs. Young's modulus	70
69	Young's modulus v.s density of different material	71
70	Sliding coupling	72
71	Frequency shift of 'Customer 2'	72
72	Flexible shaft connected to rigid wall	73
73	First and second mode shapes	74
74	Torque measurement position	75
75	Torque at different modes	76
76	Torsional stiffness of different parts of 'Customer 2'	81
77	Simulink model for optimization of 'Customer 2'	82
78	Simulink model to check sensitive parameters of 'Customer 2'	83

List of Tables

1	Damping ratio using maximum data points	38
2	Damping ratio using average data points	39
3	Known and unknown parameters	43
4	Normalized parameter of 'Customer 1'	45
5	Normalized parameter of 'Customer 2'	45
6	Results from normal modes analysis	46
7	Torsional eigenfrequencies of 'Without DUT'	47
8	Torsional frequency using operational model	54
9	Torsional frequency using operational model	57
10	Torsional frequency using operational model	60
11	Results from experiment and different models	62
12	Errors between the results	63
13	'Without DUT' model optimization	66
14	'Customer 2' model optimization	69
15	Eigenfrequencies of optimized multibody model	71

1 INTRODUCTION

Wind turbines industry is expanding and the power generating capacity, size, need for quality electronic and structural components of Wind Turbines (WTs) are also increasing. With the increasing size, the reliability of the bigger turbines is decreasing [1] and the electric device capability to handle higher loads are increasing. In 2015, Fraunhofer IWES developed and commissioned DyNaLab (Dynamic Nacelle Laboratory), in Bremerhaven, Germany to examine the sources of failure and speed-up time-to-market of a new generation of WTs [2]. Electrical certification can be achieved at DyNaLab but require the complete nacelle setup. Therefore, the need of fast, and cost-effective test bench for electronic component testing is needed. Hardware-in-the-Loop Grid Compliance test bench (HiL-Grid-CoP), located at Bremerhaven was funded by the German ministry of economic affairs (BMWi) to achieve electrical certification on test bench through minimal system testing (i.e generator, converter, and transformer). Because of this reason, generator, converter, and transformer actively contributing to electrical properties are tested, validated, and certified.

Unlike real WTs, the test bench consists of Motor, shaft-coupling, and testing equipment as shown in figure 1. Low-speed shaft and the gearbox are replaced by electric motor and shaft-coupling system. To test the electrical devices, torsional characteristics of real WT need to be applied to the generator interface but the flexible shaft and its dynamics do not allow realistic load conditions to be easily applied. Because of the test bench system dynamics, applied torque is affected by the inherent dynamics of the test bench, leading test results to differ from in-field testing. Due to this reason, damping of natural modes of the test bench is required to create a smooth environment where reference dynamic can be superimposed [2]. HiL-Grid-CoP embeds a high-speed 9 MW motor with a controllable bandwidth as high as 75 Hz. Taking advantage of high controllable bandwidth framework, power train oscillations can be damped, thanks to an accurate control design, enabled by the motor's high dynamic characteristics. HiL framework shown in fig. 2 consists of a virtual wind turbine running par-



Figure 1: Test bench setup at HiL-Grid-CoP

allel to test bench that provides the real test data and the torque-setpoints are provided to motor with the help of control environment. Feedback from motor and generator to the control environment guarantees realistic load conditions to the generator. According to [3], it is challenging to emulate realistic drive train modes in test benches with Hil set-up because of low stiffness and has proposed a control method for this problem. Similarly, advantage of HiL framework is also elaborated in [4].

With every new generator, system dynamic changes and similarly the control and overall framework has to be adjusted. If the mathematical model of system dynamics is known, the control environment can be tuned accordingly. Control requirements for the development of a closed-loop controller at high frequency represent a challenge due to the general lack of information of system behavior. Therefore, there is a need for a multibody model that can replicate the torsional dynamics of the test bench with different generator. In this thesis, generator is the only component that is added in the model and is considered as Device Under Test (DUT). Similarly, linearization of the multibody model is needed for the control purpose and faster solution.

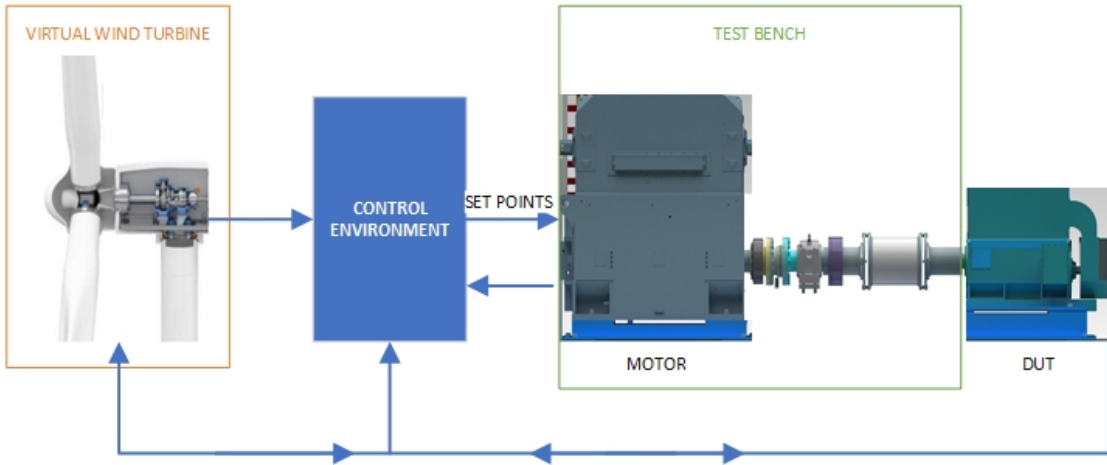


Figure 2: HiL control architecture

1.1 Aim and objectives

Knowledge of change in system dynamics is need due to different generators that are connected to the test bench. Therefore, thesis goal is to create a multibody model that duplicates the torsional behaviour with different DUT or generator and to validate and verify it. Similarly, linearization of the system is also the aim of this thesis. Following questions are set to guide towards the aim of the thesis.

1. What is signal processing and how can the results be interpreted from these signals?
2. How to build a multibody model and which software package to use?
3. What are the methods for damping calculation and its implementation in multibody model?
4. How to optimize and linearize multibody model?

1.2 Methodology

At first, multibody model is needed and MSC Adams software is used. All the parts information is received from Fraunhofer's online database, supplier, and CAD software. Siemens NX is used not only to get inertia, mass, and dimension

information but also for assembling CAD parts which are later employed in MSC Adams. Stiffness of the unknown parts are calculated from the multibody model taking advantage of flexible parts. Third-party software, ANSYS is also used for flexible body modeling. Similarly, test bench results are used to obtain the damping and torsional eigenfrequencies. Damping is then employed in multi-body model and all the above information are applied to calculate mathematical models which emulate the torsional dynamic.

Multibody model is imported to MATLAB and simulation scenarios are created to examine torsional behavior. Results from MATLAB simulation and normal mode analysis in MSC Adams are used to validate the model. Similarly, linearization of the multibody model is done in MSC Adams and the torsional behavior is analyzed in MATLAB. One of the mathematical models is later used for the optimization of the multibody model and the new parameters are verified.

1.3 Outline of the thesis

In this chapter, the topic of the thesis is introduced along with the aim, objectives, and methodology. Theoretical background, state-of-the-art, and test bench information are discussed in chapter two. Experiment and the results are analyzed in chapter three. Similarly, multibody, mathematical and operational models are described in chapters four, five, and six respectively. Linearization procedure is elaborated in chapter seven and the comparison with experiment results with different models has been delineated in chapter eight. Similarly, optimization procedure is described in detail in chapter nine. Case study is done to identify shift of eigenfrequencies in chapter ten. Finally, in the last chapter, conclusions and future work topics are brought up.

2 STATE OF THE ART

2.1 Digital signal processing

Digital Signal Processing (DSP) is a process of converting continuous input signal into discrete samples.

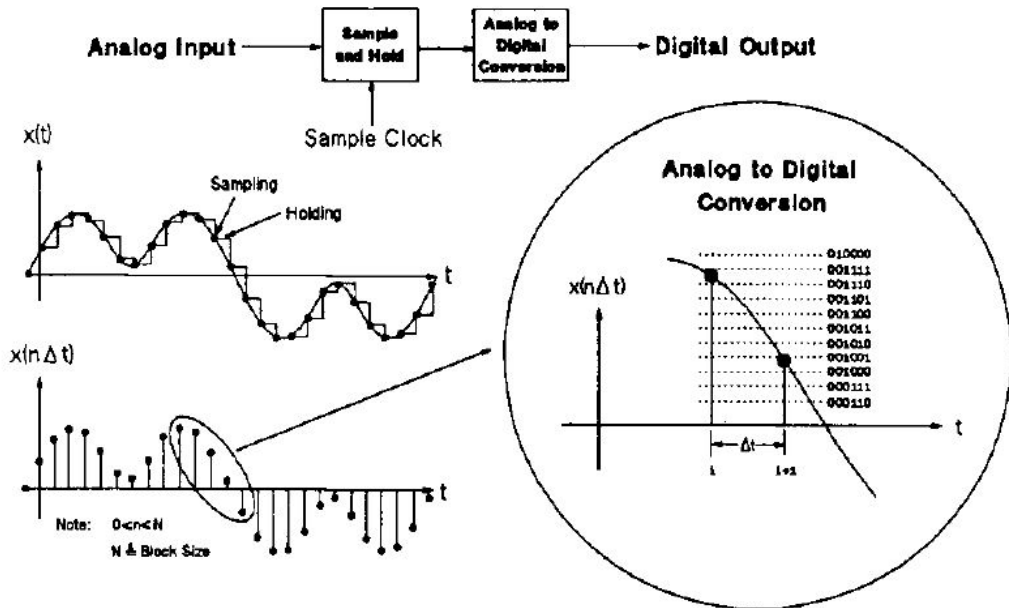


Figure 3: Digital Signal Processing (DSP) [5]

2.1.1 Sampling process in time domain

In the sampling process, two processes occur as shown in fig. 3. First is 'sample and hold' and later is Analog to Digital Conversion (ADC). In the first stage, input signals, originally analog signals are sampled in every fraction of time which is called a sampling interval (δt). Sampling frequency (f_s) can be represented by the inverse of the sampling interval shown in equation 2. If 'N' is the 'blocksize', the total observation time (T) can be represented by eq. 1.

$$T = N \delta t \quad (1)$$

$$f_s = \frac{1}{\delta t} \quad (2)$$

At the end of 'sample and hold' we have discrete analog signals. ADC converts these analog signals into digital signals. The term 'Dynamic range' describes the measurement range of a measurement device. The number of bits (k) for ADC is fixed. Another way of describing dynamic range is using deciBel (dB).

$$dB = 20 \log 2^k$$

2.1.2 Aliasing

During the sampling process, the analog signal must be recorded at a certain rate so that the exact input wave is recorded in digital form. The recording rate at which the signal is sampled is called 'sampling frequency' or 'sampling rate'. According to the Nyquist sampling theorem, we must have a sampling frequency of at least twice the highest frequency of interest in order not to lose the information of sampling data [6]. If the sampling frequency is less than the highest frequency of interest then the highest frequency is seen as the low frequency as shown in fig. 4.

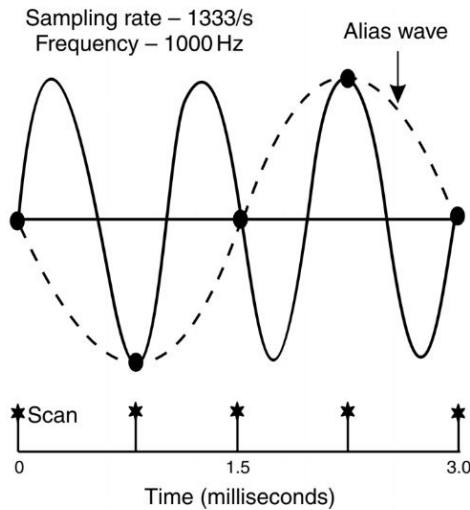


Figure 4: Aliasing during sampling [6]

In theory, there should not be the presence of any higher frequencies more than the half of sampling frequency but in reality, there is noise with higher frequen-

cies. Aliasing is one of the major problems that should be taken into consideration during data sampling. To avoid aliasing, anti-aliasing filters are used which is shown in fig. 5. Ideally, it is a low pass filter (LPF) that has a sharp cutoff frequency. They are placed before sampling and holding the analog data.

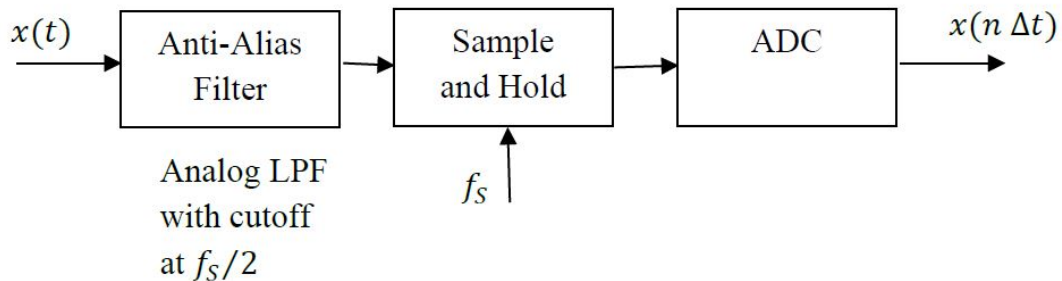


Figure 5: Anti-aliasing filter

Any real filters don't have a sharp cutoff frequency as shown in fig. 6. In most of the data acquisition software, the 'Span' and 'Bandwidth' options can be used. Span option provides the cutoff frequency at $f_s/2.56$ so that the frequency until f_s can pass. In the Bandwidth option the cutoff frequency at $f_s/2$ and higher frequencies can be seen.

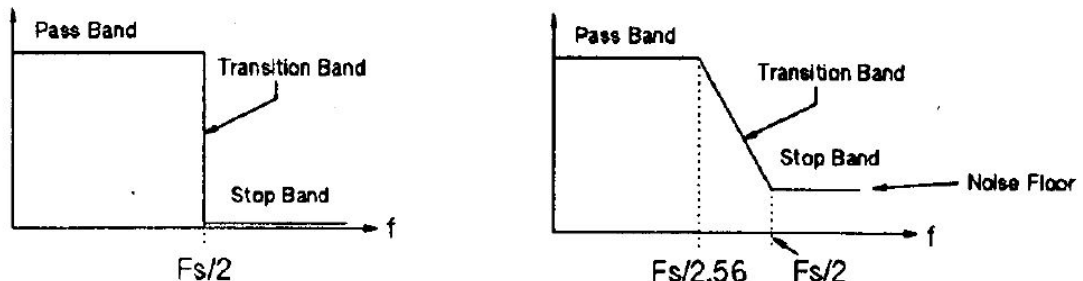


Figure 6: Ideal (left) and real (right) LPF [5]

2.1.3 Leakage and windowing

Leakage is related to the periodicity of sample data with fixed time intervals. When the sampling of the data is done at a certain fixed time interval, start and end get truncated . It caused discontinuities in the signal and frequencies around the main frequency are seen. This is known as leakage and is shown in

fig. 7. Leakage is a serious problem that cannot be avoided but can be reduced by using window.

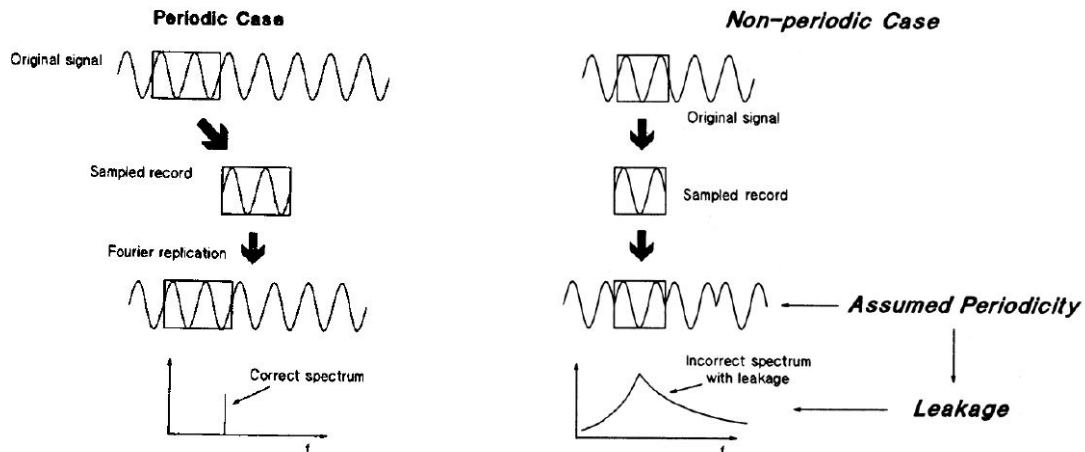


Figure 7: Leakage and truncation of data [5]

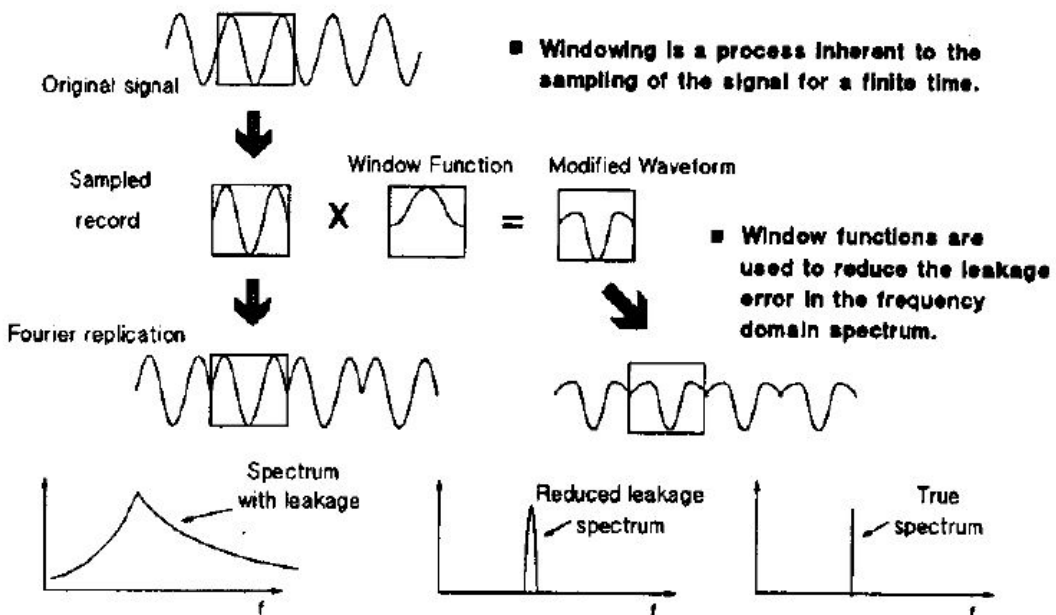


Figure 8: Windowing [5]

'Window' is a weighting function that begins and ends at zero which is shown in fig. 8. Multiplying it with the sample signal gives a periodic signal. There are different windows available and some of the windows of our interest are 'Hanning'

and 'Hamming'. Both have the same weighting function as in equation 3

$$W = A - B\cos\phi + C\cos(2\phi), \quad \phi = [0 \quad 2\pi] \quad (3)$$

Hanning window : $A = B = 0.5, C = 0$

Hamming window : $A = 0.54, B = 0.46, C = 0$

Hanning is the most common window used for random signals. It is not suitable for the measurement of small amplitude signals. Similarly, Hamming is suitable for the dynamic range of 50 dB. Hanning window is used during signal processing in this thesis.

2.1.4 Fast Fourier Transform

System vibration can be represented in time and frequency domain. In time domain the signal is represented by amplitude that varies with time. Simple sinusoidal wave with constant angular velocity is easy to examine in time domain but when it comes to complex signals with noise it is impossible to visualize the results. Therefore, all the data are represented in the frequency domain where the signal is represented as series of sine and cosine waves. MATLAB is used for FFT in this thesis.

2.1.5 Spectrogram

Spectrogram, also known waterfall plot, is the visual representation of oscillation amplitude at each operational speed. It is more powerful tool to visualize how the eigen frequencies, damping ratio in the system and its variation with time. Speed varying frequencies can be seen such as order of the system. Order are the frequencies of the system that is corresponding to the rotation speed of shaft and its harmonics. Order of the system can be easily visualized and differentiated using spectrogram. MATLAB is used to create spectrogram plots.

2.2 Finite element method (FEM)

FEM is a numerical method of solving mathematical and numerical problems. In this method, a complex body is divided into small parts called elements and the process is called discretization. There are various types of elements like 1D, 2D, and 3D elements which are used according to requirement. 1D is a one-dimensional element and is the simplest representation of a system. Similarly, 2D is mostly used for surfaces, and 3D is popularly used for solid or thick parts. For the mathematical modeling, 1D elements are used while 3D elements are used in software during multibody modeling. Detail information about FEM can be found in [7] and [8]. Collection of such nodes and elements of the entire part is called mesh. There are various software packages like ANSYS, Siemens NX, etc to provide solutions related to FEM models. In any FEM software packages types of element, order of element [8] and mesh size can be user-defined. The mass and inertia distribution of the elements in the nodes depends on whether the element has uniformly distributed mass or lumped mass. Mass and inertia of the lumped mass is concentrated at a point which can also be called a point mass. Every individual element's mass, inertia, stiffness, damping, and force can be represented in a matrix form. These element's matrices can be combined to get the structural matrix. If the element has uniformly distributed mass, the mass matrix obtained is called consistent mass matrix. Likewise, the inertia matrix obtained is called consistent inertia matrix. Similarly, the inertia matrix got from a lumped mass is called lumped inertia matrix. Using the boundary conditions forces, stress and strains can be calculated accordingly. FEM software packages do all the above work using a suitable solver and give the preprocessed results.

2.2.1 Consistent inertia model

In fig. 9, uniformly distributed isotropic cylindrical body is shown with density ' ρ ', modulus of rigidity ' G ' and length ' l '. Torque ' T_1 ' and ' T_2 ' are applied at the two ends. The angular displacement ' θ ' is assumed to be linear in ' x ' at any time

't' [9].

$$\theta(x, t) = a(t) + b(t)x \quad (4)$$

$$\theta(0, t) = \theta_1(t), \quad \theta(l, t) = \theta_2(t) \quad (5)$$

'a(t)' and 'b(t)' are constant and using the conditions 5, twist at distance 'x' can be represented as in eq. 6.

$$\theta(x, t) = N_1(x)\theta_1(t) + N_2(x)\theta_2(t) \quad (6)$$

Here, $N_1(x)$ and $N_2(x)$ are the shape functions [9].

$$N_1(x) = (1 - \frac{x}{l}), \quad N_2(x) = \frac{x}{l} \quad (7)$$

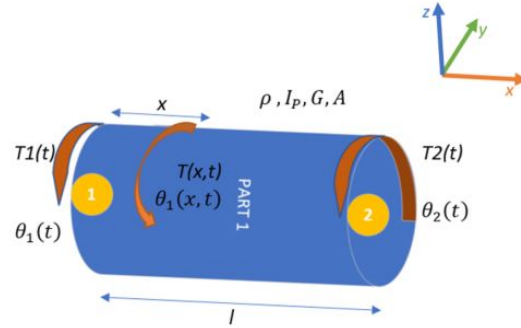


Figure 9: Uniformly distributed cylindrical mass

Kinetic energy, strain energy and virtual work [9] for pure torsion is given by eq. 8, 9 and 10.

$$T(t) = \frac{1}{2} \int_0^l \rho I_p \left\{ \frac{\partial \theta(x, t)}{\partial t} \right\}^2 dx \quad (8)$$

$$V(t) = \frac{1}{2} \int_0^l G I_p \left\{ \frac{\partial \theta(x, t)}{\partial t} \right\}^2 dx \quad (9)$$

$$\delta W(t) = \int_0^l T(x, t) \delta \theta(x, t) dx \quad (10)$$

Using eqs. 8, 9 and 10 inertia matrix 'J' and stiffness matrix 'K' formulation can be calculated as shown in eq. 11 and 12 respectively.

$$J = \frac{\rho I_p l}{6} \begin{bmatrix} 2 & 1 \\ 1 & 2 \end{bmatrix} = \begin{bmatrix} j_1/3 & j_1/6 \\ j_1/6 & j_1/3 \end{bmatrix} \quad (11)$$

$$K = \frac{G I_p}{l} \begin{bmatrix} 1 & -1 \\ -1 & 1 \end{bmatrix} \quad (12)$$

Where ' j_1 ' is the axial moment of inertia of the cylinder part and I_p is the polar moment of inertia about the centroidal axis.

In this model, there is a single body which is considered as 1D element with two nodes. Inertia distribution of the element between nodes is not equal and there is inertial interaction between the successive node. Above method can be used to generate structural inertia and stiffness matrix of the body which is the combination of such elements. For a 'n' number of elements, there are 'n+1' nodes. According to consistent inertia model, structural inertia, stiffness matrix can be defined by matrix 13 and 14 respectively.

$$[J]_{(n+1) \times (n+1)} = \begin{bmatrix} j_1/3 & j_1/6 & 0 & \dots & \dots \\ j_1/6 & j_1/3 + j_2/3 & j_2/6 & \dots & \dots \\ 0 & j_2/6 & j_2/3 + j_3/3 & \dots & \dots \\ \vdots & \vdots & \ddots & \ddots & \ddots \\ \vdots & \vdots & \ddots & \ddots & j_n/3 \end{bmatrix} \quad (13)$$

$$[K]_{(n+1) \times (n+1)} = \begin{bmatrix} k_1 & -k_1 & 0 & \dots & \dots \\ -k_1 & k_1 + k_2 & -k_2 & \dots & \dots \\ 0 & -k_2 & k_2 + k_3 & \dots & \dots \\ \vdots & \vdots & \ddots & \ddots & \ddots \\ \vdots & \vdots & \ddots & \ddots & k_n \end{bmatrix} \quad (14)$$

2.2.2 Lumped inertia model

In the lumped mass model the inertia of the rigid element is divided equally across each node. It is a diagonal matrix. Also, there is no inertial interaction

between the nodes. Structural inertia and stiffness matrix of a lumped mass model can be written as eq. 15 and 16 respectively.

$$[J]_{(n+1) \times (n+1)} = \begin{bmatrix} j_1/2 & 0 & 0 & \cdot & \cdot \\ 0 & j_1/2 + j_2/2 & 0 & \cdot & \cdot \\ 0 & 0 & j_2/2 + j_3/2 & \cdot & \cdot \\ \cdot & \cdot & \cdot & \cdot & \cdot \\ \cdot & \cdot & \cdot & \cdot & j_n/2 \end{bmatrix} \quad (15)$$

$$[K]_{(n+1) \times (n+1)} = \begin{bmatrix} k_1 & -k_1 & 0 & \cdot & \cdot \\ -k_1 & k_1 + k_2 & -k_2 & \cdot & \cdot \\ 0 & -k_2 & k_2 + k_3 & \cdot & \cdot \\ \cdot & \cdot & \cdot & \cdot & \cdot \\ \cdot & \cdot & \cdot & \cdot & k_n \end{bmatrix} \quad (16)$$

2.3 Vibration system modeling and analysis methods

A vibrating system has a potential and kinetic storing device along with energy dissipating device. For a torsional system as in figure 10, torsional stiffness is the potential energy storing device, inertia is kinetic energy storing device and damper is the energy dissipating part as described in [9]. The vibrating system can be linear or non-linear. The linear vibrating system has constant stiffness, inertia, and damping which is not always true in the real system while the non-linear vibrating system has variable stiffness, inertia, and damping [9]. A vibrating system can be defined as lumped and consistent models. Lumped and consistent model which is also called the discrete model is the simplest system representation, while a continuous model [9] can give an better results. Lumped and consistent models have a finite degree of freedom (DOF) while the continuous system has infinite numbers of DOF. The minimum number of independent coordinates required to determine completely the positions of all parts of a system at any instant of time defines the number of degrees of freedom of the system. The continuous system can be represented by the lumped model or consistent model and the accuracy of the results can be increased by increasing

DOF. Such a system is called the multi-degree of freedom system.

Analysis of vibrating system involves mathematical modeling in the first step. Important features are considered which can be further used for deriving system equations. The mathematical model is made as simple as possible and linear for easy understanding. A torsional shaft with a different diameter shaft can be represented by lumped inertia model as shown in figure 10.

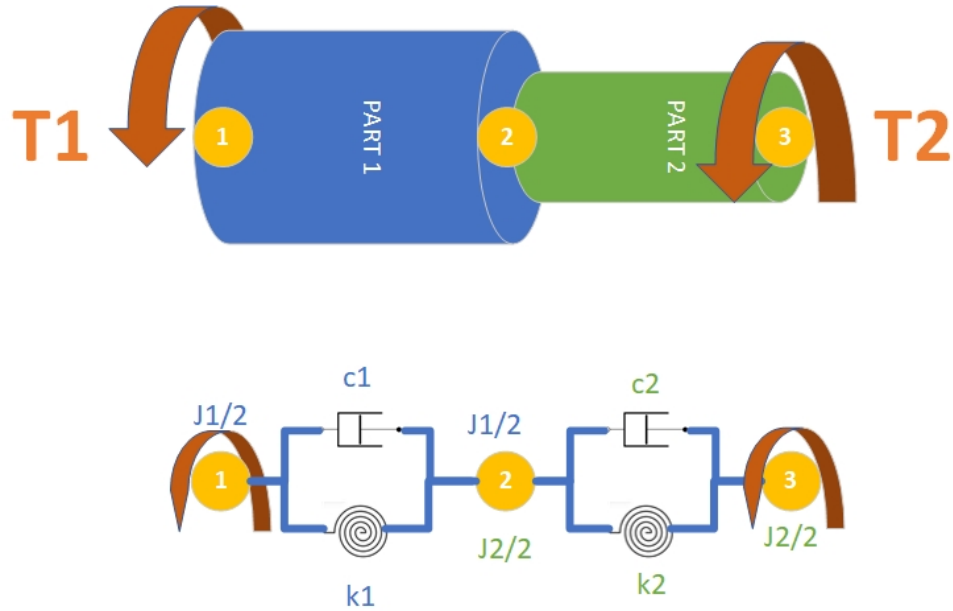


Figure 10: Two mass torsional system

The second step is to derive the governing equations. There are various methods like D'Alembert's principle, principle of conservation of energy, and Newton's second law of motion to define the governing equation of the system but Newton's second law of motion is used in this thesis. Inertial, damping and elastic torque of the shaft system are balanced by the external torque as shown by the equation 17.

$$J\ddot{\theta} + C\dot{\theta} + K\theta = T \quad (17)$$

$$J = \begin{bmatrix} j_{1/2} & 0 & 0 \\ 0 & j_{1/2} + j_{2/2} & 0 \\ 0 & 0 & j_{2/2} + j_{3/2} \end{bmatrix}, \quad K = \begin{bmatrix} k_1 & -k_1 & 0 \\ -k_1 & k_1 + k_2 & -k_2 \\ 0 & -k_2 & k_2 \end{bmatrix}$$

$$C = \begin{bmatrix} c_1 & -c_1 & 0 \\ -c_1 & c_1 + c_2 & -c_2 \\ 0 & -c_2 & c_2 \end{bmatrix}$$

J , K , C , and T are lumped-inertia, stiffness, damping and external torque matrix respectively. In the third step, using the boundary conditions the equations need to be solved and matrix method is used to solve equation 17. For a complex system, numerical methods can be used to solve the equations with the help of a computer. Finally, the results like displacement, velocity, torque, etc obtained from solving equations can be interpreted.

2.3.1 Modal analysis

Eigenvectors, also called mode shapes are calculated by solving the eigenvalue problem from the stiffness and mass matrix. Eigenvectors calculated from mathematical method in this thesis are linearly independent and orthogonal which can be used to create a new coordinate system to define the vibration of a system. This transformation from spatial coordinates to modal coordinates is called modal transformation and analysis of the vibration system in modal coordinates is called the modal analysis.

The modal coordinate is denoted by subscript ' η '. If 'V' is the eigenvector, correlation between spacial and modal coordinates can be defined as follows.

$$\theta = V\theta_\eta, \quad \dot{\theta} = V\dot{\theta}_\eta, \quad \ddot{\theta} = V\ddot{\theta}_\eta \quad (18)$$

Transforming spatial coordinate to the modal coordinate system [9], modal inertia, stiffness, and damping matrix are represented by eq. 19. Similarly, the system equation in modal coordinate is shown in eq. 20.

$$J_\eta = V^T JV, \quad C_\eta = V^T CV, \quad K_\eta = V^T KV, \quad T_\eta = V^T T \quad (19)$$

$$J_\eta \ddot{\theta}_\eta + C_\eta \dot{\theta}_\eta + K_\eta \theta_\eta = T_\eta \quad (20)$$

Modal stiffness and inertia matrix are diagonal matrices. Modal damping matrix may or may not be a diagonal matrix which means different modes are linked with each other. Therefore, a suitable damping matrix needs to be used. Every modes are independently analyzed if stiffness, inertia damping are diagonal matrix in modal coordinates. Inertia and stiffness normalization is most commonly used for easy and faster calculation. ' ω ', ' ξ ' and ' j ' are angular velocity, damping ratio and axial moment of inertia respectively.

Inertia normalization,

$$J_\eta = I, \quad K_\eta = \begin{bmatrix} \omega_1^2 & 0 & \cdot & \cdot \\ 0 & \omega_2^2 & \cdot & \cdot \\ \cdot & \cdot & \cdot & \cdot \\ \cdot & \cdot & \cdot & \omega_n^2 \end{bmatrix}, \quad C_\eta = \begin{bmatrix} 2\xi_1\omega_1 & 0 & \cdot & \cdot \\ 0 & 2\xi_2\omega_2 & \cdot & \cdot \\ \cdot & \cdot & \cdot & \cdot \\ \cdot & \cdot & \cdot & 2\xi_n\omega_n \end{bmatrix} \quad (21)$$

Stiffness normalization,

$$K_\eta = I, \quad J_\eta = \begin{bmatrix} \frac{1}{\omega_1^2} & 0 & \cdot & \cdot \\ 0 & \frac{1}{\omega_2^2} & \cdot & \cdot \\ \cdot & \cdot & \cdot & \cdot \\ \cdot & \cdot & \cdot & \frac{1}{\omega_n^2} \end{bmatrix}, \quad C_\eta = \begin{bmatrix} 2\xi_1\omega_1 j_1 & 0 & \cdot & \cdot \\ 0 & 2\xi_2\omega_2 j_2 & \cdot & \cdot \\ \cdot & \cdot & \cdot & \cdot \\ \cdot & \cdot & \cdot & 2\xi_n\omega_n j_n \end{bmatrix} \quad (22)$$

2.4 Multibody modeling

Dynamics of interconnected rigid and flexible parts can be better understood using multibody dynamics. The interconnection between the parts are defined by kinematics of the joints [10]. MSC Adams is chosen among various computational mutibody dynamics simulation software. Automatic Dynamic Analysis of Mechanical System (Adams) was developed by Mechanical Dynamics Incorporation (MDI) and later acquired by McNeill Schindler Corp (MSC). MSC Adams formulates and solves motion equations for kinematic, static, quasi-static and dynamic simulations. A multibody system must have inertial forces, the constraining forces and external forces in equilibrium [11] which is the foundation

of formulating equations of motion. These equations are calculated in terms of kinematic and potential energy of the mechanical system and Euler-Lagrange equation is used for equation formulation of motion in Adams/Solver, the computational engine of the software [10].

Lagrangian 'L' of multibody dynamics is presented in equation 23.

$$L = \sum_{i=1}^N T_j - V_j \quad (23)$$

T_j and V_j are kinematic and potential energy of each N parts of the multibody system. The equation of the motion formulated by the Adams/Solver is given by eq. 24.

$$\frac{d}{dt} \frac{\partial L}{\partial \dot{q}} - \frac{\partial L}{\partial q} + \Phi_q^T \lambda = Q \quad (24)$$

Here, q is the column matrix of generalized coordinates, Φ_q is Jacobian matrix of $n \times m$ array and λ is the column matrix of $m < n$ Lagrange multipliers [11]. 'Q' represents external, non potential forces in the model. Newton method is used to solve these equations which makes the whole simulation robust and faster [12].

2.4.1 Linearization

According to [11], implicit equations of nonlinear Adams models are written as 25.

$$G(\dot{z}, z, t) = 0 \quad (25)$$

'z' is the state vector of the model while 'G' is the system of first order differential and algebraic equations. Lagrange multipliers due to joints, variables, differential states of the system are involved in states of the model. Similarly, displacement and velocity states of flexible parts, rigid parts and point mass are also included in model states. Equation 25 can be linearized about a operating point which can either be defined by initial-condition analysis or by static, dynamic analysis [13]. During linearization, new dependent variable for each higher order derivative is applied to reduce the system to first order [11]. Linearization process of Hilber-Hughes-Taylor (HHT) solver which is C++ Adams

solver is also explained in [11]. It has the ability to linearize the system in any arbitrary user-defined coordinates and has been implemented in 2005 version of MSC.ADAMS/Solver(C++). Finally, state space representation shown by eqs. 26 and 27 is obtained by the elimination of algebraic equation from linearized representation of ordinary differential equations along with algebraic output [14].

$$\dot{x} = Ax + Bu \quad (26)$$

$$y = Cx + Du \quad (27)$$

'x', 'y', and 'u' are the vector states, outputs and inputs of the linear model respectively. Similarly, A, B, C, and D are the state-space matrices of the linear system and Adams has tools to export these matrix and operating points or linearization coordinates. Obtained linear model contains one of the states of nonlinear model of equation 25. Inputs and outputs are zero required during the modal analysis therefore, the equation 26 and equation 27 reduces to equation 28.

$$\dot{x} = Ax \quad (28)$$

If the lagrange multipliers, variables, differential states are not present in the model then,

$$x = \begin{Bmatrix} q \\ v \end{Bmatrix} \quad \text{and} \quad A = \begin{bmatrix} 0 & I \\ -M^{-1}K & -M^{-1}b \end{bmatrix} \quad (29)$$

Using above equations 28 and 29, we get familiar equation 30.

$$M\ddot{q} + b\dot{q} + Kq = 0 \quad (30)$$

'q' is the states, 'v' is the time derivative of 'q' and 'I' is the identity matrix. 'M', 'K', and 'b' represent the inertia, stiffness and damping of the system which might not be symmetric. Complex eigen value problem is solved using equation 28 instead of performing modal analysis using equation and the results are show in normal-modes-analysis section of Adams 30.

$$x = \phi e^{\lambda t} \quad (31)$$

' λ ' and ' ϕ ' are the complex eigenvalues and mode shapes respectively. Modes shapes might not be orthogonal in the case of non-symmetric behaviour of matrix 'A'. Putting equation 31 in equation 28 we obtain following equation 32.

$$A\phi^i = \lambda^i \phi^i \quad (32)$$

'i' represents the eigenvector and eigenvalue number. It is solved using QR method [15].

$$\lambda^i = \omega^i(-\xi^i + i\sqrt{1 - (\xi^i)^2}) = \lambda_r^i + i\lambda_i^i \quad (33)$$

$$\omega^i = \sqrt{(\lambda_r^i)^2 + (\lambda_i^i)^2} \quad (34)$$

$$\xi^i = \frac{-\lambda_r^i}{\omega^i} \quad (35)$$

HHT integrator damping at higher frequencies can be adjusted by ' α ' value [16] [14]. The effect of time step in the damping of implicit HHT integrator is explained by [17].

2.4.2 Flexible multibody system

Incorporating flexible body helps to predict loads and deformation with greater accuracy. Similarly, possible modes of flexible parts can be better understood with graphic interface. MSC Adams has capability to incorporate flexible body through different methods but we focus on ViewFlex and Adams Flex [14]. ViewFlex converts the rigid part to flexible file in Modal Neutral File (MNF) based flexible body within Adams using finite element analysis. Adams software don't have to rely on third parts Finite Element Software. All the information of flexible body can be through a binary file called MNF. It contains information not only about the nodes and nodes connection but also nodal mass, inertia and mode shapes. Similarly, mass, stiffness and damping ratio of each mode shapes can be received from the MNF file and damping can be adjusted in user friendly

interface. Rayleigh damping is used to calculate damping matrix. Adams Flex require third party FEA software for flexible parts that can create MNF file for later use in Adams.

2.5 Material properties

Among various materials used, isotropic metal is of our interest. Isotropic material have same properties in all the direction of the material. Mechanical, thermal, chemical and other characteristics define the metal properties and mechanical properties is of major concern in this thesis. Mechanical properties include stiffness, damping, poisson's ratio (ν), young's modulus (E), modulus of rigidity (G) etc. For a isotropic material 'G' can be defined as equation 36.

$$G = \frac{E}{2(1 + \nu)} \quad (36)$$

Similarly for a uniform cylinder of length ' L ' and polar moment of inertia ' I_p ', torsional stiffness ' $\frac{T}{\theta}$ ' can be represented by equation 37.

$$\frac{T}{\theta} = \frac{GI_p}{L} \quad (37)$$

Rayleigh damping: In this method, damping is proportional stiffness and inertia of the system and can be implemented in a vibrating system. If ' α ' is inertia proportional damping coefficient and ' β ' be stiffness proportional damping coefficient, then damping matrix 'C' can be written in spatial coordinates as equation 38.

$$C = \alpha J + \beta K \quad (38)$$

Values of ' α ' and ' β ' can be known from the modal damping ratios. Using the modal transformation equation 19, above damping equation 38 can be replaced by equation 39.

$$C_\eta = \alpha J_\eta + \beta K_\eta \quad (39)$$

Value of ' α ' is sometimes neglected in structural problems and chosen eigenfrequency can be damped by defining ' β ' [18]. To use both ' α ' and ' β ' for a given

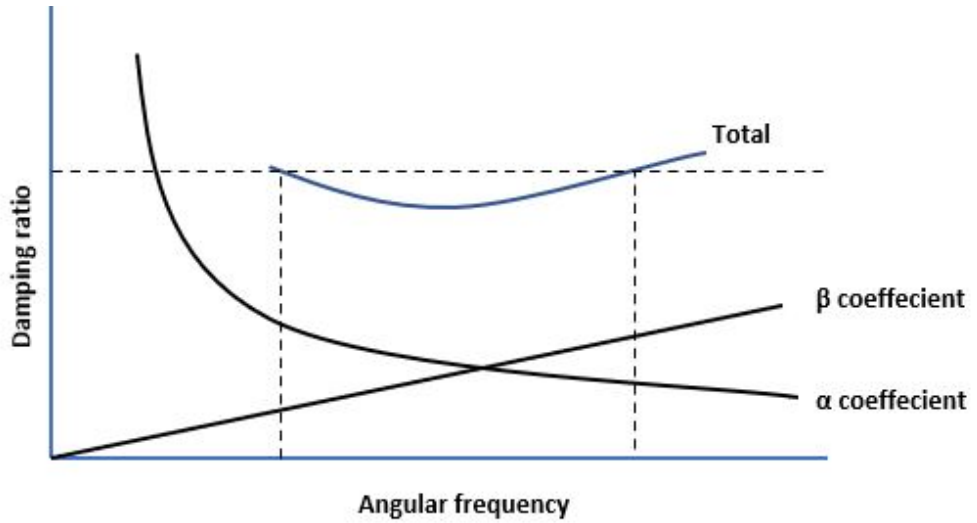


Figure 11: Rayleigh Damping

damping ratio, the sum of both constants over a range of frequency is considered constant as shown in fig. 11. If higher inertia is added to the system, ' α ' leads to undesirable results because the product of ' α ' and large inertia leads to higher damping force. Similarly, ' β ' damping can result in abnormal results in nonlinear analysis where stiffness is constantly changing. Both ' α ' and ' β ' are used in this thesis.

Half power method: In this method, oscillations of the system is represented in frequency in horizontal axis and amplitude in vertical axis. Damping ratio of each eigenfrequency can be obtained by half power method. In this method, a horizontal line is drawn 3 dB below the peak amplitude of the mode we want to investigate and is also known as 3dB method. Angular frequencies, ω_1 , ω_2 , ω_n are recorded as shown in the fig. 12.

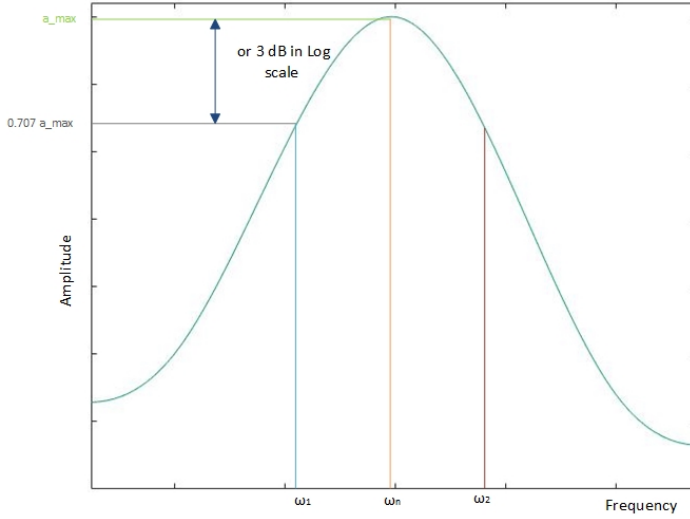


Figure 12: 3dB or Half Power Method

The recorded angular frequencies are then used in equation 40 to get the damping ratio ' ξ '.

$$\xi = \frac{\omega_2 - \omega_1}{2\omega_n} \quad (40)$$

2.6 MATLAB optimization tool

'Response Optimizer' is used which optimizes model parameters by formulating design requirements in the form of constrained minimization problem [19]. Despite performing its function, it has user friendly interface to adjust the tolerance of input and output parameter. One of the other reasons is the easy export required data into the excel file for compiling and documentation.

'Design Variables Set (DVS)', the parameters which needs to be optimized can be selected along with it's Upper Bound Magnitudes (UBM) and Lower Bound Magnitudes (LBM) which are its maximum and minimum value respectively. These bound magnitudes defines the boundary for the parameters which it cannot cross. Similarly, the boundary values of the output signals can also be set. At the end, optimized parameters are recorded in MATLAB workspace.

2.7 Test bench overview

The components of the test bench are on 600 tons of reinforced concrete structure with first eigen mode of 11 Hz and high damping. Motor, shaft, testing equipments are on the heavy concrete structure. They are considered rigidly attached to the base.

Electric motor used in the HiL-Grid-CoP is three-phase asynchronous motor with squirrel-cage rotor. It has a nominal power of 9 MW up to 30 minutes 150 % overload capacity. Nominal point is 1000 rpm and 86 KNm and torque derating need to be considered over 2200 rpm [20]. It has a shaft, rotor, and stator as shown in the fig. 13. The gap between rotor and stator is called AirGap. Torque generated by magnetic field to the rotor is the AirGap torque. Asynchronous motor works on the three-phase AC. Because of rotary magnetic field of the stator, current is induced in the rotor. The movement of the rotor cannot be synchronized with the moving stator field. The rotating magnetic field in stator created current in the rotor winding. Due to this current generated in rotor winding, force is created to rotate in the direction of stator.

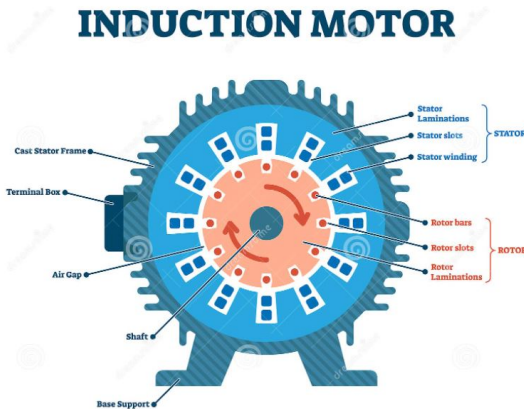


Figure 13: Asynchronous motor diagram [21]

Power Transmission Shaft System (PTSS) shown in fig. 14 is the connecting part between motor and generator which transmits the power of motor to the generator and is supported by a journal bearing in the middle. We investigate

the torque and angular velocity in between the PTSS with the help of torque measurement flange. It is a rotary strain gauge that measures torque and speed during rotation. Similarly, there are encoders at motor and generator which measure the rotational speed. Fiber coupling has the lowest stiffness and is

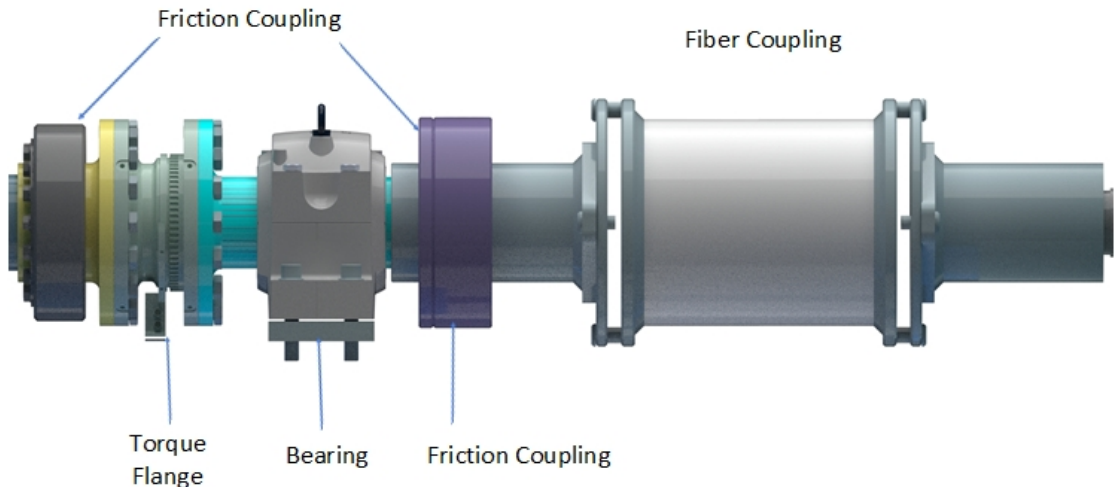


Figure 14: Power Transmission Shaft System (PTSS)

contributing to the low torsional eigenfrequency. These composite couplings are flexible and have sharp torsional failure point to protect the generator. Similarly, generator is connected at the end of the PTSS with its rotor, shaft is supported on bearing at each side.

There are three different setups of test bench which are studied in this thesis. First is 'Customer 1' whose generator denoted by DUT1 and second setup is 'Without DUT' which has no generator. Similarly, 'Customer 2' is the setup with generator named as DUT2.

2.7.1 Customer 1

It is the first setup that is tested and the components of the test bench are shown in fig. 15. We have a control room on the left side where the operator can safely work during the tests.

On the right side, we have converter and transformer. Motor and generator have fluid cooling system which is denoted by red (hot) and blue (cold) pipes. In fig-

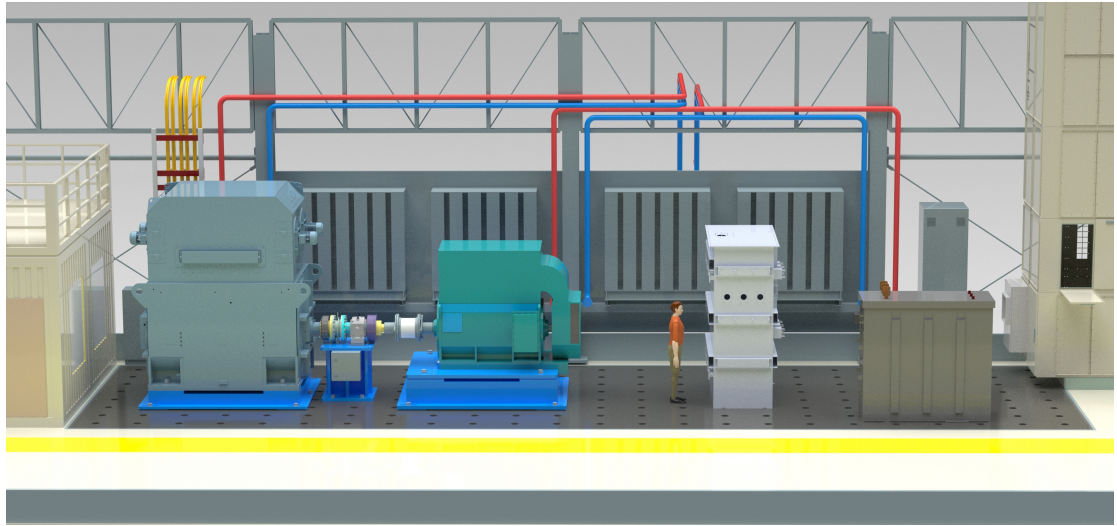


Figure 15: Testing hall overview of Customer 1

ure 16, we have major components of interest i.e motor, PTSS, and DUT1. Fiber coupling has comparatively shorter axial length and shorter distance between the motor and generator. Anti-friction roller bearing is used inside two ends of the generator.

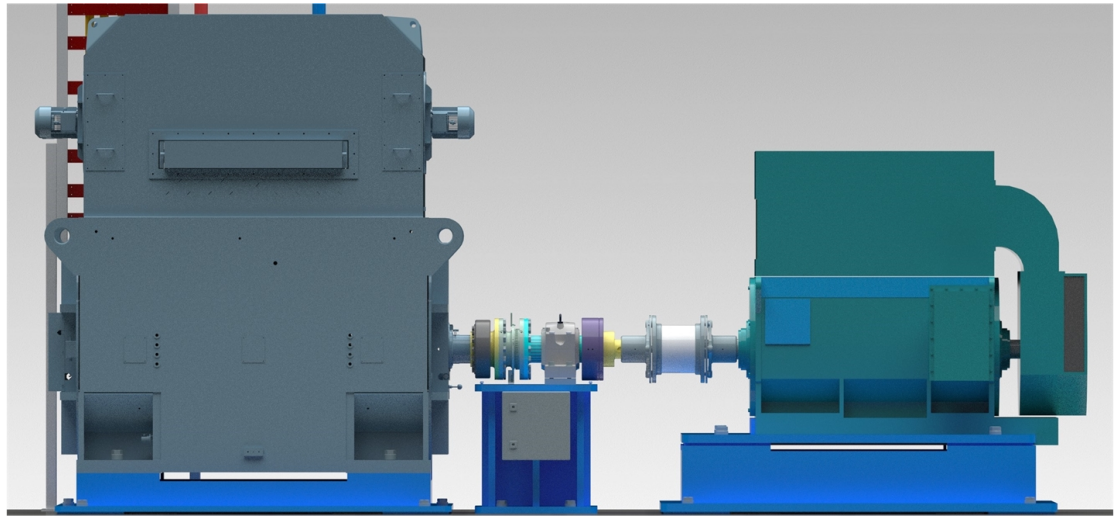


Figure 16: Components of interest of Customer 1

2.7.2 Without DUT

It has a similar orientation as the 'Customer 1' but the DUT and some torque transmitting shaft parts are missing. Shaft part is without the fiber coupling.

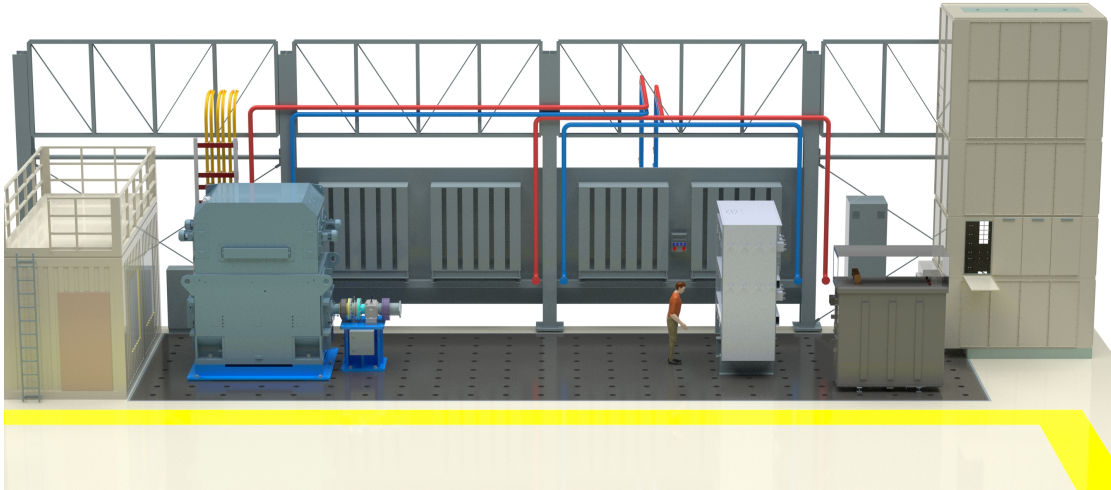


Figure 17: Testing hall overview of Without DUT

It can be clearly seen in fig. 17 and 18. Therefore, this setup consists of high inertia motor and stiffer shaft components.

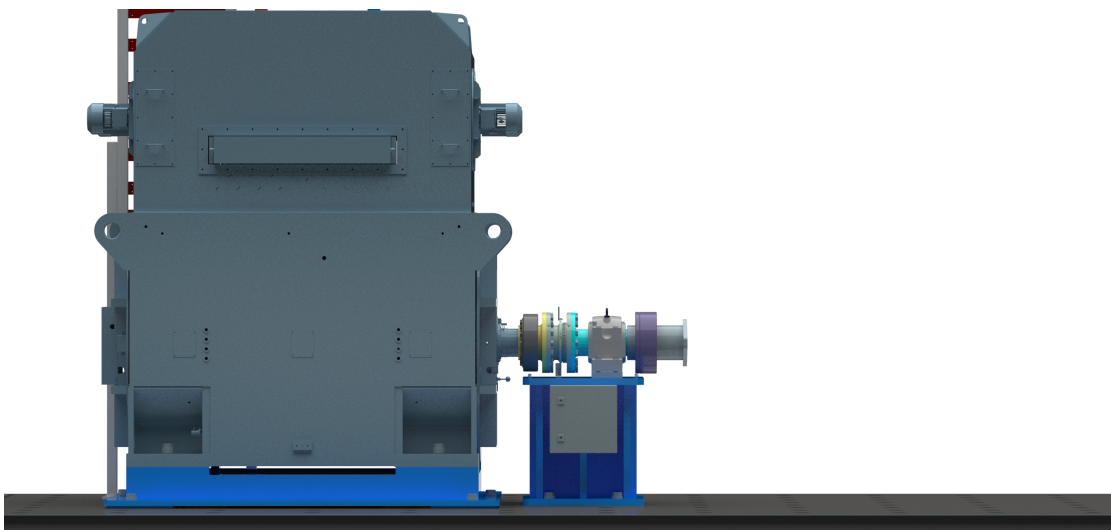


Figure 18: Components of interest of Without DUT

2.7.3 Customer 2

DUT2 was installed and all other component arrangement is same as 'Customer 1'. The axial length of flexible coupling and the distance between motor and DUT is highest compared to other setups which can also be seen in fig. 19 and

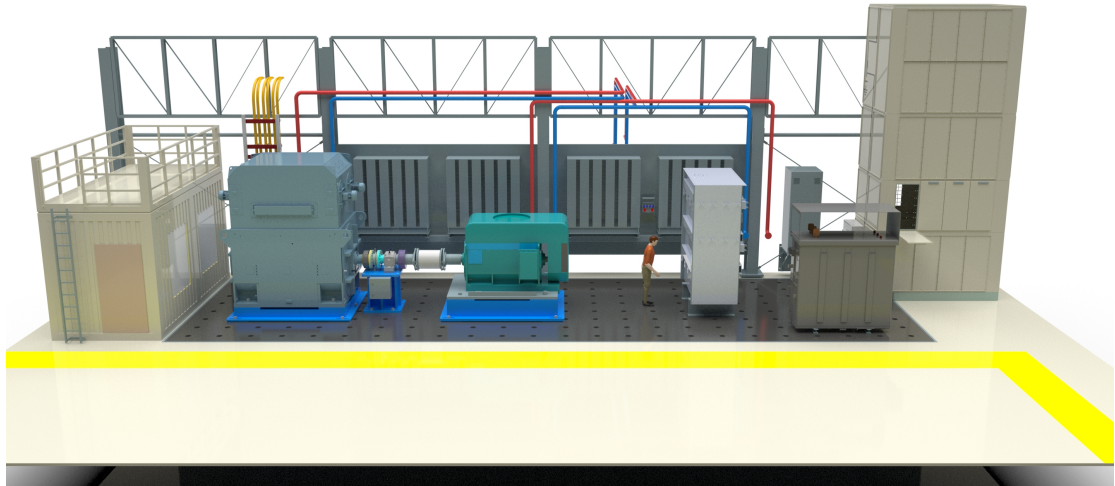


Figure 19: Testing hall overview of Customer 2

20. It has a unique sliding couplings shown in red circle in fig. 20 between fiber coupling and part of PTSS which slides when system is overloaded.

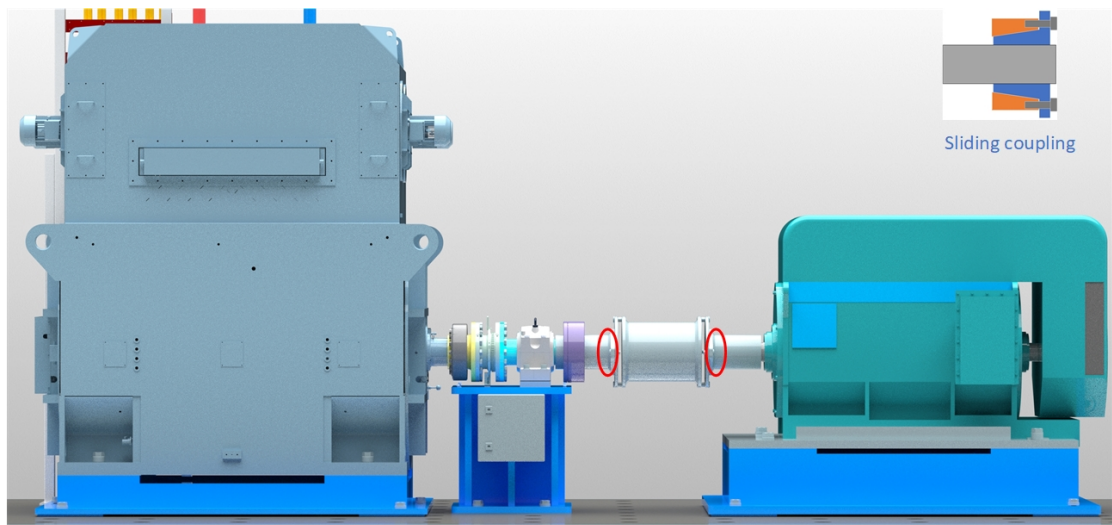


Figure 20: Components of interest of Customer 2

3 EXPERIMENTS

Main objective of this test is to identify the torsional frequencies due to the mechanical setup without electrical interference. 'Ramp up and down' and 'Coast stop' are the two major scenarios most frequently done during the testing. 'Ramp

'up' is a linear relationship between two variables with positive slope while 'Ramp down' has negative slope. Two variables in our system for Ramp up and Ramp down are shaft angular speed (RPM) and time (s). The system is ramped at 1 RPM/s if the system speed reaches from 0 RPM to 100 RPM in 100 s. A similar explanation is for 'Ramp Down' but only with negative sign i.e -1 RPM/s.

Similarly, 'Coast stop' is a condition when the motor power is switched off and the system reaches zero RPM in due course of time. There is no control over the motor and the system is unforced system without any input energy. When the 'Coast Stop' condition is active, the system rotates without external power, and the speed decreases to zero. Friction is the major cause of power loss of the system which results in decreasing speed but are not considered in the multibody model. During 'Coast stop' electrical appliances are not working therefore, the interference due to electrical devices is absent. All the results are normalized and frequencies are normalized with first eigenfrequency of the individual real test bench setup.

3.1 Experiment and results

3.1.1 Customer 1

The sensors at the flange record the shaft torque, speed and recorded signals are stored in the .csv format after signal processing. These data are loaded in MATLAB for FFT, spectrogram, and other plots for torsional vibration analysis. For this particular test setup, the system is ramped up and ramped down as shown in the fig. 21.

Similarly, another test with 'coast stop' is performed as shown in fig. 21. Pre-processing of the data from the test bench are done to get FFT and spectrogram plot. Following frequency lines are observed.

Five horizontal frequency lines are seen in the fig. 24 during ramp and frequencies are 1, 8.2, 9.6, 13.8 and 20.3 [p.u] which can be clearly seen in fig. 22. First two lower frequencies have higher energy and resonance is seen when speed-dependent frequencies or order cross them. Other three frequencies seem

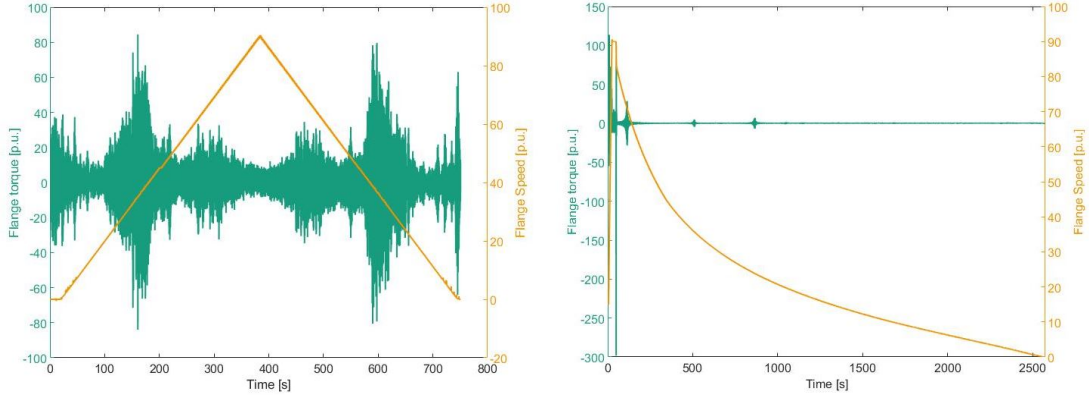


Figure 21: System torque and speed during Ramp (left) and Coast stop (right)

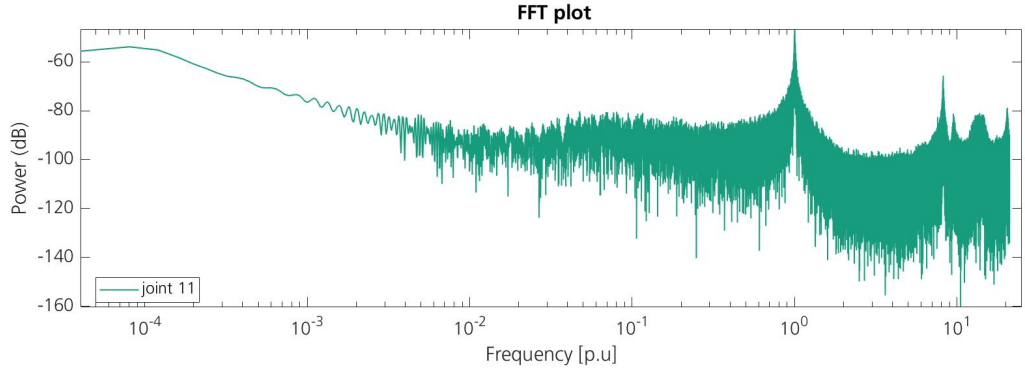


Figure 22: FFT during system ramp up and down

insensitive to the speed dependent frequency. Three horizontal lines are seen predominant in fig. 24 during 'coast stop' which could also be identified in fig. 23. Therefore, 13.8 [p.u.] frequency line is from electrical source. First, two lower frequencies are horizontal and the third frequency line starts at 9.6 [p.u] and drops to 9.3 [p.u] as the speed increases. According to [22], increase in the weight of bid causes to decrease in the bending frequency. Similarly, increasing eccentric shaft speed causes more axial force hence decreasing the bending frequency. Therefore, 9.6 [p.u] frequency line is the bending frequency. It is also observed from the multibody model that the first and second torsional modes are near to 1 and 8.2 [p.u.] frequency lines and they are confirmed to be torsional frequencies.

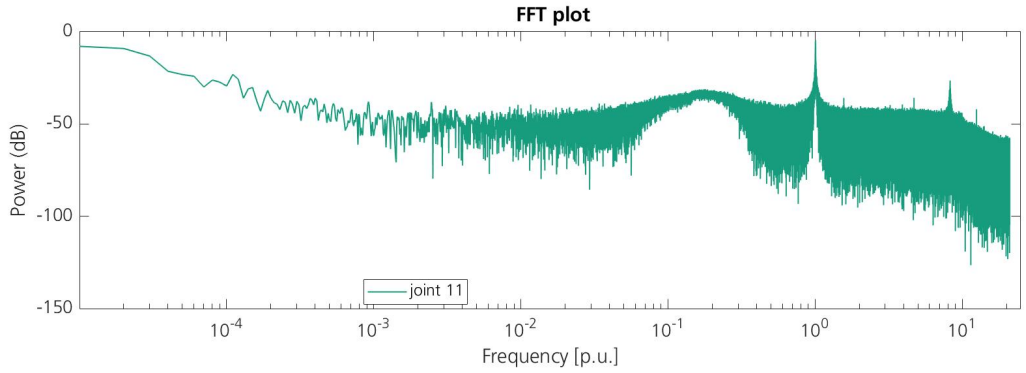


Figure 23: FFT during 'coast off'

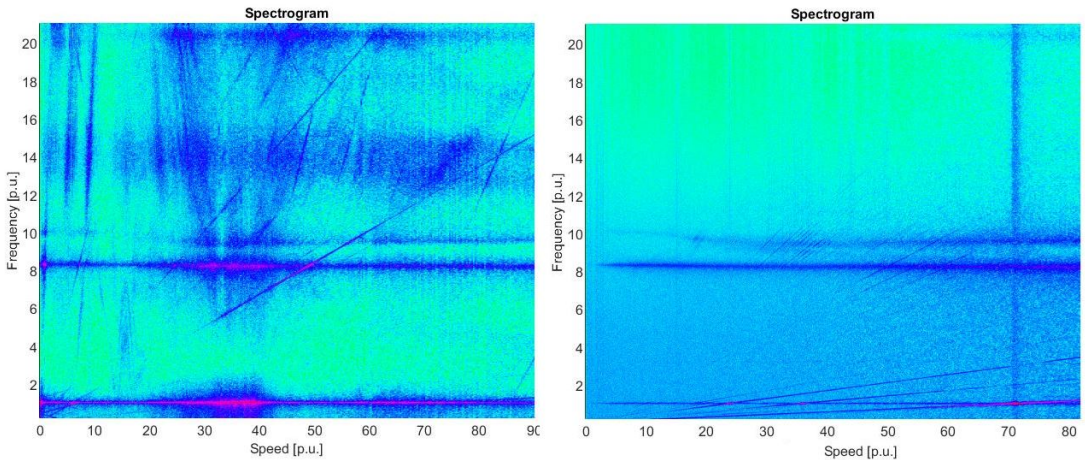


Figure 24: Spectrogram plot during 'Ramp up and down' (left) and 'Coast Stop' (right)

Similarly, inclined lines are also seen in fig. 25 that are called the order lines. Most of the vibrations are from electrical appliances like motor and converter. Harmonics of 6 order is dominant and is from the motor magnetic flux. During ramp condition orders present in the system are shown in fig. 25. Similarly, during coast stop condition orders form 1 to 26 is seen in figure 25 and are from mechanical parts only. First, four orders during coast stop in fig. 25 have higher energy, and others are only seen when they intersect the horizontal frequency lines. Common orders generated by mechanical and electrical components are seen with higher energy in ramp condition shown in fig. 25. According to [6]

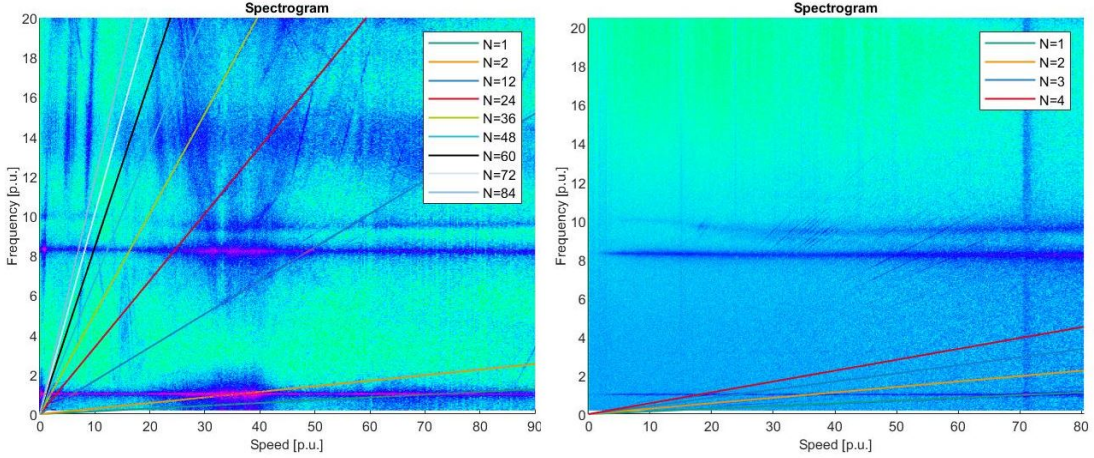


Figure 25: Order during 'Ramp up and down' (left) and 'Coast Stop' (right) system

there can be a severe misalignment in the system. It is because severe misalignment causes higher orders Of shaft speed in the system. Angular misalignment dominates because third and fourth orders have a very high amplitude compared to other orders.

3.1.2 Without DUT

Two tests 'Ramp up and down' and 'Coast Stop' are performed which can be seen in fig. 26 and 27 respectively. Similar horizontal and inclined lines are observed in the spectrogram.

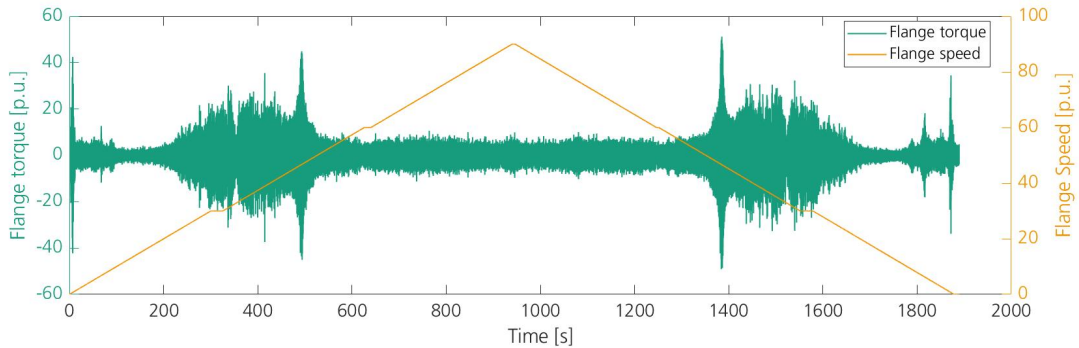


Figure 26: Flange torque and speed during 'Ramp up and down'

In figure 30, four horizontal frequency lines at 1, 1.21, 1.82 and 2.59 [p.u.] that can also be seen in fig. 28. Second frequency line is speed dependent

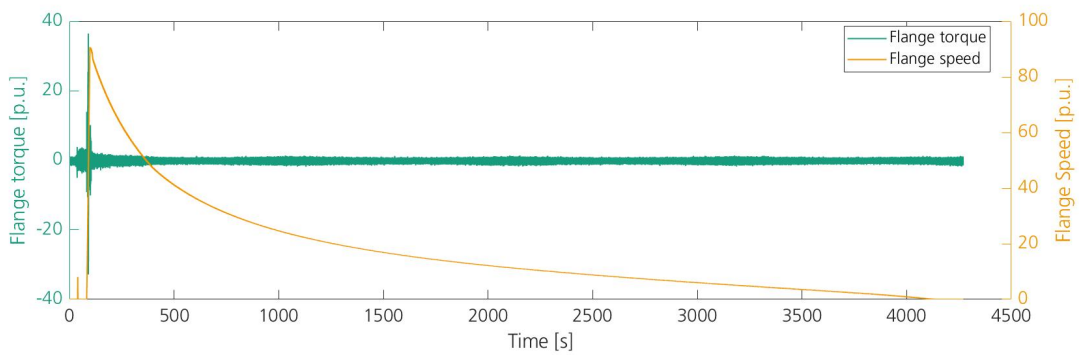


Figure 27: Flange torque and speed during 'Coast Stop'

and it decreases from 1.21 to 1.17 [p.u.]. From the previous explanation, we can say it is frequency because of bending. First and the last frequency lines have more energy while the other two have comparatively low energy. From the spectrogram plot of 'Coast Stop' condition in fig. 30 and FFT in fig. 29, we see that there are only three lines visible. Therefore, it is confirmed that 1.82 p.u frequency line is from electrical source. We can now verify that 1 and 2.59 p.u. frequency line is the torsional frequencies because torsional frequency near to these values are seen in multibody model.

During 'Ramp up and down', orders lines till 84 and more are seen in fig. 31. Harmonics of 6 order have higher energy and are generated from the motor side. Similarly, during the 'Coast Stop' condition shown in fig. 31, it can be clearly seen that first order has the highest energy. Very low energy level orders are noticed at around 12 order.

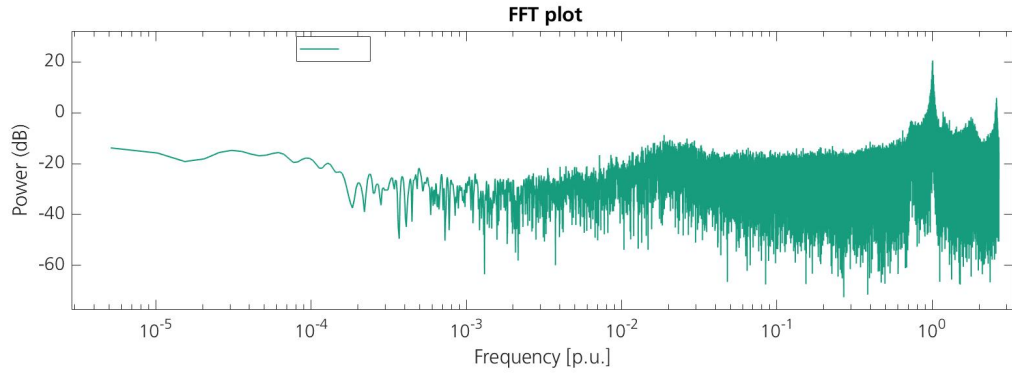


Figure 28: FFT plot of system during 'Ramp up and down'

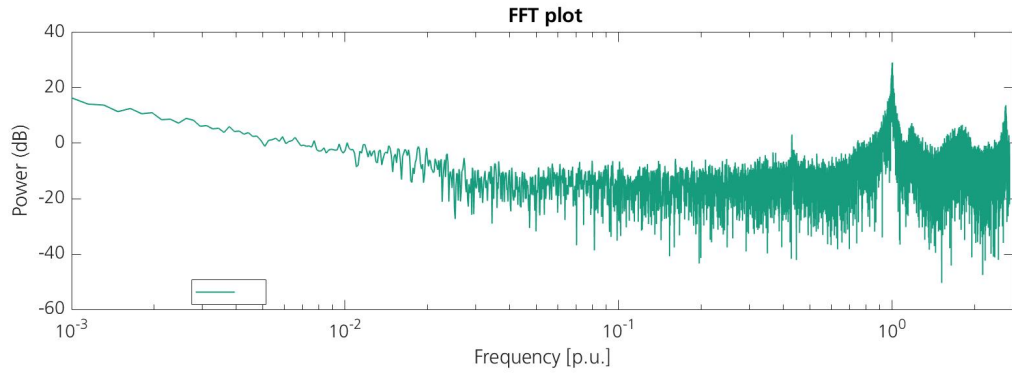


Figure 29: FFT plot of system during 'Coast Stop'

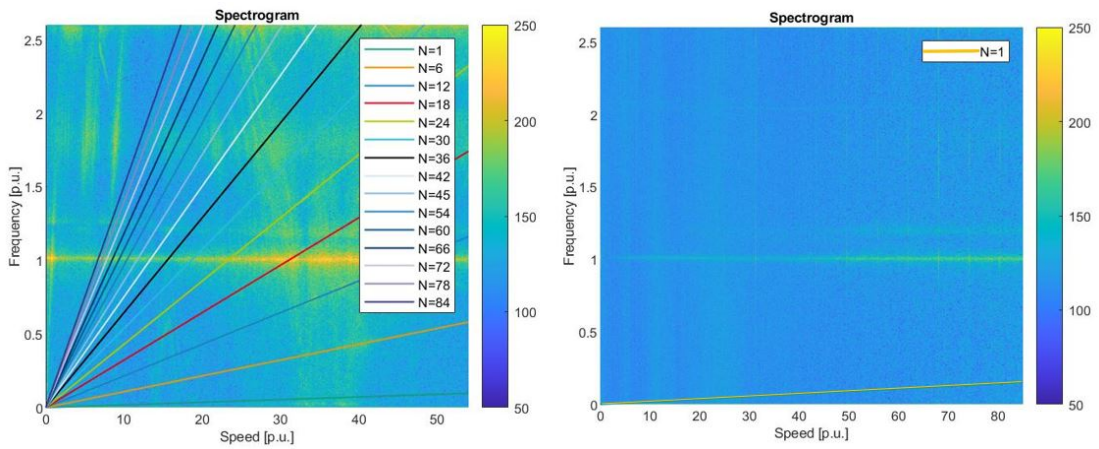


Figure 31: Order during 'Ramp up and down' (left) and 'Coast Stop' (right) system

According to [6], static imbalance is the main cause of the higher energy first

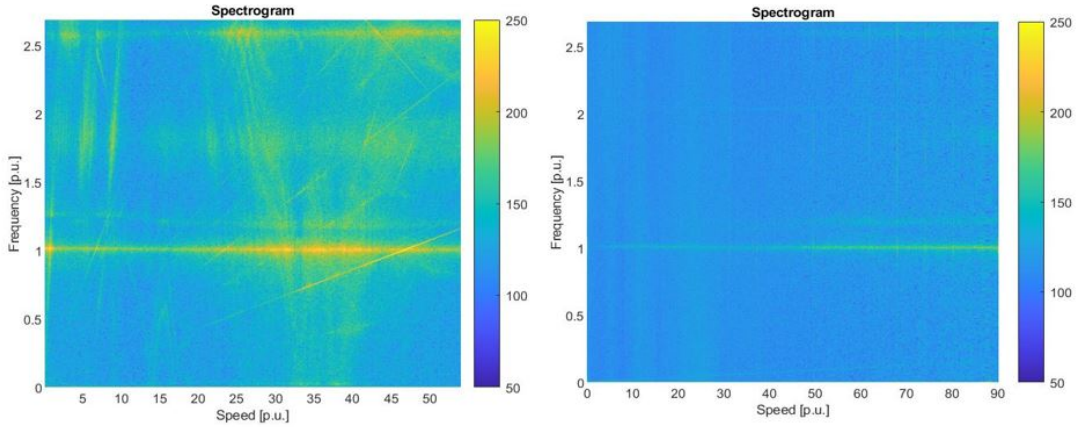


Figure 30: Spectrogram plot of 'Ramp up and down' (left) and 'Coast Stop' (right) system

order and other lower energy order. Misalignment is also another cause of higher first order energy and other low energy order during coast stop. Hence, we can conclude that there is static unbalance and misalignment is in the system. Possibly the complex geometry and assembly of motor could be a reason behind it. Static imbalance is not a serious problem at the moment but it can be solved using counterweight to balance the system.

3.1.3 Customer 2

Similar to other setups, ramp and coast stop were performed as shown in figure 32. In the spectrogram plot 35, horizontal and inclined frequency lines can be seen.

Horizontal lines at 1, 10.4 ,18.5 and 28.7 [p.u.] can be clearly seen in fig. 35 and better identified by FFT in fig. 33. Some of these frequencies are from the electrical appliances. It can be clearly identified from fig. 35 and 34 that 1 and 10.4 [p.u.] frequency lines are only present during 'coast stop' condition and the absent horizontal frequency line are from electrical sources. From previous explanation 18.5 [p.u.] is the bending mode. Multibody model of this setup gives the first two modes around 1 and 10.4 [p.u.] and it is the first two torsional frequencies of the system.

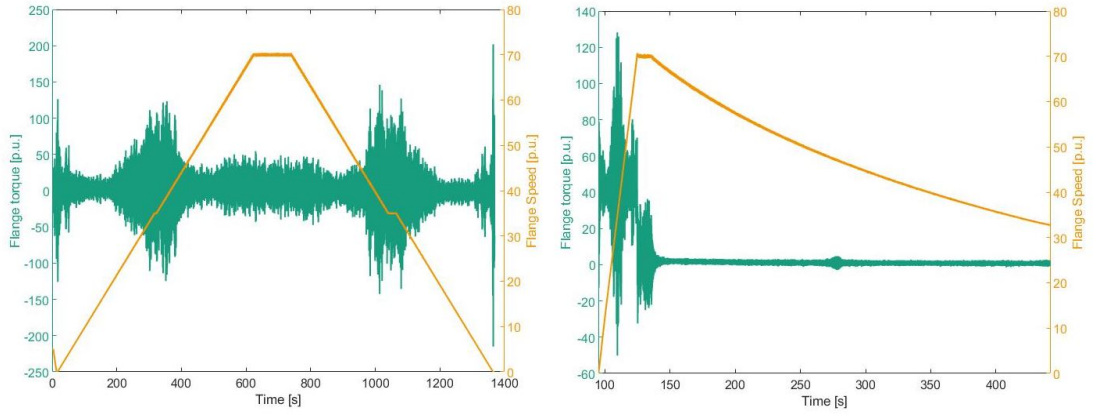


Figure 32: System torque and speed during Ramp (left) and Coast stop (right)

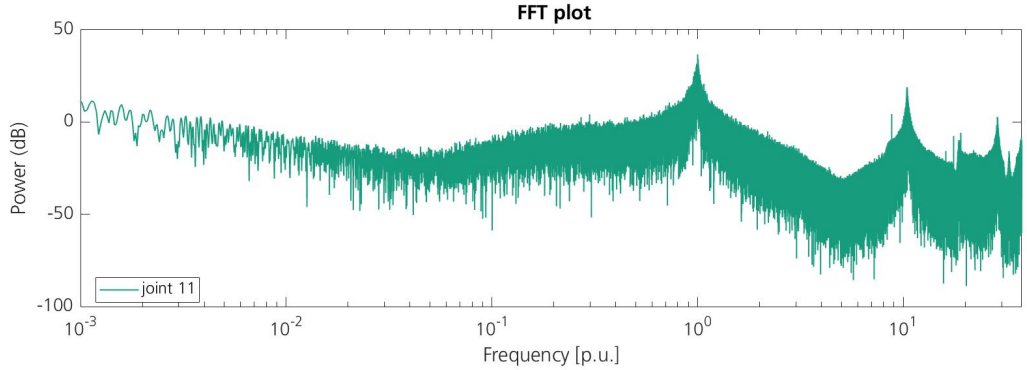


Figure 33: FFT plot of system during ramp-up and down

Order lines from 1 to 84 can be seen in fig. 36 during ramp condition. Similarly, when the motor is switched off only 1st and 2nd order is seen in figure 36. Also, the second order is seen to have more energy than 1st order. There could be two reasons according to [6]. First reason can be that the shaft is bent at the ends and the second can be because of the parallel and angular misalignment. It is known that the shaft is inclined at around 0.2 degrees with the ground and should have parallel misalignment during assembly. From above information, it can be said that second case is most probably present.

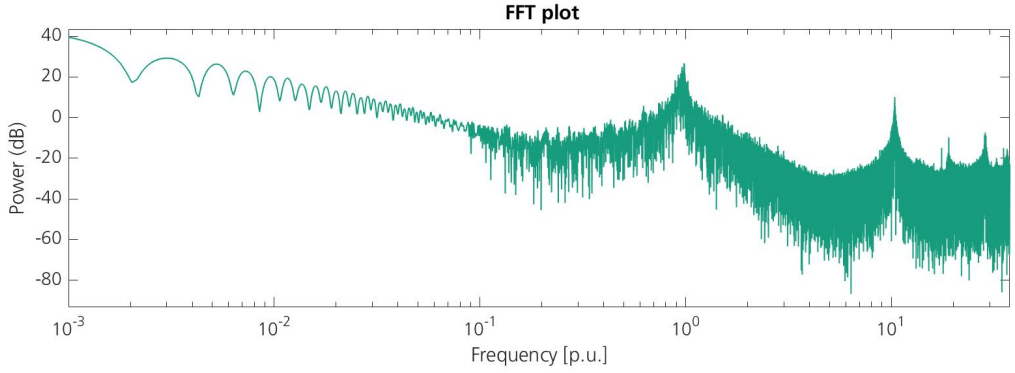


Figure 34: FFT plot of system during coast stop

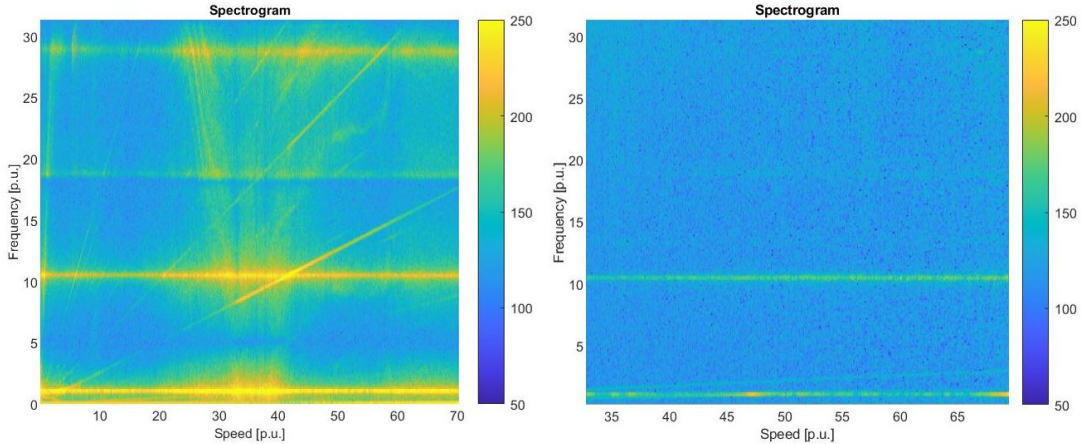


Figure 35: Spectrogram plot of ramping (left) and coast stop (right) system

3.2 Damping ratio calculation

For damping ratio calculation, 'Without DUT' setup is used because it is less complex system than other two setups. It is a two-mass model and structural matrix of the system is 3×3 order. 'Half power method' is used to calculate damping ratio of each eigenfrequency.

3.2.1 Damping from experiment data

Five scenarios are tested with first two as harmonic frequency being fed at 1500 RPM and 300 RPM respectively and are shown in fig. 37. During this process the system is torque controlled which means no control loop is involved. Similarly,

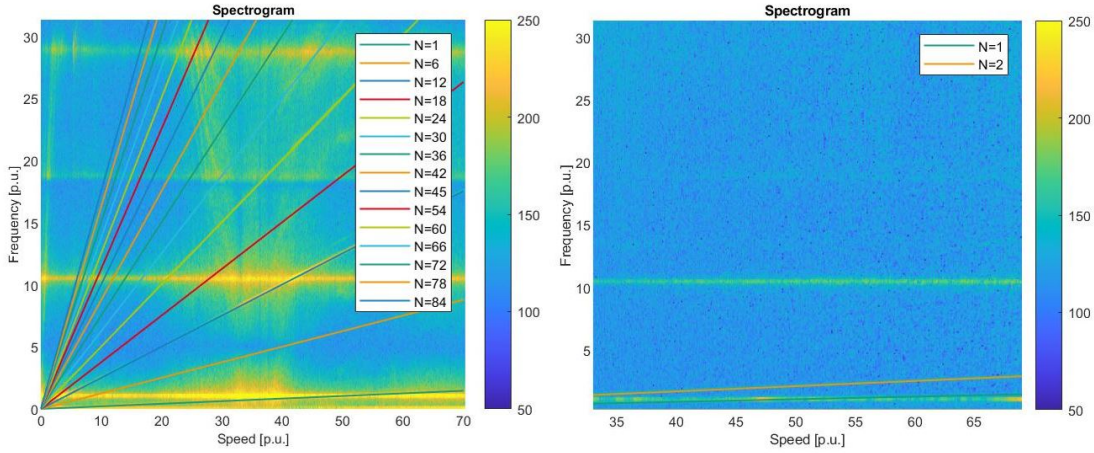


Figure 36: Oder during ramp (left) and coast stop (right) system

other three tests are speed controlled and are ramped to 1800 RPM in 900, 100, and 10 seconds respectively and shown in fig. 37.

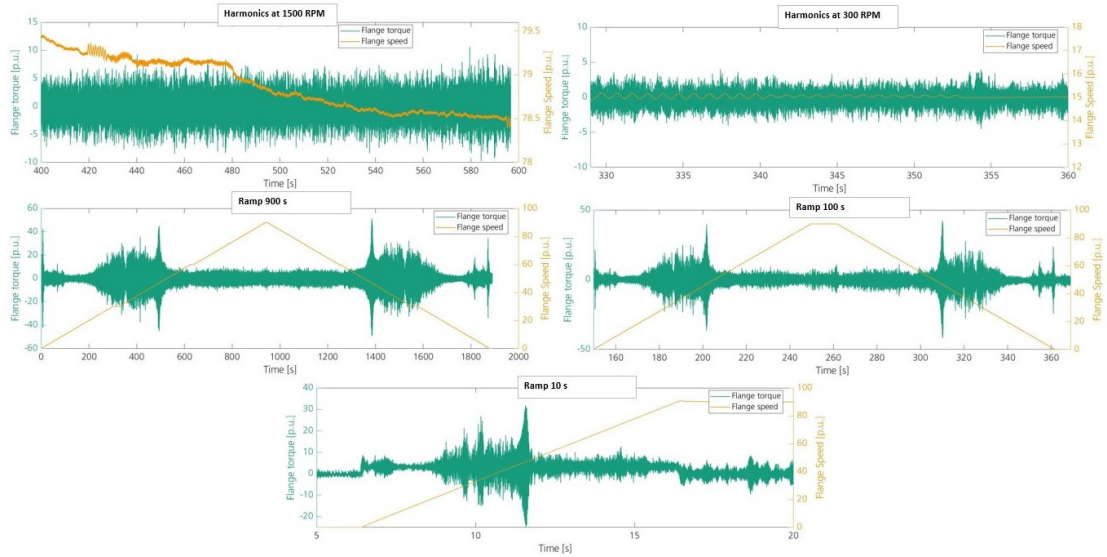


Figure 37: Torque and speed to different test

FFT plot that is received from the test data is not smooth as shown in fig. 38 and it is difficult to observe ω_1 , ω_2 , and ω_n . Noise in the signals is one of the major reasons behind it and an appropriate method needs to be used. Therefore, averaging and maximum value method to get a smooth curve. After compiling the experiment data, we get the results shown in table 1 and 2.

From both tables, damping ratio is noticed to be randomly varying and possible

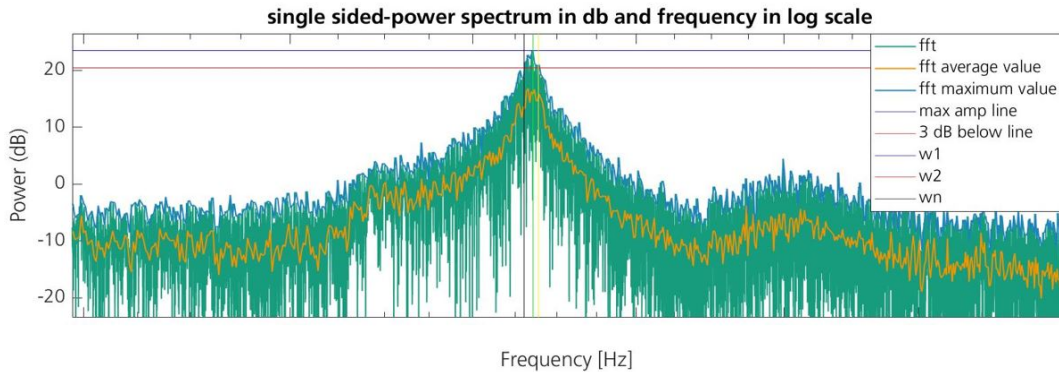


Figure 38: FFT plot using average and maximum data points

	First eig. freq.				Second eig. freq.			
Test scenarios	ω_1	ω_2	ω_n	ξ_1	ω_1	ω_2	ω_n	ξ_2
Har. 1500 RPM	0.997	1.009	1.005	0.612	2.599	2.614	2.608	0.291
Har. 300 RPM	1.003	1.010	1.005	0.365	2.582	2.608	2.599	0.488
Ramp 900s	1.001	1.011	1.006	0.544	2.579	2.604	2.591	0.480
Ramp 100s	1.000	1.010	1.006	0.479	2.581	2.600	2.594	0.376
Ramp 10s	0.992	1.011	0.997	0.921	2.592	2.625	2.618	0.627
Average				0.584				0.452

Table 1: Damping ratio using maximum data points

reason can be the errors in measurement process. FFT plot obtained using above method is not smooth or continuous with many peaks. Therefore, the correct result was not obtained and a suitable method is needed. We cannot fully rely on individual table results and the damping of the first and second eigenmode is assumed same which is average of all the data. Therefore, damping ratio of all modes is calculated as 0.53%.

3.2.2 Modal space transformation

Rayleigh damping is used to calculate the damping coefficient. The relation between Rayleigh damping and inertia normalized damping matrix in modal co-

Test scenarios	First eig. freq.				Second eig. freq.			
	ω_1	ω_2	ω_n	ξ_1	ω_1	ω_2	ω_n	ξ_2
Har. 1500 RPM	0.997	1.008	1.001	0.540	2.598	2.618	2.612	0.382
Har. 300 RPM	1.002	1.011	1.005	0.461	2.584	2.608	2.600	0.473
Ramp 900s	0.998	1.010	1.005	0.641	2.577	2.605	2.595	0.536
Ramp 100s	1.001	1.014	1.005	0.648	2.583	2.602	2.588	0.375
Ramp 10s	0.992	1.008	0.997	0.790	2.592	2.622	2.605	0.579
Average				0.616				0.469

Table 2: Damping ratio using average data points

ordinate is given by equation 41.

$$C_\eta = \alpha \begin{bmatrix} 1 & 0 & 0 \\ 0 & 1 & 0 \\ 0 & 0 & 1 \end{bmatrix} + \beta \begin{bmatrix} 0 & 0 & 0 \\ 0 & k_{\eta 2} & 0 \\ 0 & 0 & k_{\eta 3} \end{bmatrix} = \begin{bmatrix} 2\xi_0\omega_0 & 0 & 0 \\ 0 & 2\xi_1\omega_1 & 0 \\ 0 & 0 & 2\xi_2\omega_2 \end{bmatrix} \quad (41)$$

Lumped inertia and stiffness matrix is known as well as the modal inertia and modal stiffness matrix is obtained using the modal transformation. The modal inertia matrix is in normalized form and the stiffness matrix is diagonal with first diagonal element zero. ξ_0 , ω_0 is zero because of rigid mode while ξ_1 and ξ_2 have the same damping ratio got from experiment. First and second angular frequencies are denoted by ω_1 and ω_2 respectively which are known from the experiment. We get three equations from the matrix and solving the last two equations involving ' ω_1 ' and ω_2 , we get the value of $\alpha=6.4082$ and $\beta = 4.36129e-6$. To get the better damping value of the first and second eigen mode, the last two equations are solved. Transforming these values in spatial coordinates we get damping matrix as below.

$$C = 1e+03 \begin{bmatrix} 4.6097 & -0.1250 & 0 \\ -0.1250 & 0.2103 & -0.0394 \\ 0 & -0.0394 & 0.0683 \end{bmatrix}$$

$$C = \begin{bmatrix} c_1 & -c_1 & 0 \\ -c_1 & c_1 + c_2 & -c_2 \\ 0 & -c_2 & c_2 \end{bmatrix} \quad (42)$$

Here, the damping matrix is symmetric and we consider that the value of c_1 to be 125 Joules s/rad. Using the damping matrix formulation in spatial coordinates shown in 42, we get c_2 as 85 Joules s/rad.

4 MULTIBODY MODELING

4.1 Model building Procedures

There are different software where the multibody dynamics of a system can be modeled and studied like Simscape, Dymola, MSC Adams, etc. MSC Adams is used for creating the multibody model. Reason for choosing this software is because of its various features. Any complex CAD parts and assembly can be imported and it has a user-friendly interface. Various CAD parts can be combined and divided easily along with the position change in graphic interface. Isotropic and anisotropic materials of required material properties can be created or imported from libraries. Similarly, viewFlex is used to convert rigid body into flexible body. It also provides an easy and fast way to see the modal analysis of each flexible part of the assembly as well as provide functions to enable and disable modes. Because of fast equation solving capabilities, modal analysis can be performed easily. Furthermore, nonlinear and linear models can be exported to MATLAB and other software for co-simulation and control purposes. Graphic representation of the working system can be visually analyzed in the Adams during co-simulation which provides a better understanding of the system.

There are a few things to be considered during multibody modeling. Acceptable CAD format must be exported to Adams and '.CATProduct' file format is used in this thesis. Solver and integrator must be properly specified. Among C++ and FORTRAN solvers, C++ is used with HHT integrator. C++ solver is used

because of its compatibility with MATLAB. HHT solver is selected because of low calculation time and its stability with a small integration step size [14]. 'Time step' is the data sampling time as in the experiment, which defines the range of frequency that can be shown in the FFT plot. Most common time step used is 1e-03 and 6.25e-04 s. Also, units of the system must be properly defined so that the results are obtained in the required measurement.

After the above important points are considered, building multibody model is carried out. Though there are three different setups of the system, the procedures for all of them are the same. At first, the assembly are reconstructed in Siemens NX software with the desired parts. '.CATProduct' format file of the assembly are imported to Adams. Steel material from Adams library are used for all unknown parts because detailed material information are not available. After providing material information, parts are splitted and then combined according to the requirement as shown in fig. 39. Splitting or division of torque flange was done so that the torque could be measured at the sensor point.

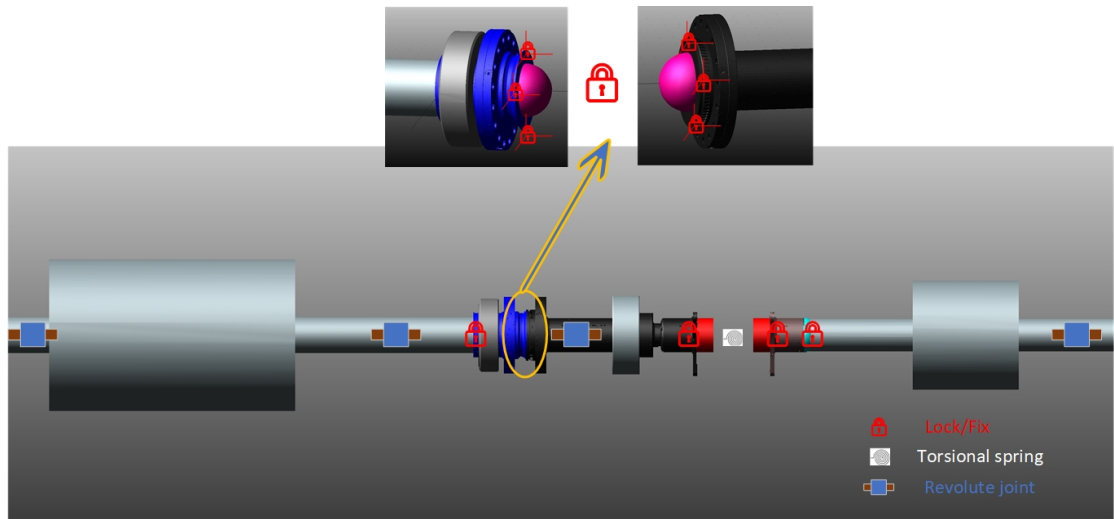


Figure 39: Constraints in multibody model

Similarly, constraints between parts are provided. One of the disadvantages using Adams is that constraints between the axial surface between two flexible body was not possible. Therefore, several markers are created on the surface and

then connected to a rigid body with negligible inertia and mass as shown in fig. 39. Similarly, it is done for the other part and the rigid bodies were connected using 'fix' joint. In this way torque measurement at the required point is possible. Revolute joints are provided at the bearing positions which are connected to the ground. Furthermore, the detailed multibody model of fiber coupling is not in the scope of the thesis and is made as two rigid parts with torsional spring between them. Inertia of the coupling is distributed equally between two rigid parts.

4.2 Realizing experimental damping ratio in multibody model

Damping ratio implementation is done in 'Without DUT' model and is explained in this subsection. There are two ways in which the damping ratio can be realized in the ADAMS model. First, damping coefficient of each part can be used which are calculated using modal transformation. It is useful for mathematical modeling where damping coefficients can be directly implemented. Damping ratio of each mode can be directly inputted into the flexible body and it is the second method. Since the damping ratio is known for all the modes from the experiment, 0.53% damping ratio is used for all modes of individual parts. Also, different damping ratio for individual frequency range can also be defined but is not required. Using the first method is time-consuming for flexible body because additional joints are required between each part and are difficult to change the model. Similarly, the damping coefficient is approximated for first two modes which needs to be confirmed before implementation. Therefore, second method is preferred which can be easily implemented and changed when required.

4.3 Known parameters

There are three major components and they are motor, PTSS, and generator. Only few information about the parts are known which are denoted by '*' in tab.3. Other parameters which are not in the table are unknown.

M=Motor, G=Generator, S=Shaft, C=Coupling

Model	M_I	M_S	M_D	G_I	G_S	G_D	C_I	C_S	C_D
Customer 1	*			*					
Customer 2	*			*				*	
Without DUT	*								

Table 3: Known and unknown parameters

M_I = motor inertia

M_S = motor stiffness

M_D = motor damping

4.4 Calculation of stiffness and inertia from multibody model

First of all multibody model of 'Customer 1' is constructed and stiffness of the parts are calculated. The PTSS is divided into four parts shown in fig. 40 and they are flexible while motor and generator are rigid. Torques is applied at the motor part and the angle of twist is measured at each of the the joint using Angle measurement tool. Measurement frames are kept in proper orientation to get the accurate results. The results of the angular twist of each part from the Adams is shown fig. 40.

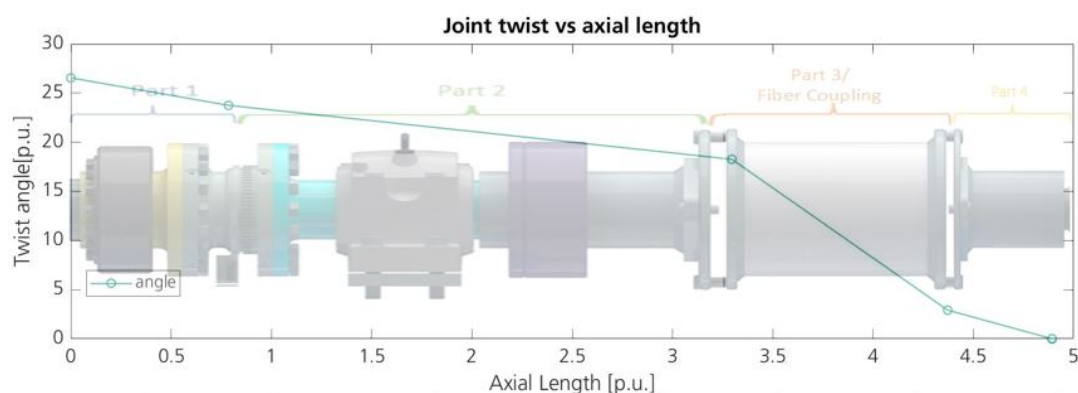


Figure 40: Angular twist vs axial length

Net angular twist and torque across the part can be calculated using formula 43

to obtain torsional stiffness (T/θ).

$$\frac{T}{\theta} = \frac{\text{Torque applied}}{\text{Net twist}} \quad (43)$$

The torsional stiffness value of the parts are also checked by varying load . The nonlinear multibody model are imported to simulink and ramp torque is given to the motor side. The torsional stiffness is calculated at each time interval and the simulation results are given in fig. 41.

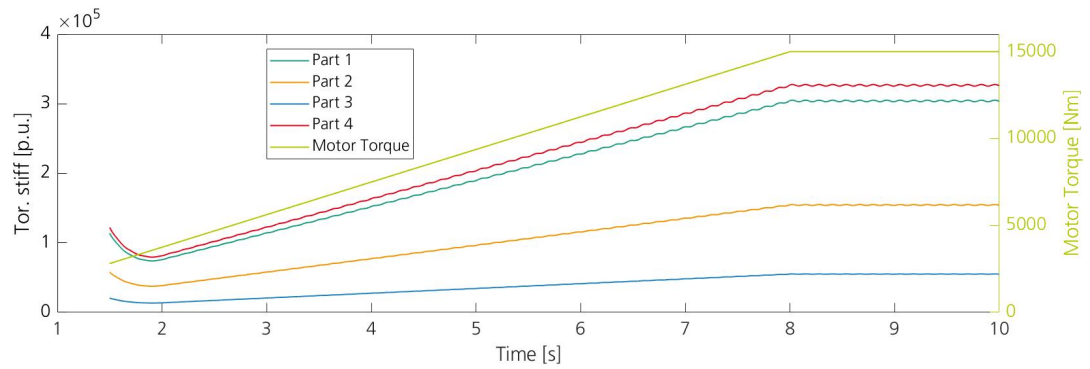


Figure 41: Torsional stiffness vs time

Torsional stiffness at the start of simulation is high because of the small angle measurement. Also, oscillation are seen because of the flexible body dynamics. After the system becomes stable, the constant value of the torsional stiffness of each parts are seen. Hence, flexible parts that are used have constant torsional stiffness.

Inertia of unknown parts are also got form that Adams/multibody model. The material properties like the density, young's modulus and poisson's ratio can define the required material properties. CAD model contains the information about the dimension. With all these inputs, Adams can automatically provide the inertia values. These values can be easily got from the interactive user interface in Adams. Material properties can be easily changed in the corresponding inertia values are automatically recalculated.

The stiffness and inertia of 'Without DUT' can be known because 'Without DUT' model has the same parts as the 'Customer 1'. For 'Customer 2', only flexible

Parts	Damping Ratio(%)	Tor. Stiff.[p.u.]	Not.	Axial MOI[p.u.]	Not.
Motor	No damp.	rigid		58.10	j_m
Part 1	0.53	307933.18	k_1	0.44	j_1
Part 2	0.53	156591.02	k_2	0.75	j_2
Part 3	No damp.	55120.04	k_3	0.06	j_3
Part 4	0.53	295285.92	k_4	0.03	j_4
Generator	No damp.	rigid		6.67	j_g

Table 4: Normalized parameter of 'Customer 1'

Parts	Damping Ratio(%)	Tor. Stiff.[p.u.]	Not.	Axial MOI[p.u.]	Not.
Motor	No damp.	rigid		58.10	j_m
Part 1	0.53	307933.18	k_1	0.44	j_1
Part 2	0.53	156591.02	k_2	0.75	j_2
Part 3	No damp.	42429.35	k_3	0.58	j_3
Part 4	0.53	295285.92	k_4	0.03	j_4
Generator	No damp.	rigid		35	j_g

Table 5: Normalized parameter of 'Customer 2'

coupling and DUT is changed and other parts are considered same. The torsional stiffness and inertia of each model is given in the table 4 and 5.

4.5 Results from normal modes analysis

Normal modes analysis in Adams displays the eigenfrequencies, modes and damping ratio. Following results are from the model which is created using viewFlex. Eigenfrequency and damping ratio of all three setups are presented in table 6. Damping ratio of 'Without DUT' is seen to be smaller than 0.53%

that was used in the flexible body model. The reason behind can be because of the computational error and linearization process which is explained in chapter two. Also, α value of HHT solver, which also controls damping might also have effect. Similarly, rigid body mode is sometime seen to have very high damping value and numerical error is the reason behind it [14]. Damping ratio of other two models are not focused in this thesis.

Setups	Mul.Body	Damp. ratio %
Customer 1		
$1^{st} eig.freq.$	1.02	0.14
$2^{nd} eig.freq.$	7.66	1.94
$3^{rd} eig.freq.$	23.98.	7.35
Without DUT		
$1^{st} eig.freq.$	0.89	0.03
$2^{nd} eig.freq.$	3.02	0.2
Customer 2		
$1^{st} eig.freq.$	0.73	0.00
$2^{nd} eig.freq.$	9.52	0.02
$3^{rd} eig.freq.$	22.53	0.05

Table 6: Results from normal modes analysis

Similarly, Adams Flex method is also used to created 'Without DUT' model and compare the results using normal modes analysis but it is unsuccessful. It is done because the parts can be better constrained. Desired nodes or complete surface nodes can be connected to point mass which has negligible mass and inertia. Point mass is assumed to have no effect in the system. In Adams, few nodes can be connected between two parts which has more concentrated loading while in ANSYS all surface nodes can be connected that provides well distributed load-

ing. All flexible parts are imported to Adams in MNF format and 'Without DUT' model are created. With same material properties, first and second torsional frequencies obtained from Adams Flex of 'Without DUT' is seen to have high first and second eigenfrequency as shown in table 7 which means the imported parts has higher stiffness because of errors.

Type	$1^{st} eig.freq.$	$2^{nd} eig.freq.$
Adams Flex	1.67	8.37
ViewFlex	0.89	3.02

Table 7: Torsional eigenfrequencies of 'Without DUT'

While creating MNF file from ANSYS units of length, force, mass and time are also written. The units of length are found to be different during import. Also, the mesh size and 'growth rate' values are also different. Rate of size transition between adjacent element is controlled by 'growth rate' [18]. Similarly, the mesh size are found different. ANSYS uses Mechanical ANSYS Parametric Design Language (MAPDL) solver target while Adams use C++ solver to create MNF file. Due to different method of obtaining flexible part and above mentioned reasons, the model using Adams Flex has higher error. Further work is continued using viewFlex.

5 MATHEMATICAL MODELING

5.1 Customer 1

Customer 1 setup can be seen in the fig. 42 and it is the simplest representation of the real system for better understanding. Shaft part is divided into four parts with motor and generator on opposite sides. The whole system is supported on five bearings. There are five nodes and represented by yellow circle with node numbers. The parameters like stiffness and inertia of the parts are either known

form the supplier or form the multibody model. The list of stiffness and inertia of the parts are given in the table 4 and 5 along with the notation.

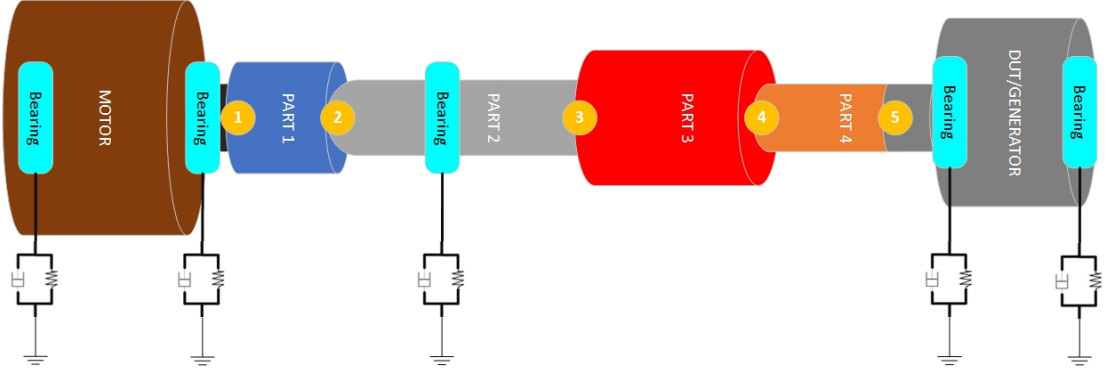


Figure 42: Simple representation of 'Customer 1' setup

The parameters needed to build a matrix model of the torsional system are available. This system is four mass model and can be represented by 5×5 order matrix. Lumped inertia of this system is denoted by eq. 44.

$$[J]_{5 \times 5} = \begin{bmatrix} j_1/2 + j_m & 0 & 0 & 0 & 0 \\ 0 & j_1/2 + j_2/2 & 0 & 0 & 0 \\ 0 & 0 & j_2/2 + j_3/2 & 0 & 0 \\ 0 & 0 & 0 & j_3/2 + j_4/2 & 0 \\ 0 & 0 & 0 & 0 & j_4/2 + j_g \end{bmatrix} \quad (44)$$

Motor is assumed as rigid and directly connected to node 1. Similarly, DUT is rigidly connected to the node 5 which can be seen in the inertia matrix. Also, the consistent model can be obtained as shown in eq. 45.

$$[J]_{5 \times 5} = \begin{bmatrix} j_1/3 + j_m & j_1/6 & 0 & 0 & 0 \\ j_1/6 & j_1/3 + j_2/3 & j_2/6 & 0 & 0 \\ 0 & j_2/6 & j_2/3 + j_3/3 & j_3/6 & 0 \\ 0 & 0 & j_3/6 & j_3/3 + j_4/3 & j_4/6 \\ 0 & 0 & 0 & j_4/6 & j_4/3 + j_g \end{bmatrix} \quad (45)$$

Stiffness matrix is same for both the models and is of order 5×5 . From the stiffness information, we can get the stiffness matrix as follows.

$$[K]_{5 \times 5} = \begin{bmatrix} k_1 & -k_1 & 0 & 0 & 0 \\ -k_1 & k_1 + k_2 & -k_2 & 0 & 0 \\ 0 & -k_2 & k_2 + k_3 & -k_3 & 0 \\ 0 & 0 & -k_3 & k_3 + k_4 & -k_4 \\ 0 & 0 & 0 & -k_4 & k_4 \end{bmatrix}$$

After getting 'J' and 'K' matrix eigenfrequencies and modes can be calculated by following formulation 46 in MATLAB and is used for all three models.

$$[V, D] = eig(K, J) \quad (46)$$

'V' contains eigen modes and D contains eigenvalues information which can be further used to calculate eigenfrequency.

5.2 Without DUT

Fig. 43 represents the simple model of 'Without DUT' model. It has only two shaft parts and three nodes. The stiffness and inertia of the system can be represented by matrix of order 3×3 and all parameters are known to build stiffness and inertia matrix.

Consistent and lumped inertia matrix of the system are denoted by eq. 47 and 48 respectively.

$$[J]_{3 \times 3} = \begin{bmatrix} j_1/3 + j_m & j_1/6 & 0 \\ j_1/6 & j_1/3 + j_2/3 & j_2/6 \\ 0 & j_2/6 & j_2/3 \end{bmatrix} \quad (47)$$

$$[J]_{3 \times 3} = \begin{bmatrix} j_1/2 + j_m & 0 & 0 \\ 0 & j_1/2 + j_2/2 & 0 \\ 0 & 0 & j_2/2 \end{bmatrix} \quad (48)$$

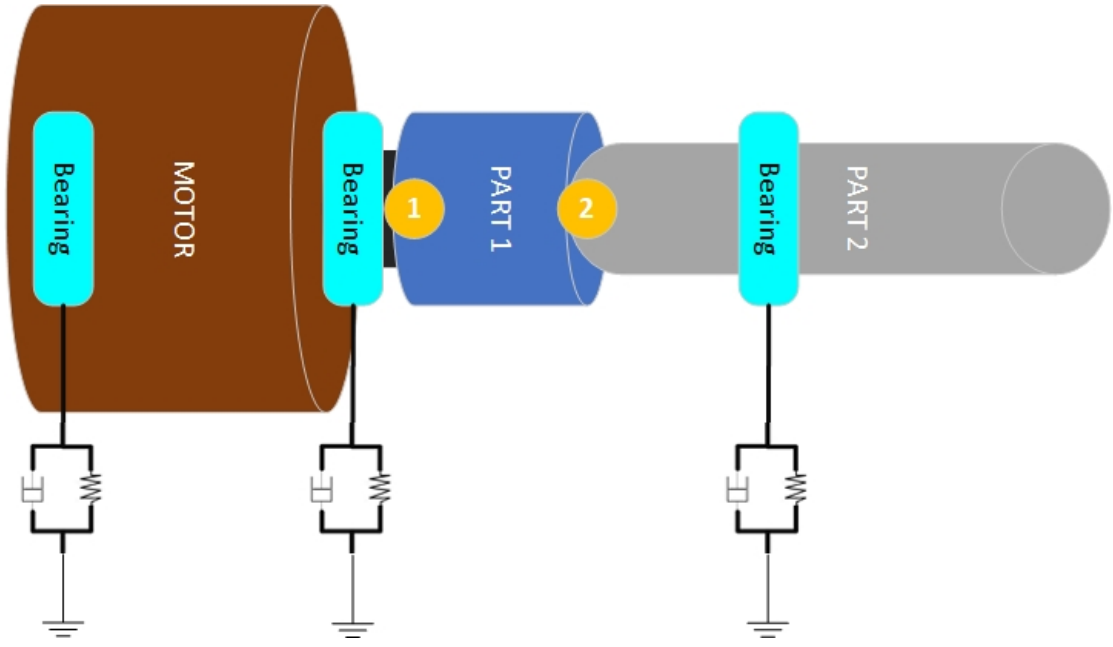


Figure 43: Simple representation of 'Without DUT' setup

Similarly, the stiffness matrix of order 3×3 can be written as follows.

$$[K]_{3 \times 3} = \begin{bmatrix} k_1 & -k_1 & 0 \\ -k_1 & k_1 + k_2 & -k_2 \\ 0 & -k_2 & k_2 \end{bmatrix}$$

5.3 Customer 2

'Customer 2' has same orientation as 'Customer 1' and can be represented by fig. 42. It has also four shaft parts and five nodes. Therefore, the structural inertial and stiffness matrix is of order 5×5 and same formation as 'Customer 1'. All the required parameters can be obtained from table 5.

6 OPERATIONAL MODEL

The torsional eigenfrequencies can be obtained by normal modes analysis of multibody model and modal analysis of mathematical model. We need a non-linear system whose measurements and data can be processed as the real system.

Therefore, operational model is required. Non-linear Adams model can be imported in MATLAB through 'Plant Export' function as 'ADAMS block' shown in fig. 44. PI controller, required input and output are added after the model is imported in Simulink (MATLAB). The system can be seen in detail in the fig. 44. Solver and time steps should be taken into consideration. The solver set-

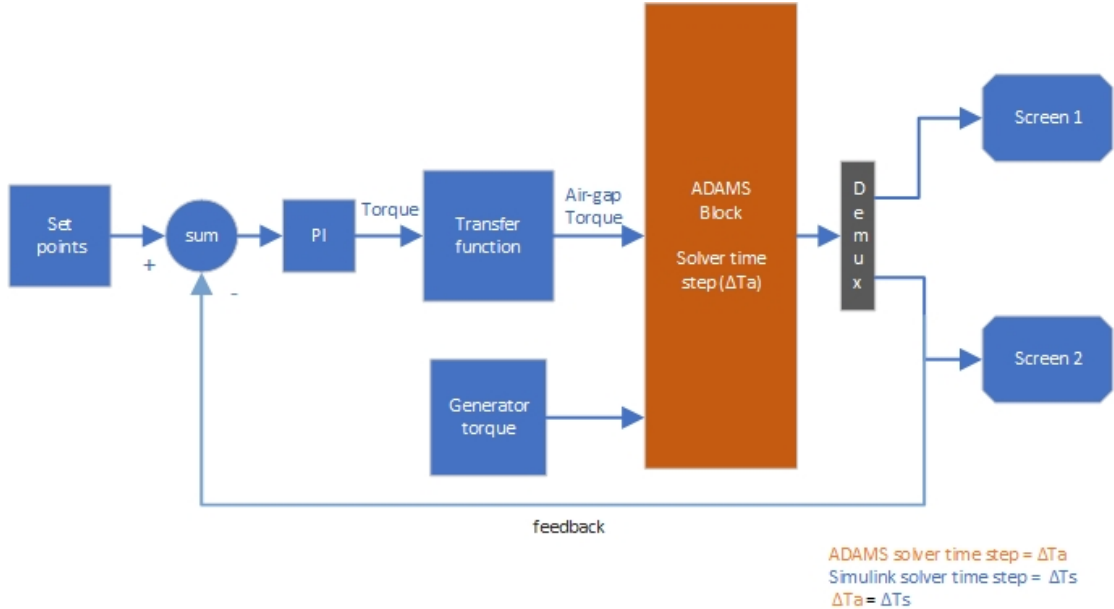


Figure 44: Operational model

tings of both Adams and Simulink should be same and C++ solver is used in this model. Solver time step for Adams and Simulink should be same and the 'communication time interval' for Adams should be same as the time step in MATLAB. Simulink provides the interface between the Adams model and the control unit. Co-simulation can also be done in operational model. In Co-simulation, the controls or required function can be built in Simulink and can be executed in Adams. In the operational model, set points in terms of motor RPM is provided to the controller. PI controller is used and flange RPM is given as feedback to the control system. Here, transfer function is used which acts as low pass filter because the motor is not sensitive to high frequency. Torque obtained after the transfer function is directly fed to rotor of motor which is called air-gap torque. Simulink communicates data with the Adams model at communication time in-

terval which is same as the time step of both models. The required output can be taken out which is predefined while exporting the Adams model to MATLAB. The required output is usually the flange torque and flange speed [RPM] The whole system can be analyzed during its operation and compared with the test results. That is why it is called as operational model. The required data can be exported from 'Scope' of the simulink to MATLAB workspace and later to the excel file. These data can be used in MATLAB for further processing and getting the desired results.

6.1 Customer 1

Two tests scenarios are examined with this setup. In the first scenario, system is ramped up with speed control while in the other scenario, the system is just given step air-gap torque without control. The air-gap torque and flange speed during ramp are given in the fig. 45. Similarly, flange torque and speed during step air-gap torque are shown in fig. 46. It is to be noticed that torque and RPM are measured at flange in the model. Therefore, FFT plot and spectrogram shows only torsional frequency.

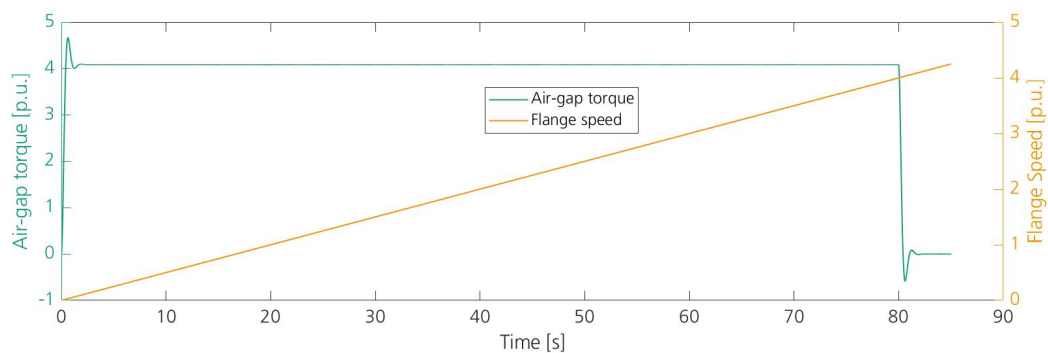


Figure 45: Air-gap torque and speed during system 'Ramp up'

Flange torque and speed in fig. 46 reveals that the system has less damping because oscillations are decaying very slowly. FFT plot in fig. 47 and 48 reveal that the torsional frequencies are 1.01, 7.19 and 20.98 [p.u.] as shown in table 8.

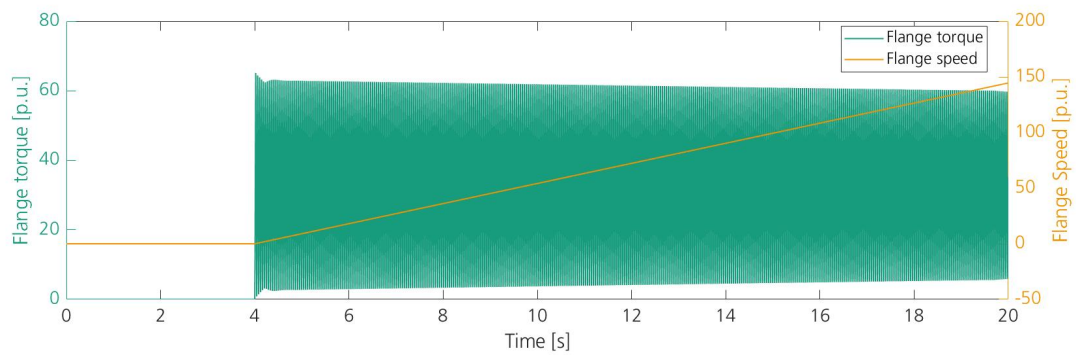


Figure 46: Flange torque and speed during step air-gap torque

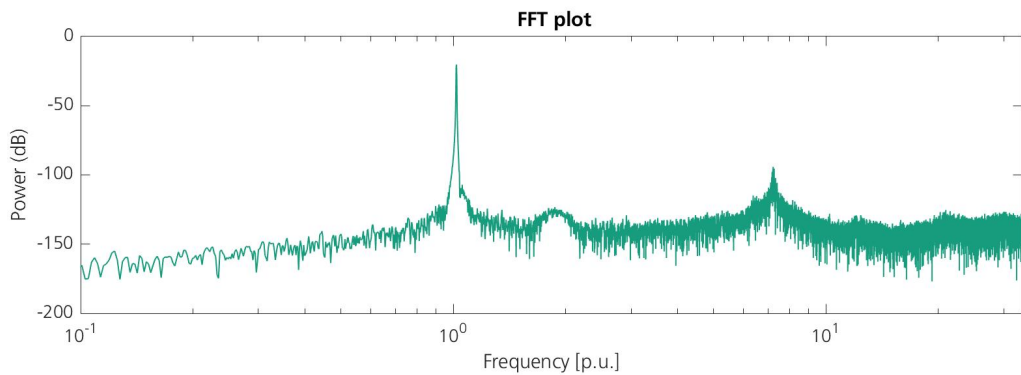


Figure 47: FFT during 'Ramp up'

Ramp condition has first two lower eigenfrequency than the step-condition because adding controller in the loop also shifts the eigenfrequencies [23]. It also noticed that these frequencies are lesser than normal modes analysis. It can be because of computational error during linearization process of normal modes analysis. Spectrogram plot of the ramp condition can be seen in fig. 49 where the two horizontal torsional frequency lines can be seen. Inclined lines are due to aliasing effect.

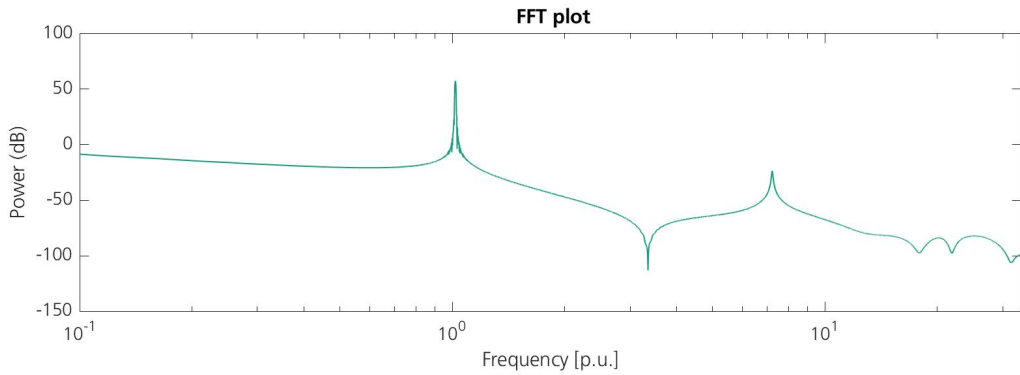


Figure 48: FFT during step air-gap torque

Scenarios	First tor. freq. [p.u.]	Second tor. freq.[p.u.]	Third tor. freq.[p.u.]
Ramp tor.	1.01	7.19	20.98
Step tor.	1.04	7.22	20.4

Table 8: Torsional frequency using operational model

6.2 Without DUT

Similar test scenarios are created with this model and the system's torque, speed can be seen in fig. 50 and 51. It is seen to have higher damping in fig. 51 therefore, half power method is used to calculate damping ratio. Damping ratio for first eigenfrequency for ramp and step torque is found to be 0.23 and 0.43 % respectively. Similarly, damping ratio of second eigenfrequency for ramp and step torque is 6.63 and 2.95 % respectively. It has higher damping ratio than the normal modes analysis which can be because of non-linearities present in the system.

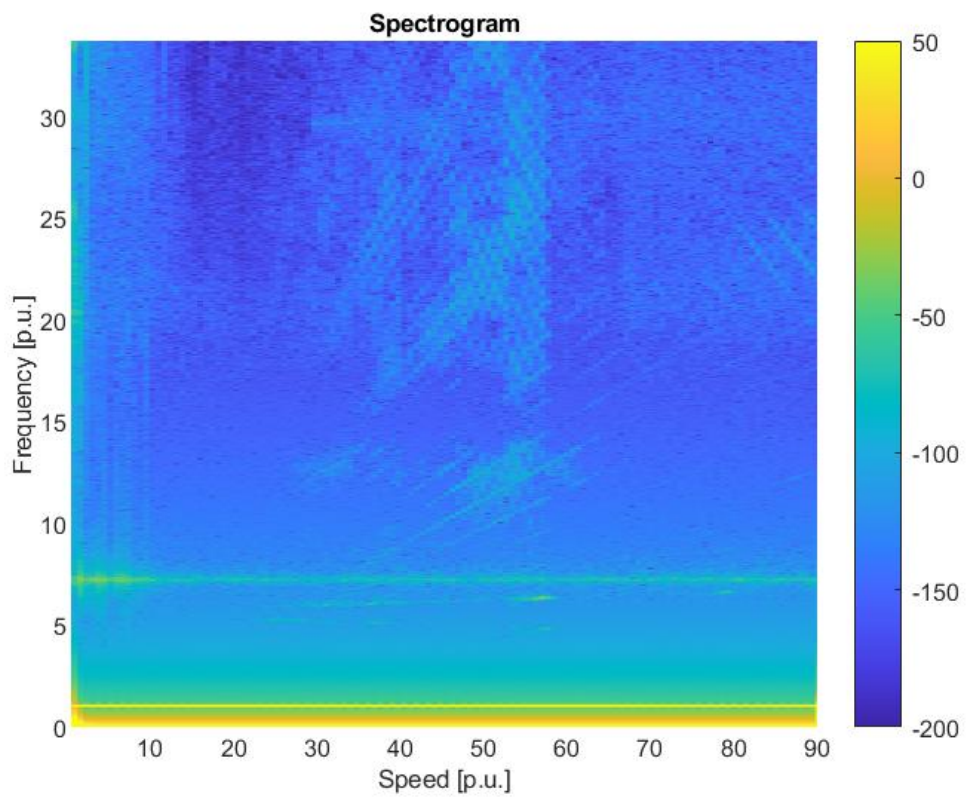


Figure 49: Spectrogram plot during 'ramp up'

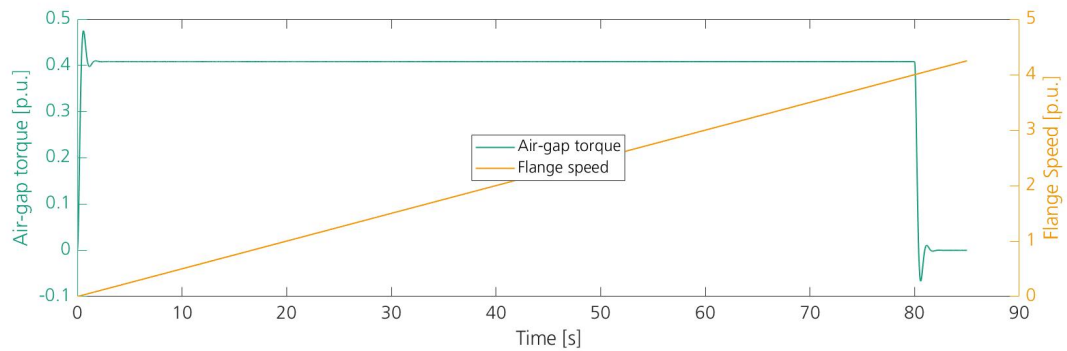


Figure 50: Air-gap torque and speed during system 'Ramp up'

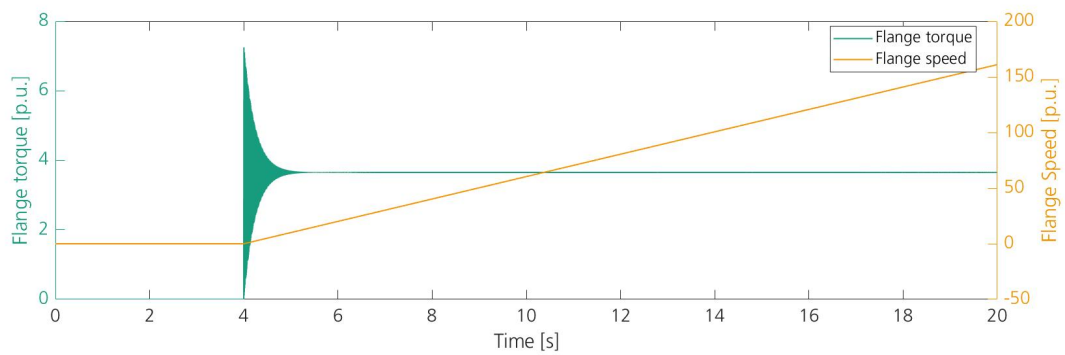


Figure 51: Flange torque and speed during step air-gap torque

Again, the eigenfrequencies during ramp are seen to have lower than the step torque condition except for the second frequency of step torque and are shown in table 9. It is due to inaccuracy in frequency determination in FFT plot shown in fig. 53. Due to aliasing effect incline lines can be seen in the spectrogram 54 and also various peaks can be noticed in FFT plot 52 and 53.

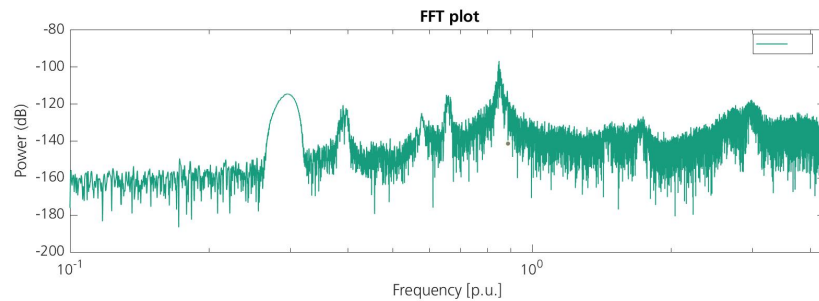


Figure 52: FFT during 'Ramp up'

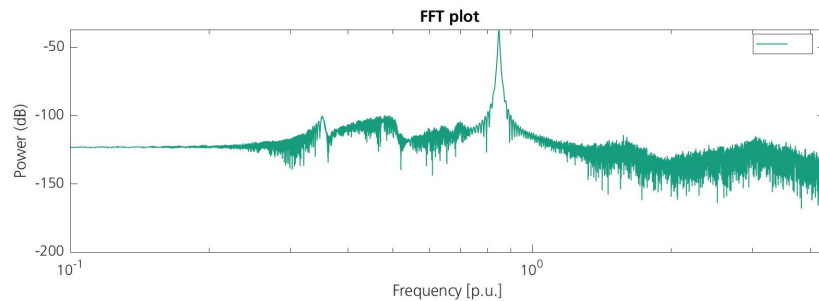


Figure 53: FFT during step air-gap torque

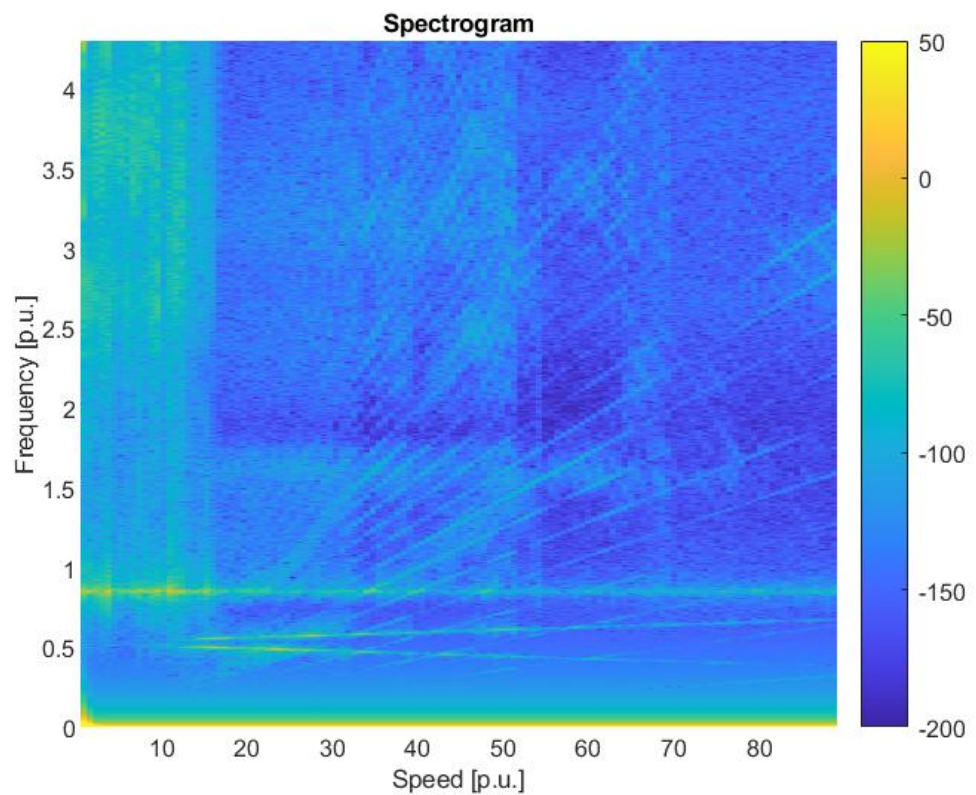


Figure 54: Spectrogram plot during 'ramp up'

Scenarios	First tor. freq. [p.u.]	Second tor. freq.[p.u.]
Ramp up	0.848	2.98
Step tor.	0.845	3.04

Table 9: Torsional frequency using operational model

6.3 Customer 2

The explanation of 'Customer 2' model can be referred to 'Customer 1'.

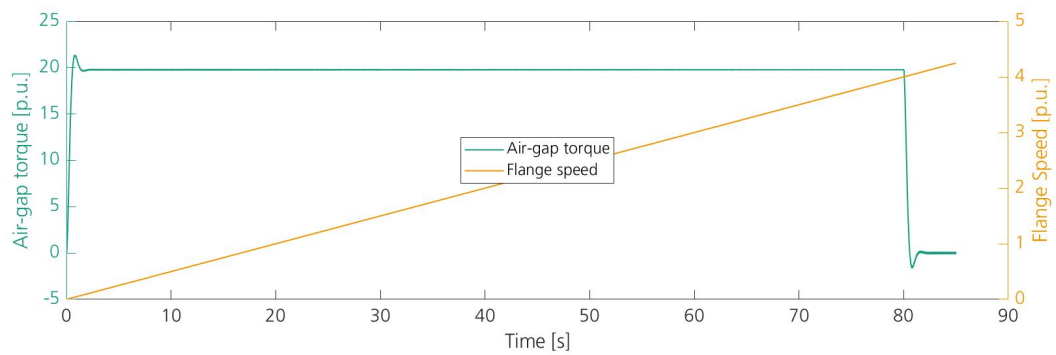


Figure 55: Air-gap torque and speed during system 'Ramp up'

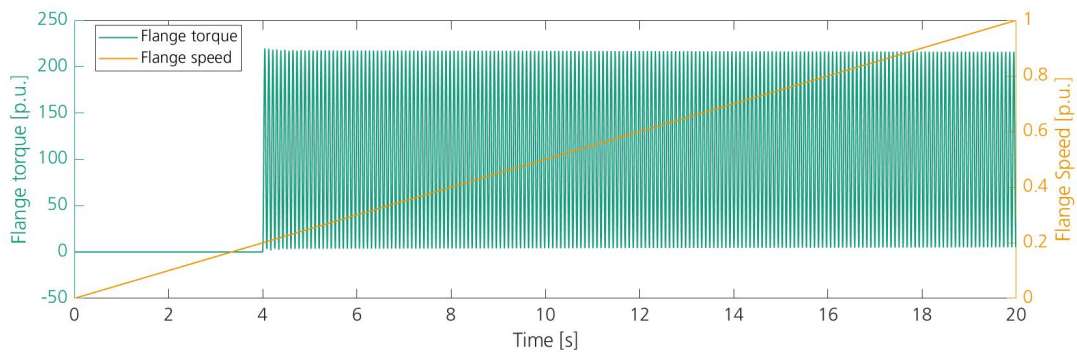


Figure 56: Flange torque and speed during step air-gap torque

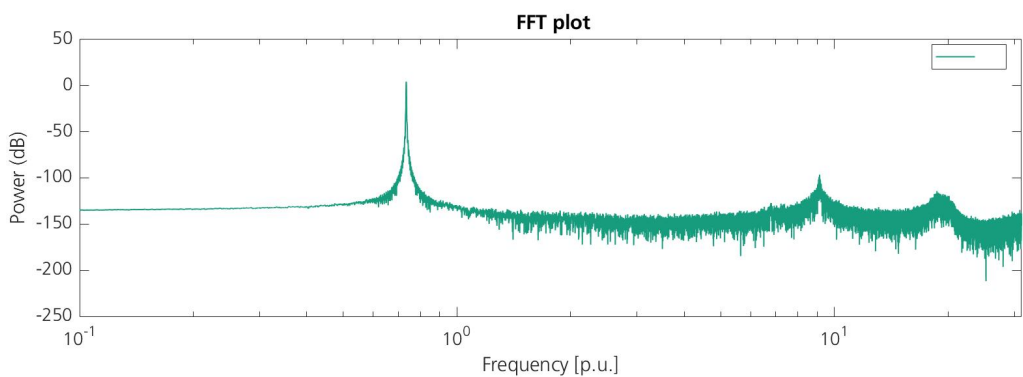


Figure 57: FFT during 'Ramp up'

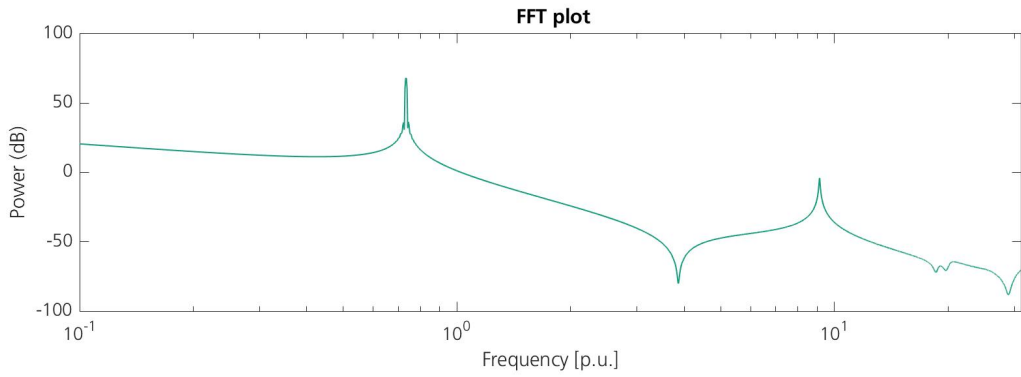


Figure 58: FFT during step air-gap torque

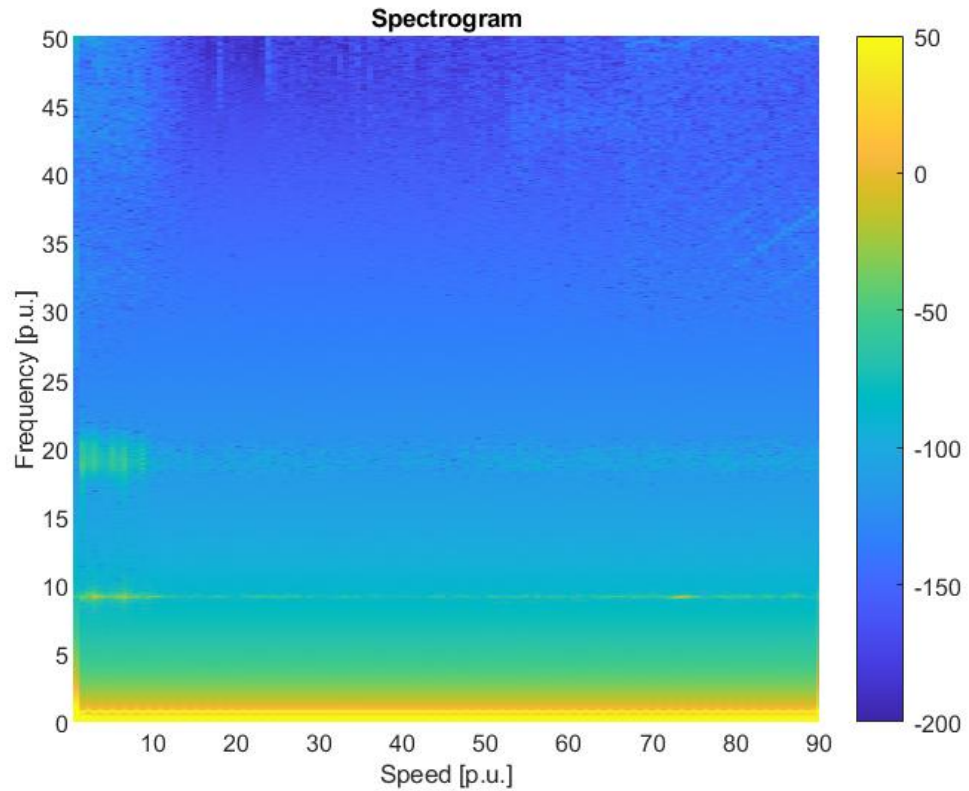


Figure 59: Spectrogram plot during 'ramp up'

Scenarios	First tor. freq. [p.u.]	Second tor. freq.[p.u.]	Third tor. freq [p.u.]
Ramp up	0.73	9.13	18.67
Step tor.	0.73	9.15	19.12

Table 10: Torsional frequency using operational model

7 LINEARIZATION OF MULTIBODY MODEL

The multibody models are nonlinear and linear model can be easily obtained in Adams. Adams user interface provide facility to export linear model to other softwares. Also, the state space matrix A, B, C, D can be easily accessed. The linearization procedure is explained in chapter two. The linear model is imported to MATLAB and bode graph is plotted using 'Gain and Phase Margin Plot' library block . The frequency response function (FRF) can also be easily take out form the model. Fig. 60, 61 and 62 are the bode plot of 'Customer 1', 'Without DUT' and 'Cusotmer 2' respectively which shows the torsional eigenfrequencies. It is same as the frequency got from normal mode analysis with negligible error.

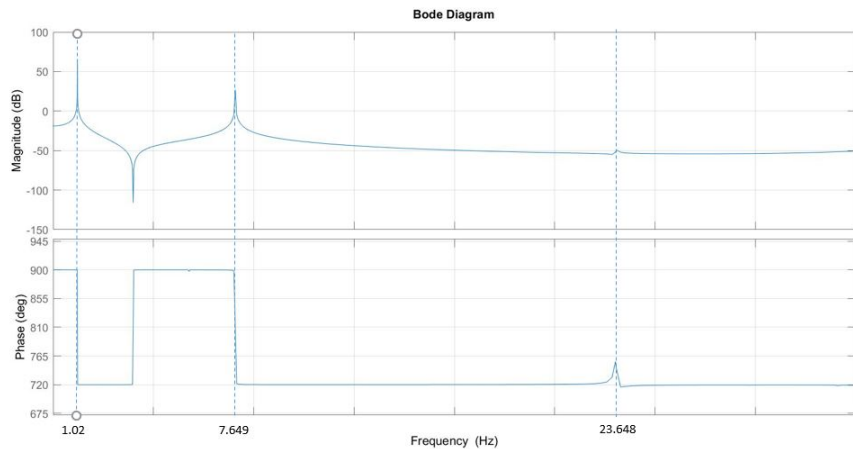


Figure 60: Frequency response of linearized model of 'Customer 1'

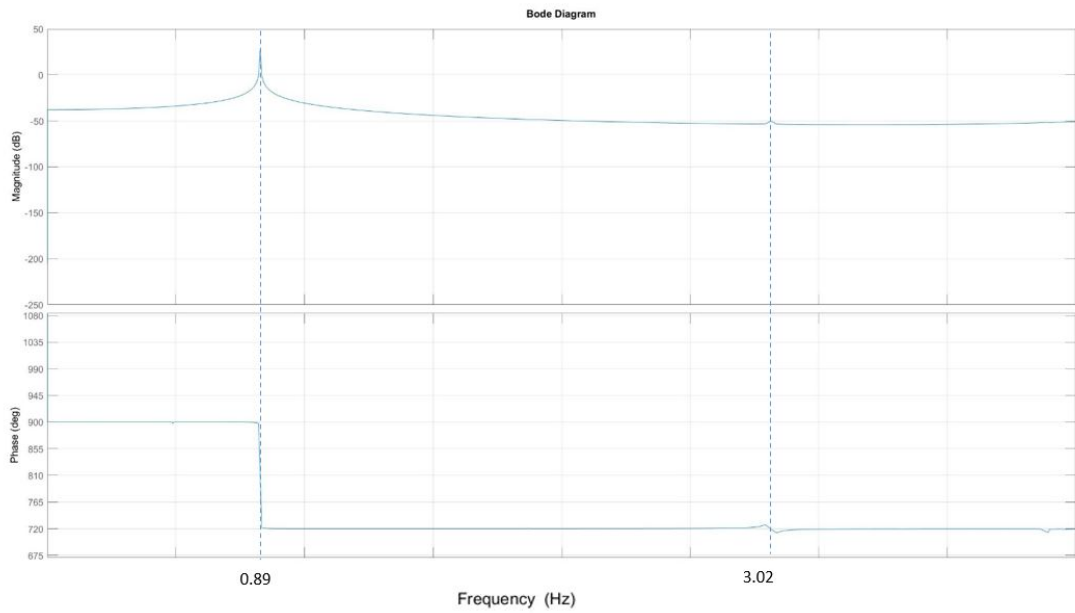


Figure 61: Frequency response of linearized model of 'Without DUT'

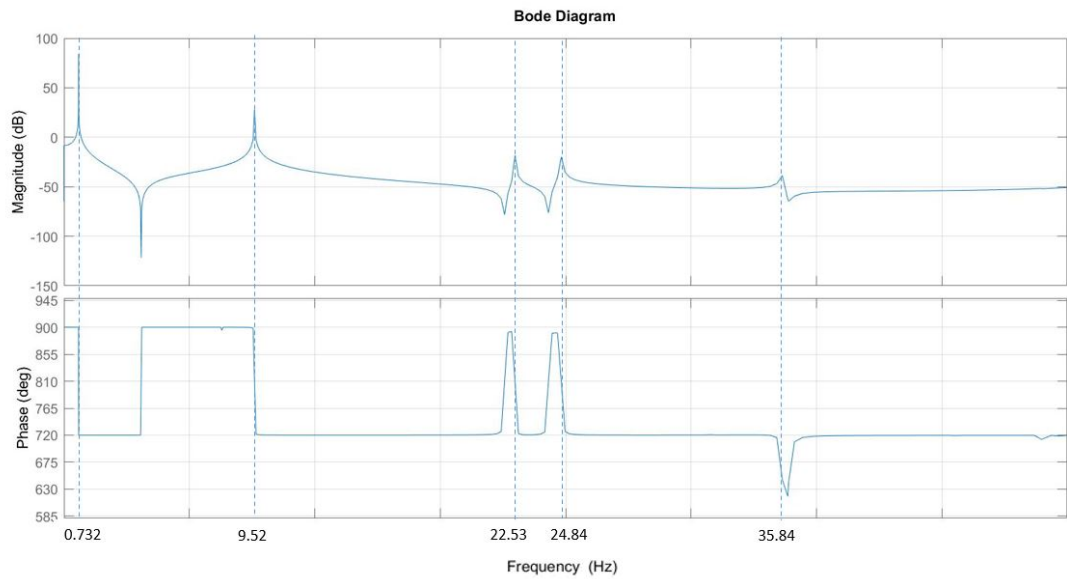


Figure 62: Frequency response of linearized model of 'Customer 2'

8 COMPARISION OF RESULTS

Torsional eigenfrequency results from the experiment, multibody model, consistent and lumped mass model, and are listed in table 11. Table 12 shows the

errors between different results. Results from the multibody model differ from the experiment and are shown in the first row of table 11. The reason behind it is the lack of accurate parameter information of the system. Only few parameters are known which are explained in chapter four. Even though the parameters are known, the multibody model assumes each part to be perfect without any defects. The material might not be of homogeneous composition which might differ in properties in various sections of the same part. Also, the experiment results are measured with the sensors and the recorded data are processed. The signal processing causes some deviation in the results. Due to all these reasons, difference in Adams and experiment results are seen.

$$Error = (reference \ value) - (obtained \ value) \quad (49)$$

$$Error \ percentage = \frac{(reference \ value) - (obtained \ value)}{reference \ value} \quad (50)$$

Setups	Experiment	Mul.Body	Consistent	Lumped
Customer 1				
1 st eig.freq.	1.00	1.02	1.02	1.02
2 nd eig.freq.	8.22	7.66	7.97	7.60
3 rd eig.freq.	20.28	23.98.	21.25	13.86
Without DUT				
1 st eig.freq.	1.00	0.89	0.88	0.84
2 nd eig.freq.	2.59	3.02	2.73	1.76
Customer 2				
1 st eig.freq.	1.00	0.73	0.73	0.73
2 nd eig.freq.	10.43	9.52	9.74	9.00
3 rd eig.freq.	28.59	22.53.	24.81	19.47

Table 11: Results from experiment and different models

	E0 _{ME} (%)	E1 _{CM} (%)	E2 _{LM} (%)	E3 _{CE} (%)	E4 _{LE} (%)
Customer 1					
1 st eig.freq.	-2.06	0.29	0.37	-1.77	-1.68
2 nd eig.freq.	6.74	-4.02	0.90	2.98	7.57
3 rd eig.freq.	-18.28	11.39	42.20	-4.81	31.64
Without DUT					
1 st eig.freq.	11.06	0.83	5.32	11.79	15.79
2 nd eig.freq.	-16.69	9.76	41.88	-5.30	32.18
Customer 2					
1 st eig.freq.	26.75	0.26	0.17	26.94	26.88
2 nd eig.freq.	8.72	-2.29	5.51	6.64	13.75
3 rd eig.freq.	21.19	-10.09	13.59	13.23	31.90

Table 12: Errors between the results

$E0_{ME}$ (%): Multibody model error with respect to experiment.

$E1_{CM}$ (%): Consistent model error with respect to multibody model.

$E2_{LM}$ (%): Lumped model error with respect to multibody model.

$E3_{CE}$ (%): Consistent model error with respect to experiment.

$E4_{LE}$ (%): Lumped model error with respect to experiment.

It is noticed that majority of error between multibody and the consistent inertia model is less compared to the lumped inertia model. Error and error percentage is denoted by equation 49 and 50. It denotes that the consistent model predicts the multibody model better. Also, the consistent model can compute higher eigenfrequencies better than the lumped model. The reason is because of the inertia of an element being linked across its nodes and is explained in detail in chapter two. Similarly, it is seen that the error between the consistent model and the experiment results are lesser except for the first eigenfrequency of 'Customer

1' and 'Customer 2'. Therefore, the consistent model can better represent the multibody model.

9 MODEL OPTIMIZATION

Optimization of 'Customer 1' and 'Customer 2' Adams model is the motive of this section so that it can show more promising dynamic results against the experiment. The outcome from the above explanation reveals that the consistent model describes the Adams model better. Therefore, Optimization is done using the consistent model. It is easier to know the parameters that needs to be changed using mathematical model. Therefore, mathematical model is optimized at first followed by multibody optimization in Adams.

9.1 Optimization of mathematical model

'Customer 1' and 'Customer 2' model can be individually optimized but a new approach is adopted. Among three Adams models 'Without DUT' is common in both other models as shown in fig. 63 which means that the parts used in the 'Customer 1' and 'Customer 2' models are identical with the same parameters as the 'Without DUT' model. If 'Without DUT' model is optimized then optimizing other models is easier, faster, accurate and also decreases the complexity of handling a higher number of variables. Therefore, the 'Without DUT' model is first optimized and the parameters are used in 'Customer 1' and 'Customer 2'.

Tolerance and tolerance % is defined by equation 51 and 52 respectively. During the 'Without DUT' optimization, tolerance of first and second eigen frequency is $\pm 1\%$ and $\pm 2\%$ respectively. Initially the tolerance of known parameters is $\pm 5\%$ and unknown parameters is $\pm 10\%$. The optimization process is not successful. Therefore, the sensitive parameters are calculated and are shown in fig. 64. Sensitive parameters are those which influence the eigenfrequencies more. The stiffness of k_1 and k_2 has more effect on first and second eigen frequency.

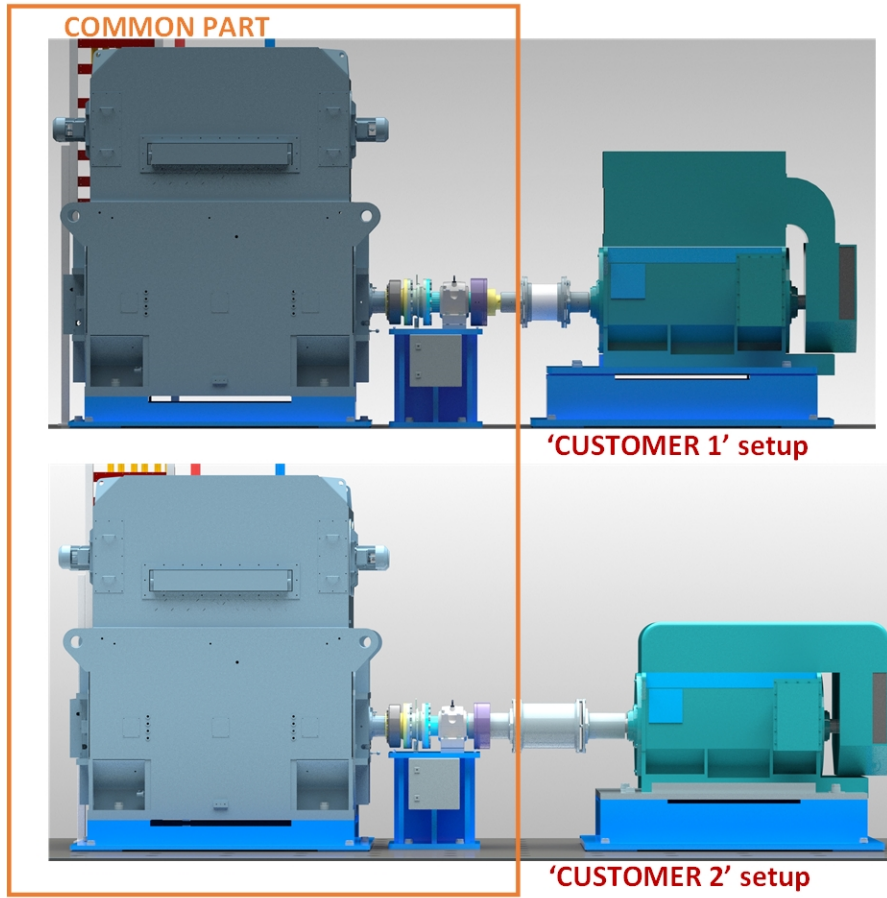


Figure 63: Common part of 'Customer 1' and 'Customer 2' model

Also, the inertia j_1 and j_2 influence the higher eigenfrequency. Above four parameters are called sensitive parameters and their tolerance is made higher until the optimization is successful and the results are shown in table 13.

$$\text{Tolerance} = (\text{initial value}) - (\text{maximum/minimum value}) \quad (51)$$

$$\text{Tolerance percentage} = \frac{(\text{initial value}) - (\text{maximum/minimum value})}{\text{initial value}} \quad (52)$$

k_1 and k_2 has the highest percentage of change because the first and second eigenfrequencies have a higher percentage of error with experiment results. Also, k_1 highly influences the first and second eigen frequencies. It is noticed that k_2 is more sensitive to the higher eigen frequencies and its new value is

Var.	Opt. val	Max. val.	Min. val.	Ini. val.	% change
j_1	0.57	0.22	0.66	0.44	-28.35
j_2	0.61	0.38	0.09	0.75	18.84
j_m	55.19	55.19	61.00	58.10	5.00
k_1	425262.00	153966.59	461899.77	307933.18	-38.10
k_2	109683.12	78295.51	234886.53	156591.02	29.96
r_1	125.02	112.50	137.50	125.00	-0.02
r_2	85.25	76.50	93.50	85.00	-0.30

Table 13: 'Without DUT' model optimization

lower than the initial value. Also, j_1 has higher influence on the second eigen frequency and it is increased during optimization. j_2 is sensitive to first and second eigen frequency and is noticed to be declined. Similarly, inertia of motor and damping ratio has negligible influence in the first and second eigen frequencies.

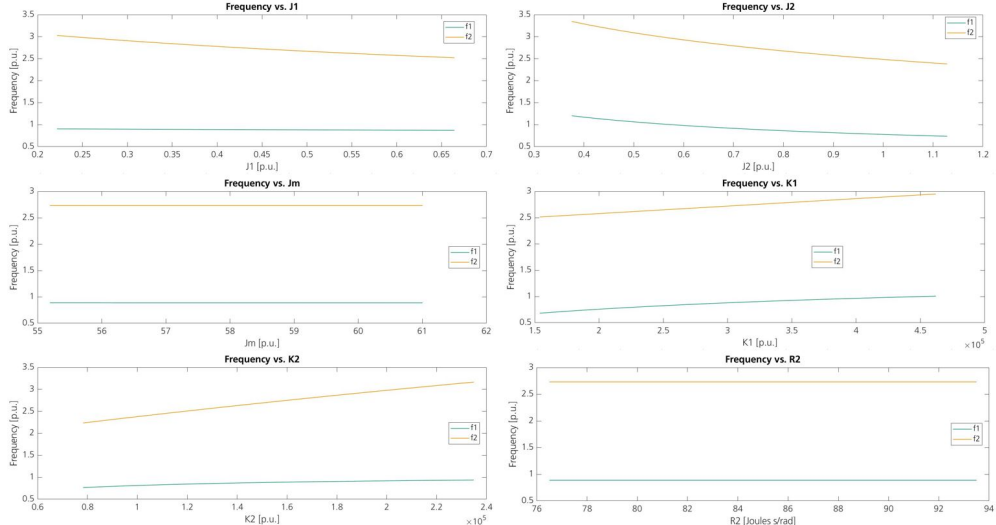


Figure 64: Change in frequency against inertia, stiffness and damping of 'Without DUT'

Small damping value of part 3 (r_3) and part 4 (r_4) are also added in 'Customer 1' and 'Customer 2' which has negligible effect on system dynamics. The new parameters got from the 'Without DUT' model are used in the optimization of

'Customer 1' model. The initial tolerance of eigen frequency for first and second mode is same as 'Without DUT'. Unknown parameters has $\pm 10\%$ tolerance while known parameters has a tolerance of $\pm 5\%$. Using these values, the optimization of second eigen frequency is not successful. Therefore, the effect of each parameter is analyzed. ' j_3 ' shows higher sensitivity to the second eigen frequency and can be seen in fig. 65. It is maximum value during optimization is set to 158.06% more than its initial value and the optimization of 'Customer 2' is successful.

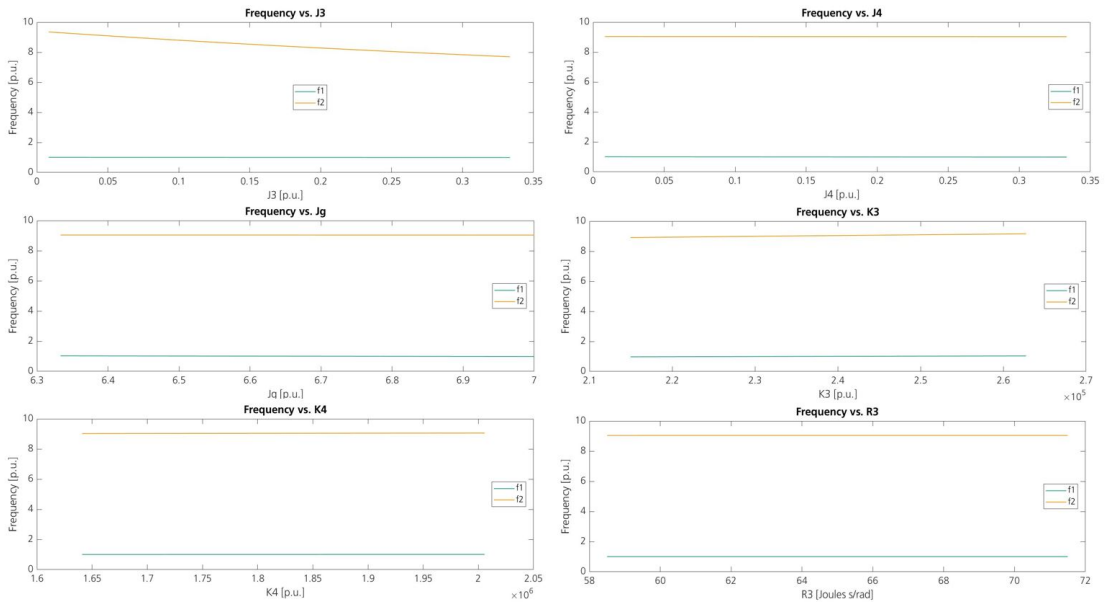


Figure 65: Change in frequency against inertia, stiffness and damping of 'Customer 1'

Similarly, the optimization of 'Customer 2' is done using the similar method used in 'Customer 1' but parameters of part 2 are also used because some components of part 2 are changed in real test bench. With the initial tolerance as the 'Customer 1', optimization is not successful and sensitive parameters are calculated which are shown in fig. 66. It is seen that j_2 and k_2 have a higher effect on second eigen frequency. Similarly, k_2 , k_3 and k_4 has impact on the first eigen frequency. Even though the tolerance of the above sensitive values are increased to $\pm 10\%$ optimization do not converge but it is noticed that the results are better.

Therefore, to achieve the required optimization, tolerance of above parameters are made higher which can be seen in table 14.

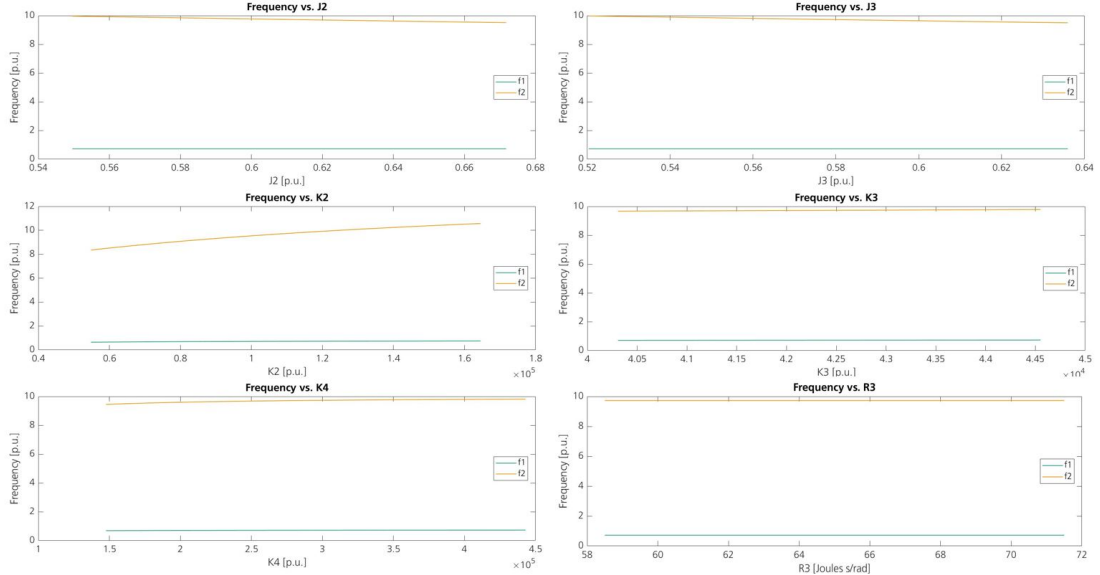


Figure 66: Change in frequency against inertia, stiffness and damping of 'Customer 2'

The optimization procedure is more dependent on k_3 and has higher percentage change although the value is known from the supplier. There is a possibility of change in the stiffness of the coupling during fabrication process.

9.2 Optimization of Adams models

From the mathematical optimization, new parameters are known which need to be employed in Adams model. The material density of flexible bodies in whole system is assumed same. Inertia of part 1 needs to be increased and can be achieved either by increasing the density or adding inertia to the rigid bodies. Changing density of the flexible part within the plausible range doesn't achieve required increased inertia. Therefore, second method is adopted. Plausible density of steel is from 7750 to 8050 Kg/m^3 . Density of Part 1 is kept as $8050Kg/m^3$. Similarly, optimized inertia of part 2 is lesser and inertia of rigid parts are reduced but the density is kept same as part 1.

Var.	Opt. val	Max. val.	Min. val.	Ini. val.	% change
j_2	0.67	0.31	0.67	0.61	-10.00
j_3	0.64	0.29	0.64	0.58	-10.00
j_4	0.03	0.03	0.04	0.03	6.91
j_g	33.25	33.25	35.70	35.00	5.00
k_2	157173.77	54841.56	548415.58	109683.12	-43.30
k_3	152477.45	21214.68	212146.76	42429.35	-259.37
k_4	172528.01	147642.96	442928.89	295285.92	41.57
r_2	85.48	76.73	93.78	85.25	-0.27
r_3	65.01	58.50	71.50	65.00	-0.01
r_4	64.98	58.50	71.50	65.00	0.03

Table 14: 'Customer 2' model optimization

Dimensions of the optimized parts are same. Therefore, torsional stiffness depends on the modulus of rigidity of material. Using the relation between G, E and ν , stiffness of parts can be changed. Poisson's ratio is kept 0.29 and young's modulus is varied to get the required stiffness. This process is used for both part 1 and part 2. Stiffness is recorded with varying young's modulus of each part but the relation between them is not perfectly linear which is shown in fig. 67 and 68. It is because of measurement errors in the Adams model and numerical calculation process. Graphical method is used to calculate approximate value of Young's modulus which doesn't perfectly determine the optimized torsional stiffness but gives a reliable value with -1.19 and -1.15 % error for k_1 and k_2 respectively.

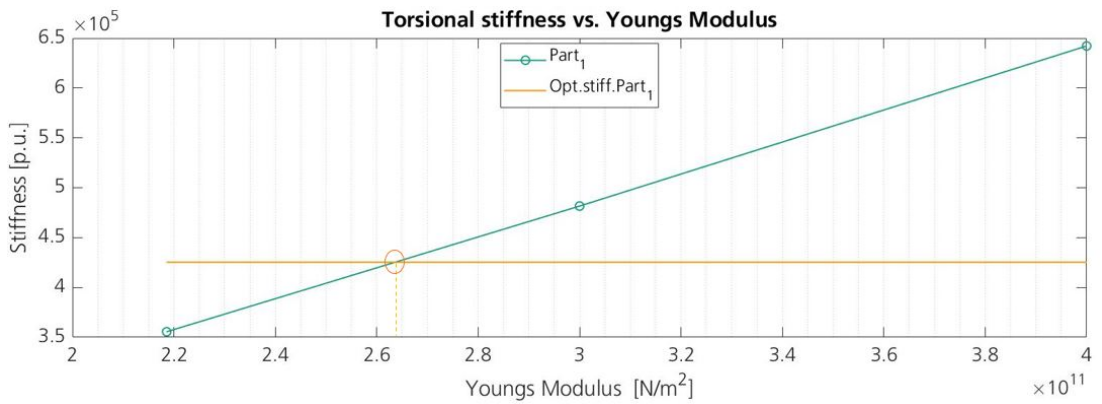


Figure 67: Torsional Stiffness of part 1 vs. Young's modulus

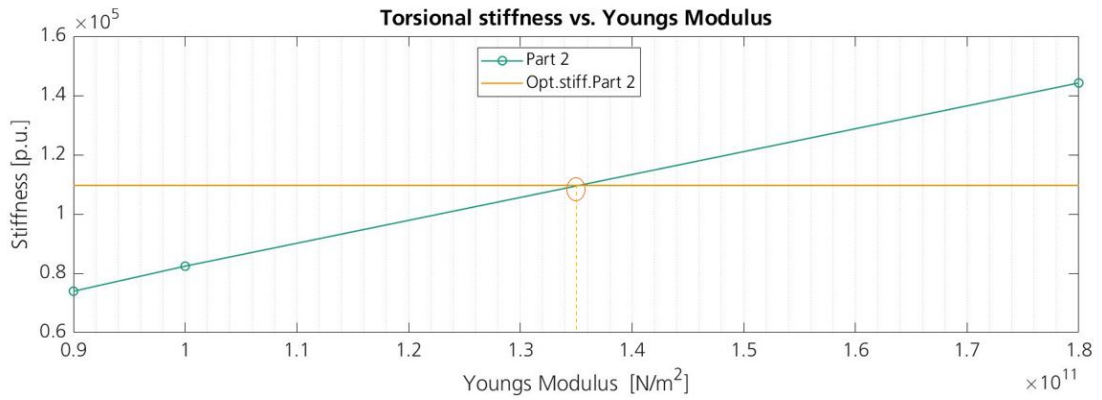


Figure 68: Torsional Stiffness of part 2 vs. Young's modulus

After getting the required parameters, Adams model is modified and the modal analysis is done which are shown in table 15. First eigen frequency has an error of -2.12% while second eigen frequency as -9.07% with the experiment results as shown in table 15. Errors of the optimized model are lesser than previous model but the errors are still high. Major reason is the addition of inertia to the rigid bodies. The increment or decrements of the inertia of each part should be uniformly distributed rather than accumulated to rigid body. The other reason is error in determination of stiffness in the Adams model. It signifies that the consistent mass model can be used to optimize the Adams model better. Similar method can be used for optimization of the 'Customer 1' and 'Customer 2' Adams model.

Material density and young's modulus of optimized 'Part 1' and 'Part 2' are shown

Eig. freq	Opt. val	% error
f1	1.02	-2.12
f2	2.83	-9.07

Table 15: Eigenfrequencies of optimized multibody model

by red circle in fig. 69. It shows the density and young's modulus range of available materials. Poisson's ratio is 0.29 which is the default value of steel in Adams. Both parts have the properties in the metal region near to the steel. The properties can also be tuned during optimization by varying density and poisson's ratio. Similarly, it might not be accurately in steel region because all the material are assumed same and perfect contact between parts which is not true in reality.

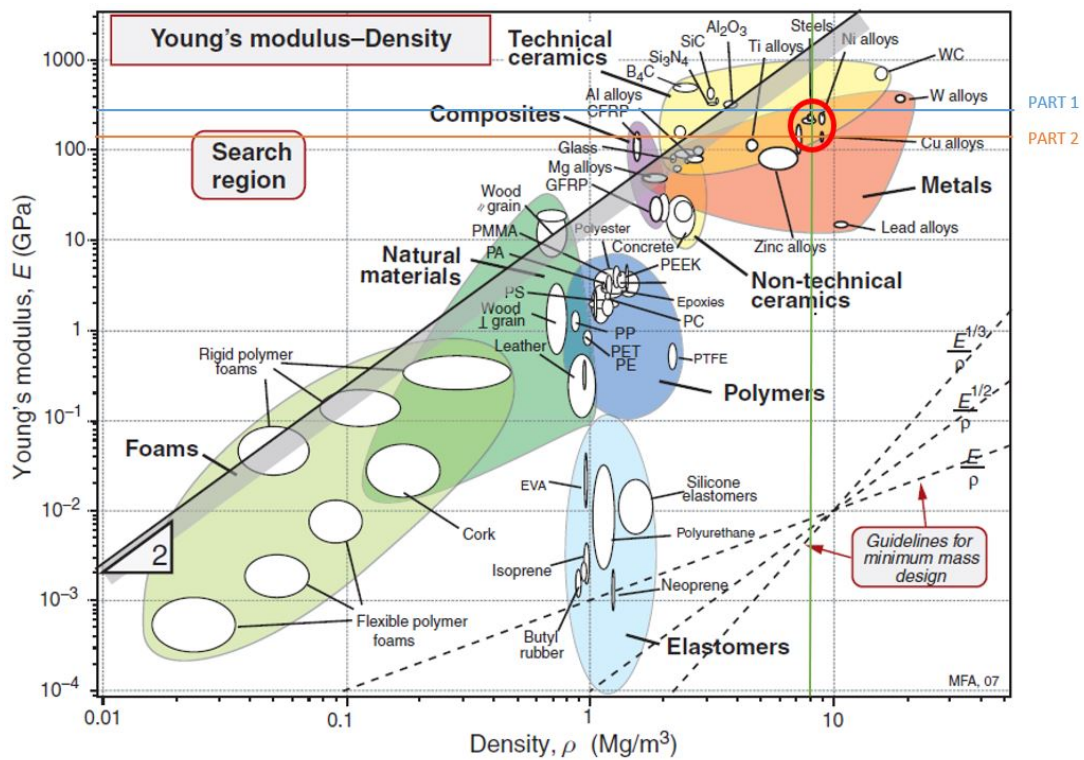


Figure 69: Young's modulus v.s density of different material [24]

10 CASE STUDY OF LOW EIGENFREQUENCIES

During the testing of the 'Customer 2' setup the eigenfrequencies are noticed to be shifted to a lower value. It is found that there is sliding between the parts of sliding coupling. As shown in figure 70, sliding coupling has 'part x' and 'part y' connected to 'part z'. 'Part x' and 'part y' are conical shape so that the pretension in the bolts provide required compression between 'part y' and 'part z'. Because of the resulting friction force acting between these parts torque can be transmitted.

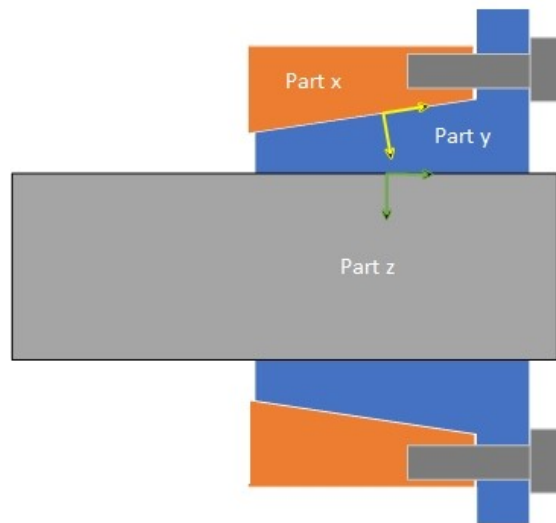


Figure 70: Sliding coupling

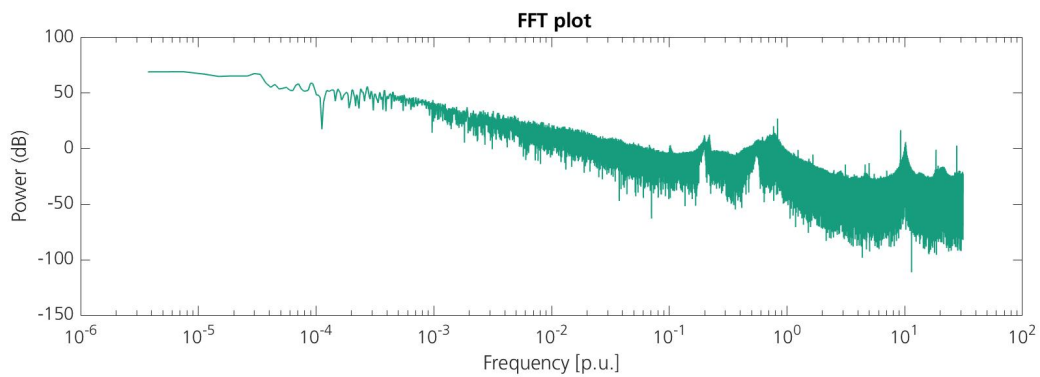


Figure 71: Frequency shift of 'Customer 2'

[25] has described fault diagnosis of wind turbine drive train using torsional vibration. In this paper, causes of the shift of the eigenfrequencies including the coupling defects are explained. Sensitive analysis is done which shows the parameters that affect the eigenfrequencies. Also, a method to detect damage using the frequency shift curve (FSC) for cylindrical shell is explained in [26]. Similarly, [27] has presented a method to predict the effect of small geometrical changes on the resonance frequency. According to this paper, eigenfrequency change is dependent on the strain energy of static solutions that can be got for small cracks and other small cut-outs.

In the fig. 71, FFT plot shows that first eigenfrequency decreases by 23.25%

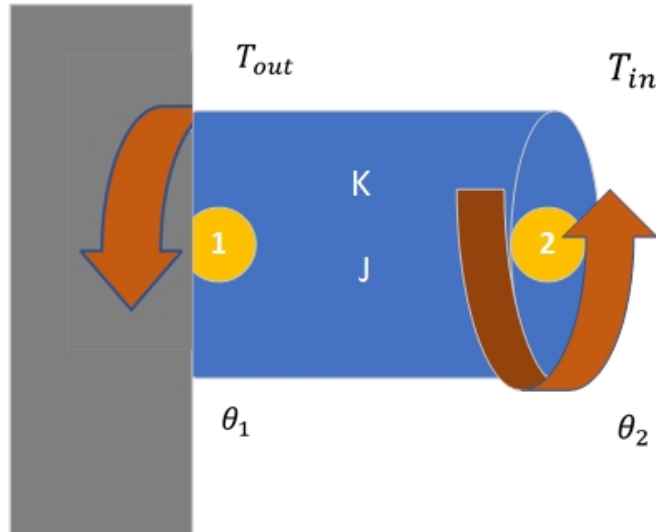


Figure 72: Flexible shaft connected to rigid wall

while second eigen frequency decreases by 3.05%. The defect is assumed only in the stiffness of the part because inertia contributing to such a high difference in frequency is small. Optimized parameters are used for calculation of eigenfrequencies. If stiffness of part 2 is assumed to be varied then the first eigenfrequency matches to changed frequency only when the stiffness is decreased to 40% of its optimized value which is very less. Also, if the stiffness of both part 2 and part 3 are assumed to be changed then the required low frequency is obtained with approximately 50% of each part's stiffness. In either case, the stiffness needs to be sharply decreased. The second eigenfrequency

is also highly reduced using this assumption which cannot be the cause of the shifted frequency.

Above explanation is related to stiffness change during static condition. Let's consider a flexible shaft connected to rigid wall as shown in the fig. 72. 'J' and 'K' are the inertia and torsional stiffness respectively. T_{in} is the torque at node 2 which is zero in the system while T_{out} is the reaction of the wall to cylinder at node 1. Similarly, the angular deflection at node 2 is θ_2 and there is no damping in the system. The dynamics condition of the system can be represented by eq. 53.

$$T_{out} = J\ddot{\theta}_2 + K\theta_2 \quad (53)$$

We notice that if the inertia and angular acceleration of the part is high, the torque exerted at the wall interface is also high. Fig. 73 represents the modes of first and second eigenfrequency from the Adams model which is approximate value taken from mode animation. In the first mode nodes N3 and N4 move in the opposite direction which represents higher relative angular acceleration. N4 and N5 are in the same direction and high inertia generator is connected to N5 which results in very high torque in part 2. Due to high torque, the coupling is predicted to slide. Similarly, in the second mode all the nodes except N5 move in the same direction. Due to this, the torque during dynamic conditions is relatively small, and second eigenfrequency is not highly shifted.

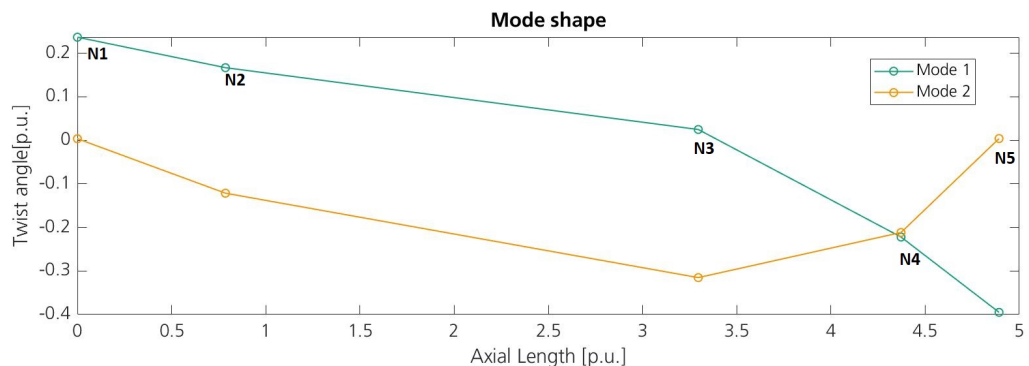


Figure 73: First and second mode shapes

To verify above prediction, validated multibody model of 'Customer 2' is used

because it represents the torsional dynamic of real test bench. Sinusoidal torque with first and second eigenfrequencies are provided to motor with same amplitude. When first eigenfrequency is provided to the system, it oscillates with the first eigenmode and torque is measured. Torque measurement position is between part 2 and part 3 as shown in fig. 74.

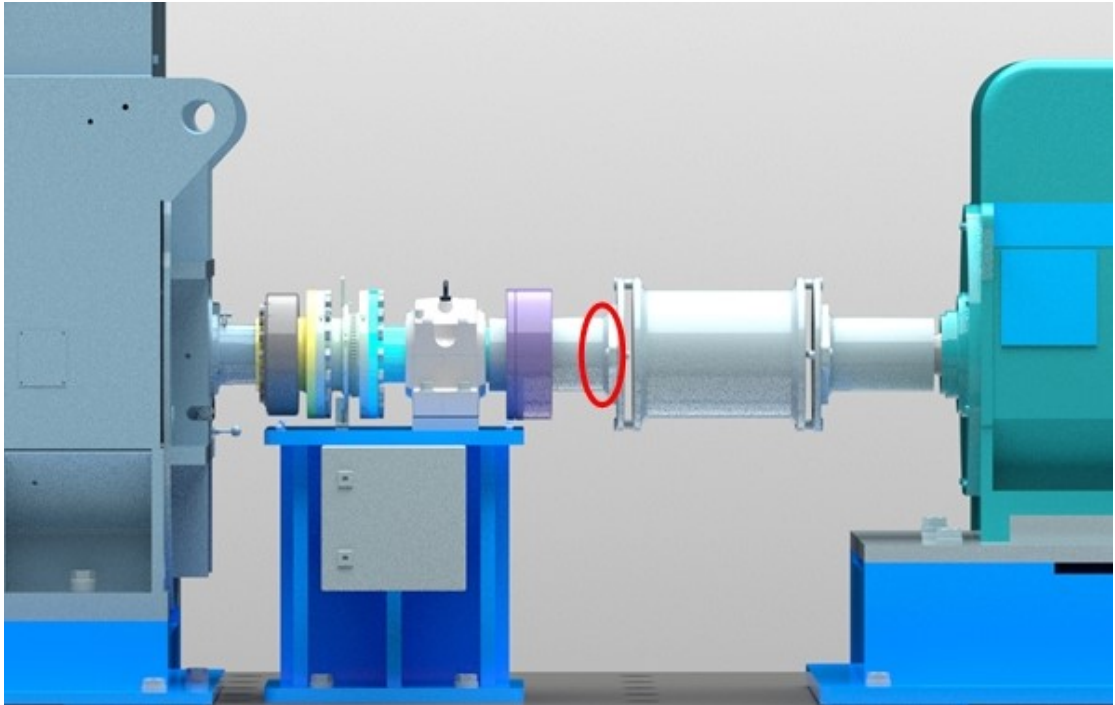


Figure 74: Torque measurement position

Results obtained from two cases are shown in the fig. 75. It can be clearly seen that torque between part 2 and part 3 is higher at first mode which causes the sliding. Amplitudes in both modes are increasing because it is in resonance condition and the poles lies in the negative x-axis which denotes that the system is stable in closed loop.

11 CONCLUSIONS AND FUTURE PROSPECTS

The multibody models of three different test bench setups are validated against torsional eigenfrequencies of empirical results. Experiment's damping ratio is implemented in 'Without DUT' multibody model but the damping ratio got from

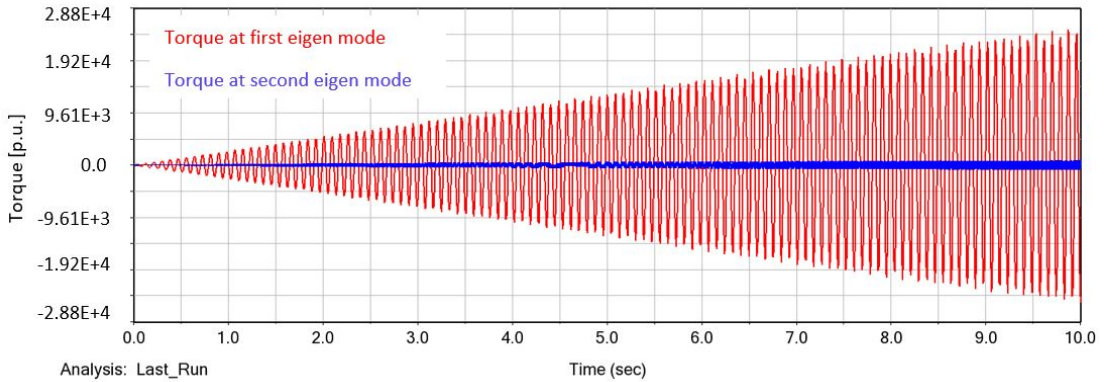


Figure 75: Torque at different modes

normal mode analysis is less than experiment's damping ratio. Non-linear multi-body model of 'Without DUT' shows higher damping ratio than normal mode analysis which is got from linearization process. Also, Unusual damping and eigenfrequency of rigid mode are seen during linearization and flexible parts from ANSYS are also used for normal modes analysis which shows higher eigen-frequencies. Consistent model is seen to predict higher frequencies better and it is also noticed that consistent model represents multibody and experiment results accurately than lumped mass model. Errors are found in the multibody model and a suitable optimization method is used which provides improved torsional dynamics. The optimized parameters are also verified against available material properties. Operational model are applied to test nonlinear multibody models in controlled loop and the eigenfrequencies obtained are found lesser than normal modes analysis and linearized model. During testing of 'Customer 2' setup, first eigenfrequency is seen to be dropped by higher percentage than second eigenfrequency. Sliding of the coupling due to higher dynamic loading during first mode is the reason behind it which is confirmed from the multibody simulations.

Therefore, a suitable system is created where a new generator with known required parameters can be added to the existing multibody system and its torsional behavior can be predicted. Control logic can be tested in the operational model which can help to provide beforehand information of tuning parameters.

Similarly, the unknown parameters of the system can also be identified with the help of Adams model and results from the test bench.

Multibody model can be further optimized to achieve higher accuracy in the eigenfrequencies. Damping ratio calculation method and implementation in multibody model can be further improved to get more accurate damping values. Flexible parts using ANSYS needs to be further examined because solving the units problem can give better results and constraints between bodies can be well defined. Since the sensitive parameters of each setup are known, defects in the system parts can also be identified and studied. Bearing damping and friction, bending modes, misalignment, etc are not involved in the model. These conditions can be incorporated in the multibody model to observe and validate non-rotational modes. Control logic can also be further implemented and checked with the multibody model. Sensitive parameters can be used to predict the defective parts and the progression of defects like cracks, misalignment etc in the system.

References

- [1] L. Bertling, J. Ribrant, Bertling, Lina, Ribrant, and Johan, *2007 IEEE Power Engineering Society general meeting: Tampa, FL, 24 - 28 June 2007*. Piscataway, NJ: IEEE Service Center, 2007.
- [2] G. Curioni, “Robust drive-train test bench control framework via hardware-in-the-loop with mechanical inertia emulation capability,” in *2019 IEEE 58th Conference on Decision and Control (CDC)*, pp. 1931–1936, IEEE, 2019.
- [3] B. Fischer, C. Mehler, A. Zuga, and M. Shan, “Control design for mechanical hardware-in-the-loop operation of dynamometers for testing full-scale drive trains,” *Wind Energy*, vol. 19, no. 10, pp. 1889–1901, 2016.
- [4] M. Neshati, P. Feja, A. Zuga, H. Roettgers, A. Mendonca, and J. Wenske, “Hardware-in-the-loop testing of wind turbine nacelles for electrical certification on a dynamometer test rig,” *Journal of Physics: Conference Series*, vol. 1618, no. 3, p. 032042, 2020.
- [5] H. Packard, “The fundamentals of signal analysis,” *HP application note*, vol. 243, 1985.
- [6] C. S. Paresh Girdhar, “Practical machinery vibration analysis and predictive maintenance,” 2004.
- [7] D. L. Logan, “A first course in the finite element method,” 2016.
- [8] D. V. Hutton, “Fundamentals of finite element analysis,” 2004.
- [9] S. S. Rao, *Mechanical vibrations*. Upper Saddle River N.J.: Prentice Hall, 5th ed. ed., 2011.
- [10] R. R. Teixeira, S. R. Moreira, and S. Tavares, “Multibody dynamics simulation of an electric bus,” *Procedia Engineering*, vol. 114, pp. 470–477, 2015.

- [11] J. B. McConville and J. F. McGrath, “Introduction to adams theory,” *Mechanical Dynamic Inc*, 1998.
- [12] A. Khaghani and K. Cheng, “Investigation on multi-body dynamics based approach to the toolpath generation for ultraprecision machining of freeform surfaces,” *Proceedings of the Institution of Mechanical Engineers, Part B: Journal of Engineering Manufacture*, vol. 234, no. 3, pp. 571–583, 2020.
- [13] D. Negrut and J. L. Ortiz, “A practical approach for the linearization of the constrained multibody dynamics equations,” *Journal of Computational and Nonlinear Dynamics*, vol. 1, no. 3, pp. 230–239, 2006.
- [14] *ADAMS/PRE Online Documentation*.
- [15] N.S. Achar and G.H. Gaonkar, “An exploratory study of a subspace iteration method as an alternative to the qr method for floquet eigenanalysis,” *Mathematical and Computer Modelling*, vol. 19, no. 3, pp. 69–73, 1994.
- [16] HILBER, H. M., HUGHES, T. J. R., AND TAYLOR, R. L., “Improved numerical dissipation for time integration algorithms in structural dynamics,” *Earthquake Engineering and Structural Dynamics*, vol. 5, pp. 283–292, 1977.
- [17] X. Qu, C. Qi, G. Fu, and X. Li, “Effects of time integration schemes on discontinuous deformation simulations using the numerical manifold method,” *International Journal for Numerical Methods in Engineering*, vol. 112, no. 11, pp. 1614–1635, 2017.
- [18] *ANSYS Online Documentation*.
- [19] MATLAB, version 9.11.0.1809720 (R2021b). Natick, Massachusetts: The MathWorks Inc., 2021.
- [20] G. Q. Gabriele Curioni, Torben Jersch, “Hil-grid-cop: Wind turbine minimal system test bench design.”

- [21] Wikipedia, *Asynchronous motor*. 2022. [Online; accessed 22-July-2004].
- [22] R.-J. Shyu, “Bending vibration of rotating drill strings,” 1989.
- [23] N. S. Nise, “Control systems engineering, sixth edition,”
- [24] M. F. Ashby, H. Shercliff, and D. Cebon, *Materials: Engineering, science, processing and design*. Amsterdam and Boston: Butterworth-Heinemann, 1st ed. ed., 2007.
- [25] F. K. Moghadam and A. R. Nejad, “Theoretical and experimental study of wind turbine drivetrain fault diagnosis by using torsional vibrations and modal estimation,” *Journal of Sound and Vibration*, vol. 509, p. 116223, 2021.
- [26] Y. Zhang, S. T. Lie, Z. Xiang, and Q. Lu, “A frequency shift curve based damage detection method for cylindrical shell structures,” *Journal of Sound and Vibration*, vol. 333, no. 6, pp. 1671–1683, 2014.
- [27] P. Gudmundson, “Eigenfrequency changes of structures due to cracks, notches or other geometrical changes,” *Journal of the Mechanics and Physics of Solids*, vol. 30, no. 5, pp. 339–353, 1982.

APPENDICES

A Flexible parts and units

If the same part is made flexible twice recent flexible part is saved in the same name. It was one of the major problem during optimization because the previous flexible parts information was lost. Special attention should be taken while reusing the same flexible part in Adams. Precision of results must be increased by including more decimal numbers especially in the case of normalizing results. Units should be mm, gm, N, s and degree because it gives better precision than MKS system.

B Stiffness calculation from multibody model

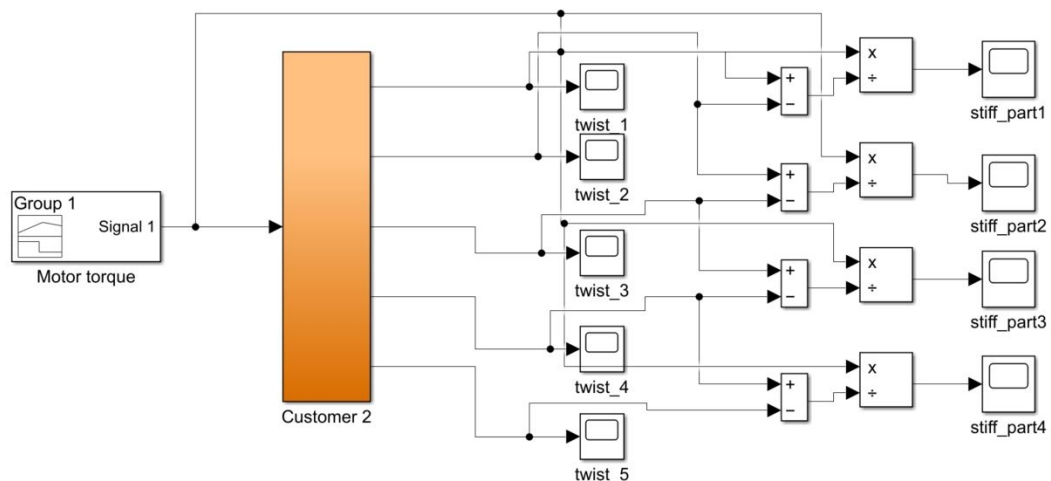


Figure 76: Torsional stiffness of different parts of 'Customer 2'

C Simulink model for optimization

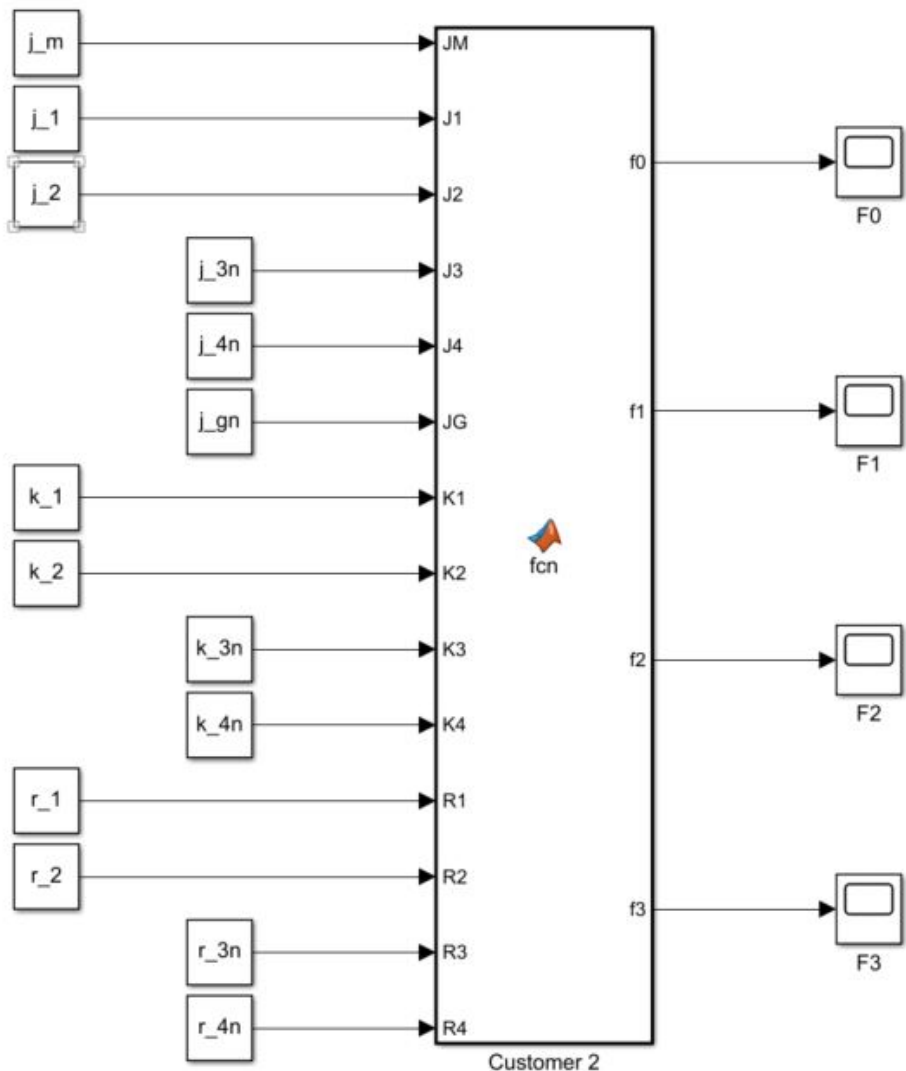


Figure 77: Simulink model for optimization of 'Customer 2'

D Simulink model to check sensitive parameters

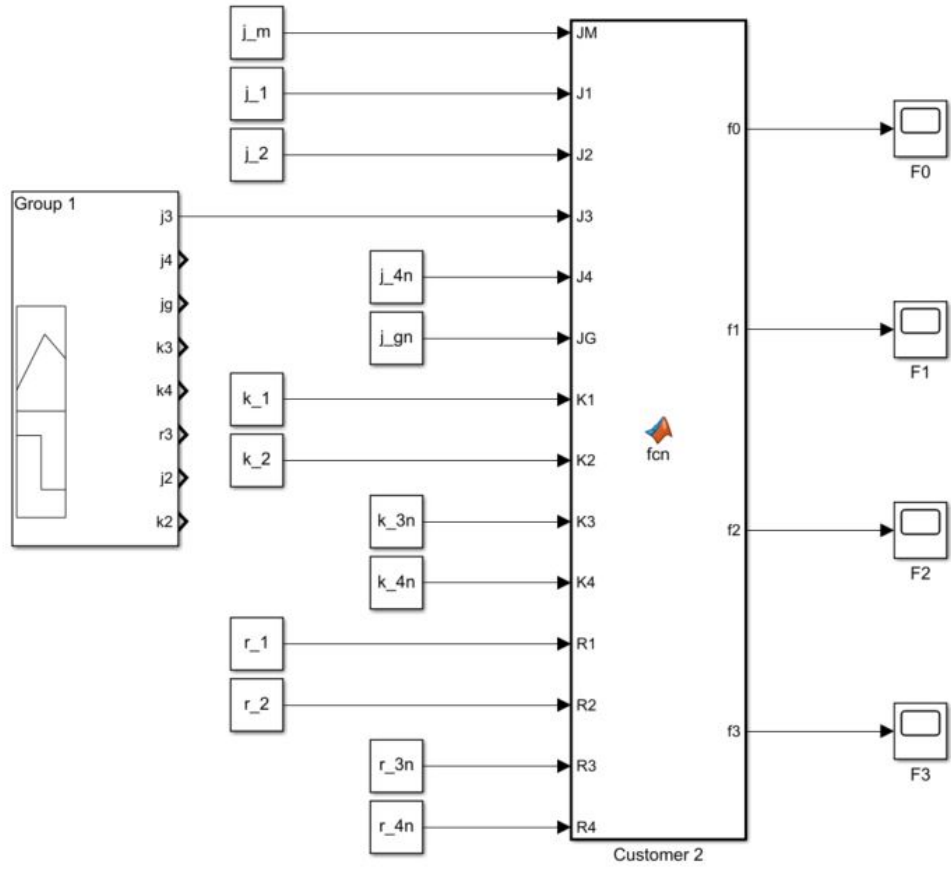


Figure 78: Simulink model to check sensitive parameters of 'Customer 2'